RM No. L7I15
Copy No.

NACA

RESEARCH MEMORANDUM

HIGH-SPEED WIND-TUNNEL INVESTIGATION OF THE LATERAL CONTROL CHARACTERISTICS OF PLAIN AILERONS ON A WING WITH VARIOUS AMOUNTS OF SWEEP

By

Arvo A. Luoma, Ralph P. Bielat, and Richard T. Whitcomb

Langley Memorial Aeronautical Laboratory
Langley Field, Va.

NATIONAL ADVISORY COMMITTEE FOR AERONAUTICS

WASHINGTON

December 19, 1947

NATIONAL ADVISORY COMMITTEE FOR AERONAUTICS

RESEARCH MEMORANDUM

HIGH-SPEED WIND-TUNNEL INVESTIGATION OF THE LATERAL-CONTROL CHARACTERISTICS OF PLAIN AILERONS ON A WING WITH VARIOUS AMOUNTS OF SWEEP

By Arvo A. Luoma, Ralph P. Bielat, and Richard T. Whitcomb

SUMMARY

A three-dimensional investigation of straight-sided-profile plain ailerons on a wing with 30° and 45° of sweepback and sweepforward was made in the Langley 8-foot high-speed tunnel for aileron deflections from −10° to 10° and at Mach numbers from 0.60 to 0.96. The wing when unswept had an NACA 65-210 section, an aspect ratio of 9.0, and a taper ratio of 2.5:1.0. Sweep was obtained by rotating the wing semispans about an axis perpendicular to the chord plane of the wing at the center line of the wing. Rolling-moment, wing normal-force, and wing pitching-moment coefficients were determined from pressure-distribution measurements. Aileron hinge-moment data were obtained by an electrical strain gage. No corrections have been made to the data as a result of bending of the swept wing. The results presented in this report, therefore, are specifically applicable to a wing with flexural characteristics similar to those of the model wing tested.

The severity of the large changes in rolling-moment and aileron hinge-moment coefficients observed for an unswept wing as a result of compression shock was reduced, and the speeds at which such changes occurred were delayed to higher Mach numbers by 30° of sweepback and sweepforward. The configurations with 45° of sweepback and sweepforward had rolling-moment and hinge-moment characteristics which, for the speeds covered, were not materially affected by change in Mach number. At the higher speeds, the configurations with sweepforward generally developed more rolling moment than the configurations with an equal amount of sweepback; at low speeds, the reverse was true. The configuration with 30° of sweepback generally had smaller aileron hinge moments than the configuration with an equal amount of sweepforward; for 45° of sweep, however, sweepforward gave smaller hinge moments. The variations in wing pitching-moment coefficient with Mach number for all the sweep angles tested were large.

INTRODUCTION

Investigations made in Germany and in this country have shown that the use of sweep delays the onset of the radical changes in aerodynamic characteristics associated with the presence of shock on the wing. More recent investigations have added appreciably to existing information on the characteristics of wings with sweep in the subsonic, transonic, and supersonic speed ranges. Among these is an investigation of the effects of 30° and 45° of sweepback and sweepforward on the characteristics of a wing at Mach numbers up to 0.96 (reference 1). Some low-speed investigations, such as reference 2, have studied the lateral-control characteristics of swept wings. However, there is a lack of lateral-control data for swept wings at very high speeds.

The tests presented herein were made to determine the aerodynamic characteristics at high subsonic speeds of plain ailerons on a wing having 30° and 45° of sweepback and sweepforward. Wind-tunnel data, including rolling-moment coefficients, wing normal-force coefficients, wing pitching-moment coefficients, and aileron hinge-moment coefficients were obtained for aileron deflections from −10° to 10°, for various wing angles of attack, and at Mach numbers from 0.60 to 0.96.

SYMBOLS

The symbols used in this report are defined as follows:

X — line of intersection of reflection plane and chord plane of wing (X-axis); positive direction shown in figure 1

Y — line perpendicular to reflection plane and intersecting X-axis at origin O (Y-axis) (See fig. 1.)

x, y — coordinates of any point in chord plane of wing, referred to X- and Y-axes

Y' — principal reference line in the wing (Y'-axis), obtained by passing line through quarter-chord points of section chords of unswept wing

X' — line perpendicular to Y'-axis at origin O and lying in chord plane of wing (X'-axis)

x', y' — coordinates of any point in chord plane of wing, referred to X'- and Y'-axes

Λ_r — sweep angle, measured between Y-axis and Y'-axis; sweepback is considered positive and sweepforward negative

α	angle of attack of wing, measured by angle between X-axis and direction of undisturbed stream
δ_a	aileron deflection, measured in plane perpendicular to aileron hinge axis; positive for down deflection
$\Delta\delta_a$	absolute value of total aileron deflection with ailerons at equal positive and negative deflections
V	velocity in undisturbed stream
p	static pressure in undisturbed stream
p_l	local static pressure at point on airfoil section
ρ	mass density in undisturbed stream
μ	coefficient of viscosity in undisturbed stream
a	speed of sound in undisturbed stream
q	dynamic pressure in undisturbed stream $\left(\frac{1}{2}\rho V^2\right)$
P	pressure coefficient $\left(\frac{p_l - p}{q}\right)$
M	Mach number $\left(\frac{V}{a}\right)$
R	Reynolds number $\left(\frac{V\rho\bar{c}_W}{\mu}\right)$
b	span of model, measured parallel to Y-axis
$b'/2$	swept semispan, distance along Y'-axis from origin 0 to tip chord $\left(\frac{b/2}{\cos \Lambda}\right)$
r_{st}	radius of straight-sided part of fuselage at wing-fuselage juncture; model value, 1.88 inches
y'_i	distance along Y'-axis from origin 0 to aileron inboard end
y'_o	distance along Y'-axis from origin 0 to aileron outboard end
b_a'	span of aileron, measured parallel to Y'-axis $\left(y'_o - y'_i\right)$
c	section chord of wing, measured parallel to X-axis
c'	section chord of wing, measured parallel to X'-axis; in this report this chord is considered to be limited by fuselage for those sections partially covered by the fuselage

c_g tip chord of wing, measured parallel to X-axis

c_r root chord of wing, measured parallel to X-axis (See fig. 1.)

t'_{max} maximum thickness of section with chord c'

S_w area of wing outboard of fuselage $\left(2\int_{r_{st}}^{b/2} c\ dy\right)$

S_e total area of wing extended through fuselage $\left(\frac{(c_r + c_g)b}{2}\right)$

A aspect ratio $\frac{b^2}{S_e}$

$\bar{c}_w$ mean aerodynamic chord of wing outboard of fuselage $\left(\frac{2}{S_w}\int_{r_{st}}^{b/2} c^2\ dy\right)$

c_a' section chord of aileron, measured parallel to X'-axis, from hinge axis to trailing edge of airfoil (0.20c')

$\bar{c}_a'$ root-mean-square chord of aileron $\left(\sqrt{\frac{1}{b_a'}\int_{y'_i}^{y'_o} c_a'^2\ dy'}\right)$

$\bar{x}_w$ distance from the origin 0 to the lateral axis which is parallel to Y-axis and passes through the quarter-chord point of mean aerodynamic chord $\bar{c}_w$ $\left(\frac{2}{S_w}\int_{r_{st}}^{b/2} cx\ dy\right)$ where x is abscissa of quarter-chord point of any chord c

H_a aileron hinge moment

C_{h_a} aileron hinge-moment coefficient $\left(\frac{H_a}{qb_a'\bar{c}_a'^2}\right)$

ΔC_{h_a} absolute value of total hinge-moment coefficient of ailerons at equal positive and negative deflections

c_n' section normal-force coefficient of wing (section parallel to X'-axis) $\left(\frac{1}{c'}\int_{L.E.}^{T.E.} (P_L - P_U)\ dx'\right)$

L.E. leading edge of section chord c'

T.E. trailing edge of section chord c'

c_t' section twisting-moment coefficient of wing about Y'-axis (section parallel to X'-axis) $\left(\frac{1}{c'^2}\int_{L.E.}^{T.E.} (P_U - P_L)\ x'\ dx'\right)$

C_{N_w} normal-force coefficient of semispan wing (based on air loads outboard of fuselage) (See figs. 1 to 4 for limits of integration.) $\left(\frac{2}{S_w}\int_{y'_a}^{y'_b} c_n'\ c'\ dy'\right)$

C_{m_w} pitching-moment coefficient of semispan wing (based on air loads outboard of fuselage) about lateral axis which is parallel to Y-axis and passes through quarter-chord point of mean aerodynamic chord $\bar{c}_w$ (See figs. 1 to 4 for limits of integration.)

$$\left[\frac{2}{S_w\bar{c}_w}\left(\cos\Lambda\int_{y'_a}^{y'_b} c_t' c'^2\ dy' - \sin\Lambda\int_{y'_a}^{y'_b} c_n' c' y'\ dy'\right) + \frac{C_{N_w}\bar{x}_w}{\bar{c}_w}\right]$$

C_l rolling-moment coefficient (based on air loads outboard of fuselage), due to single aileron deflection, about X-axis

$$\left[\frac{-1}{S_e b}\left(\cos\Lambda\int_{y'_a}^{y'_b} \Delta c_n' c' y'\ dy' + \sin\Lambda\int_{y'_a}^{y'_b} \Delta c_t'\ c'^2\ dy'\right)\right]$$

$\Delta c_n'$ change in section normal-force coefficient c_n' due to aileron deflection

$\Delta c_t'$ change in twisting-moment coefficient c_t' due to aileron deflection

ΔC_l absolute value of total rolling-moment coefficient of wing with ailerons at equal positive and negative deflections

Subscripts:

U upper surface

L lower surface

APPARATUS AND METHODS

Apparatus.— The tests were made in the Langley 8-foot high-speed tunnel, which is of the single-return, closed-throat type.

The wing-aileron model used in the wind-tunnel investigation of the effects of sweep on the characteristics of plain ailerons was the same model used in the lateral-control tests of a wing with no sweep reported in reference 3. The unswept wing had an NACA 65-210 airfoil section, an aspect ratio of 9.0, a taper ratio of 2.5:1.0, and no twist or dihedral. The ordinates of the tip of the unswept wing and the NACA 65-210 section are given in reference 3. The aileron was of the plain type with no aerodynamic nose balance. The chord of the aileron was 20 percent of the local wing chord, and the profile of the aileron was defined by straight lines tangent to the nose radius and passing to the trailing edge, resulting in a trailing-edge angle of 11.1°. (See fig. 5.) The aileron span of the unswept wing was 37.5 percent of the wing semispan with the inboard end of the aileron at the 60-percent-semispan station. Two hinges located approximately 25 percent of the aileron span from either end of the aileron supported the aileron.

Twenty static-pressure orifices in lines perpendicular to the quarter-chord line of the unswept wing were placed at each of eight stations along the wing span. The four inboard stations were placed on the left half of the wing, and the four outboard stations on the right half. The locations of the pressure stations are given in table I; stations A to E were inboard of the aileron, and stations F, G, and H were included within the aileron span.

The wing was supported in the wind tunnel by a vertical steel plate which had a modified-ellipse section of 50-inch chord and 0.75-inch maximum thickness. The surfaces of this plate formed reflection planes for the two wing semispans. Additional information about the support plate and the tunnel setup is to be found in reference 4. The various swept configurations were obtained by rotating the wing with respect to the support plate about the main fastening screw, which was perpendicular to the chord plane and intersected the chord at the center line of the wing at the 0.4-chord station. The axis of rotation is shown in figures 1 to 4. Wall-pressure measurements indicated that the flow over the model on one side of the plate had very little effect, even at the highest test Mach numbers, on the flow on the other side of the plate. A given test configuration with the wing rotated represented, therefore, not a yawed model but half of a sweptback model and half of a sweptforward model.

The wing tips, which were revised for each swept configuration, were elliptical with ordinates determined in a similar manner as those of the unswept wing. For the sweep tests a fuselage was simulated by the addition of two half bodies of revolution to the wing at the surfaces of the support plate (fig. 1). The center lines of the half bodies of revolution lay in the chord plane of the wing. Dimensions of the swept configurations are given in table II.

Procedure.– Normal-force, pitching-moment, and rolling-moment characteristics were determined from pressure-distribution measurements taken at the eight spanwise stations on the wing and are for sealed-gap aileron conditions. Hinge-moment data were obtained by electrical-strain-gage measurements. The hinge moments were measured on the left aileron, which had no pressure stations within its span. Because of the small size of the model and the high loads encountered during these tests, it was not feasible to include a seal on this aileron which did not interfere with hinge-moment measurements. The hinge-moment data are therefore for an unsealed aileron, with a gap approximately 0.003 of the wing chord c'.

The angles of attack and Mach numbers at which pressure measurements were made are given in table III. The data were obtained at Mach numbers up to a maximum of either 0.925 or 0.96, depending on model configuration. Aileron deflections of -10°, -5°, 5°, and 10° were tested with the configurations having 30° of sweepback and sweepforward, and aileron deflections of -10° and 10° were tested with the configurations having 45° of sweepback and sweepforward. Data for the swept configurations with undeflected aileron were obtained from the tests of reference 1. The angle of attack was estimated to be set to within $\pm 0.1^{\circ}$ and the aileron deflection to within $\pm 0.15^{\circ}$.

Reynolds numbers.– The variation of test Reynolds number, based on the mean aerodynamic chord of the model wing, with test Mach number for the various swept configurations is given in figure 6 together with similar data for the unswept wing. The variation of dynamic pressure with Mach number in the wind tunnel is also shown in figure 6.

Corrections.– No tunnel-wall interference corrections have been applied to the data, since the methods now available for estimating corrections at high subsonic Mach numbers are especially limited in application to swept wings. The corrections, however, would be small – the corrections to the dynamic pressure and Mach number are indicated to be less than 1 percent for the swept configurations at a Mach number of 0.925. The tunnel choked in the present tests at a Mach number of approximately 0.98. As brought out in reference 1, some tendency toward choke can be expected at a Mach number of 0.96 for the swept configurations. Under such conditions, the reliability of the data at a Mach number of 0.96 is probably impaired; the general trends shown by the data, nevertheless, are believed to be correct.

The model wing was made of brass and was relatively stiff. Since the wing contained cut-outs for instrumentation, static bending tests were made to determine the effective flexural rigidity EI (where E is the modulus of elasticity and I is the section moment of inertia about the neutral axis) of the model wing. Taking a value for the modulus of elasticity of brass of 13×10^{6} pounds per square inch, the section moment of inertia of the model wing was found to equal $c' t'_{max}{}^3/26$. The wing twisting produced by the air loads was estimated to be small for all the test conditions. The bending of a swept wing, however, introduces an effective change in angle of attack, which tends to augment the bending loads in the sweptforward case and alleviate the bending loads in the sweptback case. Some calculations were made to estimate the magnitude of the effects of bending on the aerodynamic coefficients. Using the experimental spanwise loading and the measured flexural rigidity, the spanwise change in angle of attack due to bending of the model wing was determined. Then, the spanwise loading resulting from the spanwise change in angle of attack was obtained approximately by a computation procedure based on Schrenk's method (reference 5). The results of these computations indicate that the bending effects are appreciable. For example, for the configuration with 45° of sweepforward the calculated bending effects at the maximum Mach number of 0.96 are of the order of magnitude of 10 percent of the measured values of wing normal-force coefficient and 15 percent of the measured values of rolling-moment coefficient. Since no corrections as a result of wing bending have been made to the coefficients presented in this report, the data shown, therefore, are specifically applicable to a wing with flexural characteristics similar to those of the model wing tested. For actual aircraft, which would have wing flexural rigidities probably less than the flexural rigidity of the model wing tested, the bending effects can be expected to be greater than those indicated for the model wing. Plots of the spanwise variation in section loading of the wing included in this report will be an aid in the modification of the data of this report for application to wings of different stiffnesses.

REDUCTION OF DATA AND RESULTS

In the reduction of the data, the section pressure distributions at the wing pressure stations parallel to the X'-axis were plotted, and then the plots were mechanically integrated to give section normal-force coefficient c_n' and section twisting-moment coefficient c_t'. Using the section coefficients, plots of $c_n' c' \frac{b'}{S_e}$ and $c_t' c'^2 \frac{b'^2}{S_e}$ along the Y'-axis were made and then mechanically integrated. The wing normal-force coefficient C_{N_w} and the wing pitching-moment coefficient C_{m_w} were determined, as in reference 1, from these integrations. The rolling-moment coefficient C_l, the change ΔC_{N_w} in wing normal-force coefficient resulting from aileron deflection, and the change ΔC_{m_w} in wing pitching-moment coefficient resulting from aileron deflection were also determined from these integrations together with similar integrations for the swept configurations with undeflected aileron.

The rolling-moment coefficient for the wing with the sealed aileron is shown plotted against Mach number in figure 7. The variation with Mach number of the total rolling-moment coefficient of the wing with ailerons at equal positive and negative deflections is shown in figure 8. Data for total deflections of 10° (±5°) and 20° (±10°) are shown, together with values from reference 3 for the unswept wing. The hinge-moment data of these tests are for an unsealed aileron with a gap approximately equal to 0.003c'. The general effects of compressibility on aileron hinge-moment coefficient are brought out in figure 9. The variation with Mach number of the total hinge-moment coefficient of the ailerons at equal positive and negative deflections is shown in figure 10. Included in figures 9 and 10 also are data for the unswept wing from reference 3.

The variation with Mach number of the wing normal-force coefficient C_{N_W}, the normal-force-curve slope $\Delta C_{N_W}/\Delta\alpha$, and the incremental value ΔC_{N_W} of wing normal-force coefficient resulting from aileron deflection are shown in figures 11, 12, and 13, respectively. The normal-force-curve slopes shown are the average values for an angle-of-attack range from 0° to 4°. The spanwise variations along the Y'-axis of the section loading $c_n'c'\frac{b'}{S_e}$ based on the air loads outboard of the fuselage are given in figures 14 to 17 for the various sweep angles and aileron deflections. In these tests the lines of pressure orifices were perpendicular to the Y'-axis, and the loading curves were plotted along the Y'-axis in terms of $\frac{y'}{b'/2}$. The chord c' used in the loading plots was limited by the fuselage surface for those wing sections partially covered by the fuselage. This chord was zero at the spanwise location $\frac{y'}{b'/2}$ corresponding to the intersection of the trailing edge of the wing and the fuselage surface for the sweptforward configurations and to the intersection of the leading edge of the wing and the fuselage surface for the sweptback configuration. (See figs. 1 to 4.) It is to be noted that the value of $\frac{y'}{b'/2}$ for a value of c' of zero is on the negative side of $\frac{y'}{b'/2} = 0$ for the sweptforward configurations and on the positive side of $\frac{y'}{b'/2} = 0$ for the sweptback configurations (figs. 1 to 4). The loading curves shown in this report differ, therefore, from usual load distributions in that the loading becomes zero at the inboard spanwise location $\frac{y'}{b'/2}$ where c' is zero. The loading data for an aileron deflection of 0° are from the tests of reference 1. In the present tests it was found that the loading curves at inboard stations could be satisfactorily faired from the corresponding plots for an aileron deflection of 0°, so in order to reduce the large amount of computing involved, some of the inboard pressure data were not worked up.

The effects of compressibility on the wing pitching-moment coefficient C_{m_W} and the change ΔC_{m_W} in wing pitching-moment coefficient resulting from aileron deflections are shown in figures 18 and 19, respectively.

DISCUSSION

Variables

Since the aspect ratio, wing section, taper ratio, and Reynolds number range changed in the present tests when the sweep angle was changed, the results shown do not indicate the effects of sweep alone. The effects of the changes in these other variables on most of the variations of characteristics with Mach number, however, are probably small with respect to the effects of the corresponding sweep. As mentioned previously, the data have not been corrected for wing bending so the results presented in this report apply specifically to a wing with flexural characteristics similar to those of the model wing tested.

Rolling-Moment Coefficient

The rolling-moment-coefficient curves for the configuration with 30° of sweepback generally show losses in effectiveness at high Mach numbers (fig. 7(c)). The rolling-moment data for the wing with 30° of sweepforward, however, show appreciably smaller losses in effectiveness at the same high speeds (fig. 7(b)). For sweep angles of ±45° there are smaller changes in rolling-moment coefficient with Mach number (figs. 7(a) and 7(d)) than for ±30°.

The effect of sweep on the total rolling-moment coefficient ΔC_l is illustrated in figure 8. The data for the unswept wing for angles of attack to 4° are characterized by marked losses in aileron effectiveness associated with the formation of a strong compression shock on the wing at high supercritical Mach numbers. Sweeping the wing back to 30° reduces the severity of the losses and delays the occurrence of the losses to higher Mach numbers. Sweep angles of −30° and ±45° show further improvement in aileron effectiveness characteristics at high Mach numbers. At low Mach numbers the ailerons on the wing with 30° of sweepback produce more rolling moment than on the wing with 30° of sweepforward. At high Mach numbers, however, the ailerons on the wing with 30° of sweepforward are more effective than on the wing with 30° of sweepback. The ailerons on the wing with 45° of sweepback generally produce more rolling moment than on the wing with 45° of sweepforward for most of the speed range covered by these tests. At the highest speeds the ailerons on the wing with 45° of sweepforward are more effective than on the wing with 45° of sweepback.

Hinge-Moment Characteristics

The configuration with 30° of sweepback experienced marked changes in aileron hinge-moment characteristics at high Mach numbers, but these changes were much smaller than the large, irregular changes in hinge-moment characteristics experienced by the unswept configuration (fig. 9). The changes in hinge-moment characteristics with variation in Mach number were appreciably less for the configuration with 30° of sweepforward than for the configuration with 30° of sweepback. The compressibility effects on the hinge-moment coefficients for the configurations with ±45° of sweep were small.

Sweeping the wings, as would be expected, also reduces the variation with Mach number of the total aileron hinge-moment coefficient as experienced by the unswept configuration (fig. 10). In these tests 30° of sweepforward generally resulted in higher total hinge-moment coefficients than 30° of sweepback, whereas 45° of sweepforward gave lower values than 45° of sweepback.

Normal-Force Characteristics

The effects of compressibility on the wing normal-force coefficient of the swept configurations with aileron deflected are, in general, approximately the same as the effects observed for the swept configurations with undeflected aileron (figs. 11(a) to 11(d)). Compressibility effects on normal-force-curve slope $\Delta C_{N_W}/\Delta\alpha$ for the wings with -45°, 30°, and 45° of sweep, and with the aileron deflected, are essentially the same as noted for the corresponding swept configurations with undeflected aileron (fig. 12). The slopes for the configuration with 30° of sweepforward become less with increase in aileron deflection at high Mach numbers. This trend is also generally true but to a lesser extent for the configuration with 30° of sweepback. The variations with Mach number of the incremental wing normal-force coefficient ΔC_{N_W} resulting from aileron deflection are quite small, for the most part, for all the swept configurations (fig. 13) and are seen to be very similar to the variations with Mach number of the rolling-moment coefficient (fig. 7). The greatest changes in ΔC_{N_W} with Mach number are to be noted for the configuration with 30° of sweepback and these changes are small in magnitude.

The irregular load distributions and large changes in angle of zero normal force observed for the unswept wing at Mach numbers above 0.83 (reference 3) were notably improved by 30° and 45° of sweepforward and sweepback (figs. 14 to 17). The load distributions for the swept wings are quite similar throughout the Mach number range of the tests. Of the sweep angles investigated, the loading curves for 30° of sweepback were affected most by Mach number variation.

Pitching-Moment Characteristics

The wing pitching-moment coefficient about the quarter-chord point of the mean aerodynamic chord shows considerable variation with Mach number for all the sweep angles tested (fig. 18). The effects of compressibility on the incremental wing pitching-moment coefficient ΔC_{m_w} resulting from aileron deflection are also large and quite irregular (fig. 19).

CONCLUDING REMARKS

A three-dimensional wind-tunnel investigation was made of plain ailerons on a wing with 30° and 45° of sweepback and sweepforward at Mach numbers from 0.60 to 0.96. The results presented in this report, specifically applying to a wing with flexural characteristics similar to those of the model wing tested, indicated the following:

1. Wing configurations with 30° of sweepback and sweepforward generally reduced the severity of the large changes in rolling-moment and aileron hinge-moment coefficients experienced by the unswept wing configuration as a result of compression shock and extended to higher Mach numbers the speeds at which such changes occurred. The use of 45° of sweepback and sweepforward resulted in rolling-moment and hinge-moment coefficients which, for the Mach numbers covered by these tests, did not materially change with speed.

2. At low Mach numbers the configuration with 30° of sweepback developed more rolling moment than the configuration with 30° of sweepforward; at high Mach numbers, however, 30° of sweepforward was more effective. The configuration with 45° of sweepback generally developed more rolling moment than the configuration with 45° of sweepforward for most of the speed range covered by these tests; at the highest speeds 45° of sweepforward was more effective.

3. The configuration with 30° of sweepback generally had smaller aileron hinge moments than the configuration with 30° of sweepforward. The configuration with 45° of sweepforward, however, gave smaller hinge moments than the configuration with 45° of sweepback.

4. The changes with Mach number in the wing pitching-moment coefficient of the swept configurations were large.

Langley Memorial Aeronautical Laboratory
National Advisory Committee for Aeronautics
Langley Field, Va.

REFERENCES

1. Whitcomb, Richard T.: An Investigation of the Effects of Sweep on the Characteristics of a High-Aspect-Ratio Wing in the Langley 8-Foot High-Speed Tunnel. NACA RM No. L6J01a, 1946.

2. Letko, William, and Goodman, Alex: Preliminary Wind-Tunnel Investigation at Low Speed of Stability and Control Characteristics of Swept-Back Wings. NACA TN No. 1046, 1946.

3. Luoma, Arvo A.: An Investigation of a High-Aspect-Ratio Wing Having 0.20-Chord Plain Ailerons in the Langley 8-Foot High-Speed Tunnel. NACA RM No. L6H28d, 1946.

4. Whitcomb, Richard T.: Investigation of the Characteristics of a High-Aspect-Ratio Wing in the Langley 8-Foot High-Speed Tunnel. NACA RM No. L6H28a, 1946.

5. Schrenk, O.: A Simple Approximation Method for Obtaining the Spanwise Lift Distribution. NACA TM No. 948, 1940.

[redacted]

TABLE I

LOCATIONS OF PRESSURE ORIFICE STATIONS FROM ORIGIN O ALONG

Y'-AXIS IN PERCENT OF SWEPT SEMISPAN b'/2

Station \ Λ_r	-45°	-30°	30°	45°
A	5.2	7.6	12.7	14.4
B	14.0	16.3	21.3	22.9
C	23.7	26.0	30.9	32.4
D	36.4	38.6	43.4	44.7
E	49.1	51.1	55.8	57.0
F	56.9	58.9	63.5	64.7
G	72.5	74.4	78.8	79.8
H	87.1	88.9	93.2	94.0

NATIONAL ADVISORY
COMMITTEE FOR AERONAUTICS

[redacted]

[redacted]

TABLE II

MODEL DIMENSIONS

Symbol \ Λ_r	-45°	-30°	30°	45°
b, in.	27.4	33.8	34.2	28.2
$b'/2$, in.	19.4	19.5	19.7	19.9
c_r, in.	9.03	7.23	6.64	7.97
c_g, in.	3.33	2.66	2.53	3.07
c_r/c_g	2.70	2.72	2.63	2.60
S_e, sq in.	169.2	167.4	157.0	155.6
S_w, sq in.	137.0	141.2	133.0	127.0
A	4.4	6.8	7.4	5.1
$\bar{c}_w$, in.	6.10	4.99	4.62	5.45
$\frac{y'_i}{b'/2}$	0.529	0.550	0.596	0.609
$\frac{y'_o}{b'/2}$	0.895	0.913	0.956	0.963

NATIONAL ADVISORY
COMMITTEE FOR AERONAUTICS

[redacted]

TABLE III

[redacted]

ANGLES OF ATTACK (DEG) AND MACH NUMBERS AT WHICH PRESSURE DATA WERE OBTAINED

M \ δ_a	-10°	10°	-10°	10°
	$\Lambda_r = -45^\circ$		$\Lambda_r = 45^\circ$	
0.60	-2, 2, 7	2, 7, 10	-2, 2, 7, 10	2, 7, 10
.80	-2, 2, 7, 10	-2, 2, 7, 10	-2, 2, 7, 10	-2, 2, 7, 10
.89	-2, 2, 7	-2, 2, 7	-2, 2, 7	-2, 2, 7
.925	-2, 2, 7	-2, 2, 7	-2, 2, 7	-2, 2, 7
.96	-2, 2, 7	-2, 2, 7	-2, 2	-2, 2, 7
M \ δ_a	**-10°**	**-5°**	**5°**	**10°**
	$\Lambda_r = -30^\circ$			
0.60	-2, 0, 2, 4, 7, 10	-2, 0, 2, 4, 7, 10	-2, 0, 2, 4, 7, 10	-2, 0, 2, 4, 7, 10
.80	-2, 0, 2, 4, 7	-2, 0, 2, 4, 7	-2, 0, 2, 4, 7	-2, 0, 2, 4, 7
.85	-2, 0, 2, 4, 7	-2, 0, 2, 4, 7	-2, 0, 2, 4, 7	-2, 0, 2, 4, 7
.89	-2, 0, 2, 4, 7	-2, 0, 2, 4, 7	-2, 0, 2, 4, 7	-2, 0, 2, 4, 7
.925	0, 2, 4, 7	0, 2, 4, 7	0, 2, 4, 7	0, 2, 4, 7
.96	0, 2, 4, 7		- - - -	- - - -
	$\Lambda_r = 30^\circ$			
0.60	0, 2, 4, 7, 10	-2, 0, 2, 4, 7, 10	-2, 0, 2, 4, 7, 10	-2, 0, 2, 4, 7, 10
.80	-2, 0, 2, 4, 7	-2, 0, 2, 4, 7	-2, 0, 2, 4, 7	-2, 0, 2, 4, 7
.85	-2, 0, 2, 4, 7	-2, 0, 2, 4, 7	-2, 0, 2, 4, 7	-2, 0, 2, 4, 7
.89	-2, 0, 2, 4, 7	-2, 0, 2, 4, 7	-2, 0, 2, 4, 7	-2, 0, 2, 4, 7
.925	0, 2, 4, 7	0, 2, 4, 7	0, 2, 4, 7	0, 2, 4, 7
.96	0, 2, 4, 7		- - - -	- - - -

[redacted]

NACA

[redacted]

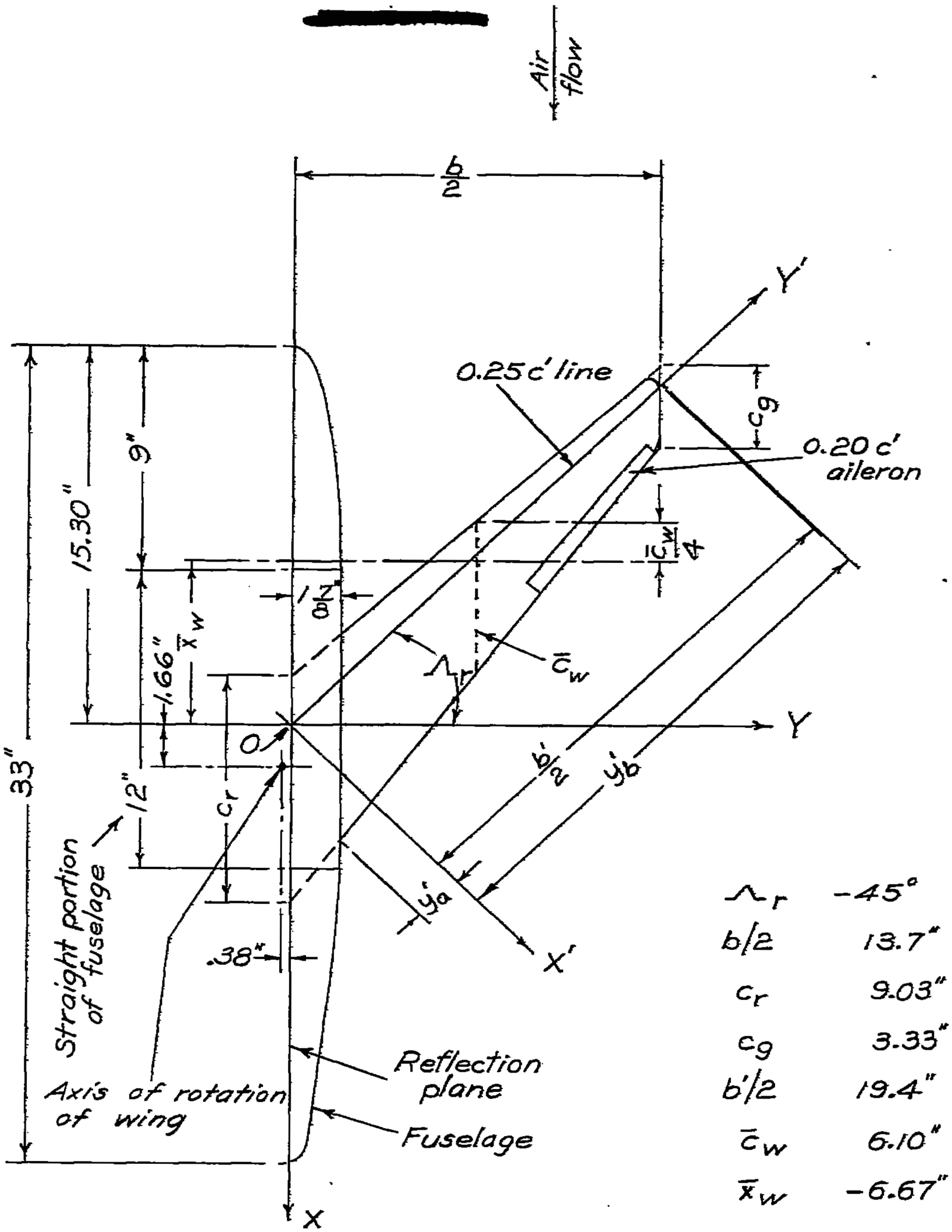

NATIONAL ADVISORY COMMITTEE FOR AERONAUTICS

Figure 1.– Plan form and general dimensions of model wing-fuselage configuration with 45° sweepforward.

[redacted]

[redacted]

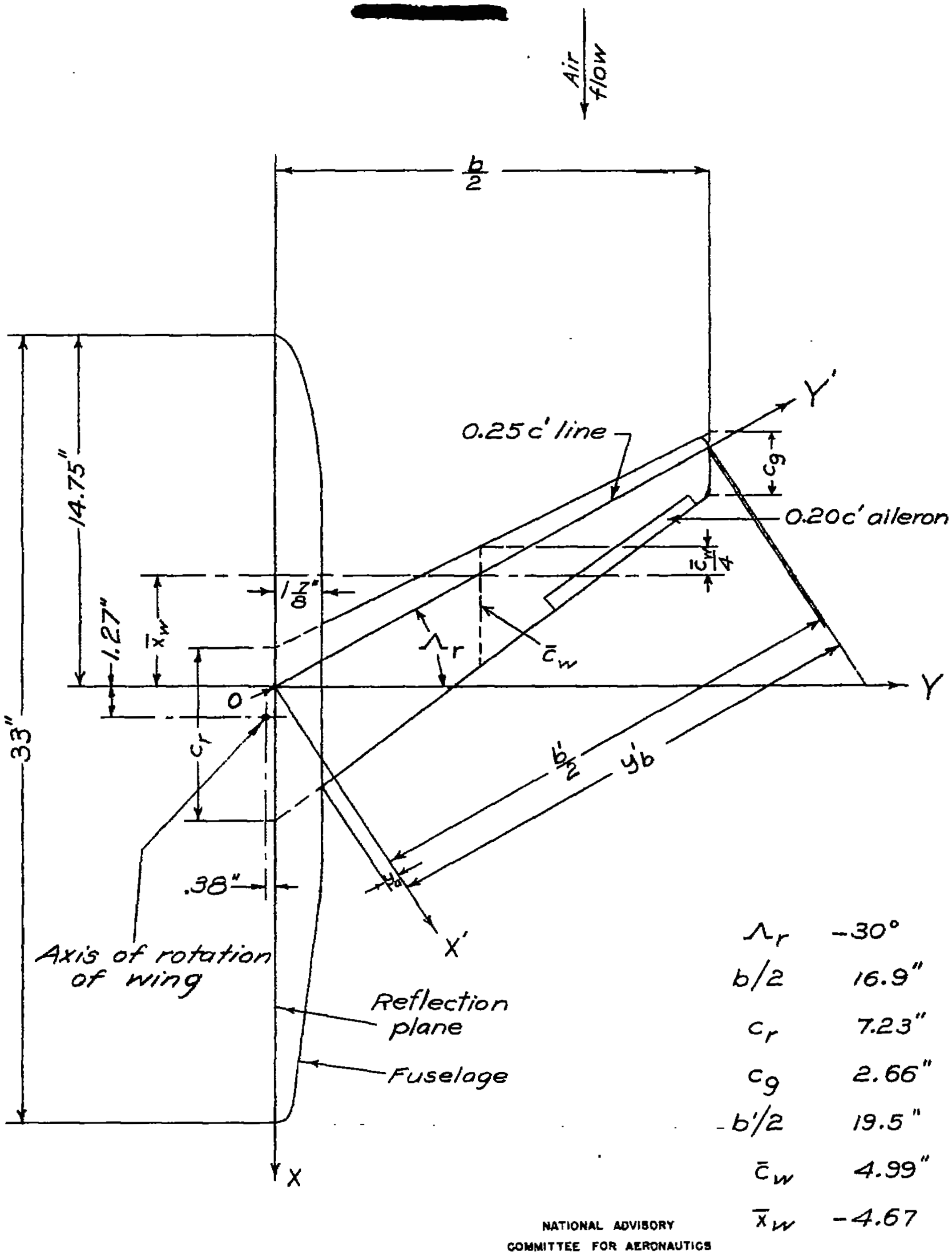

Figure 2.- Plan form and general dimensions of model wing-fuselage configuration with 30° sweepforward.

[redacted]

[redacted]

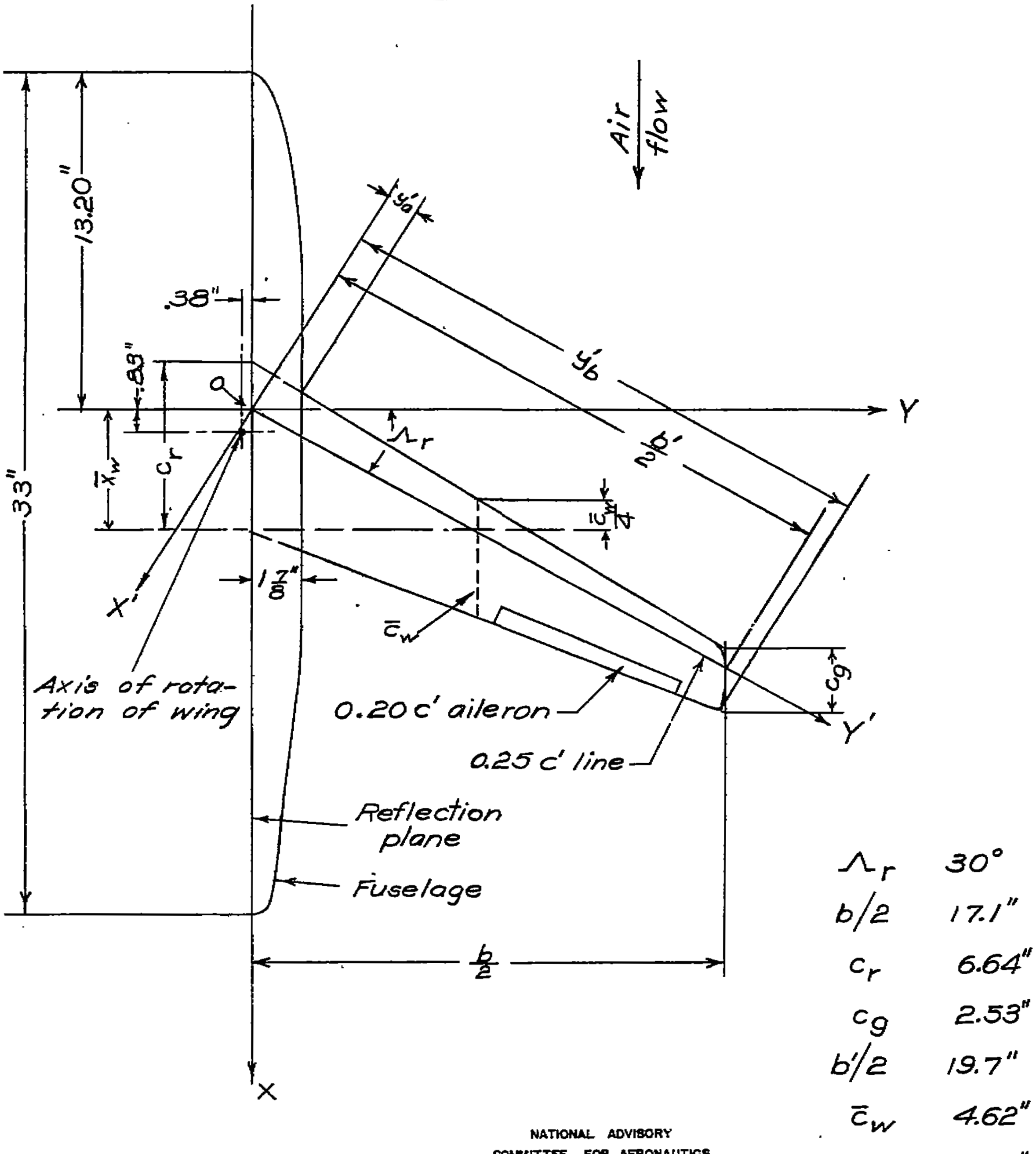

[redacted]

Figure 3.— Plan form and general dimensions of model wing-fuselage configuration with 30° sweepback.

[redacted]

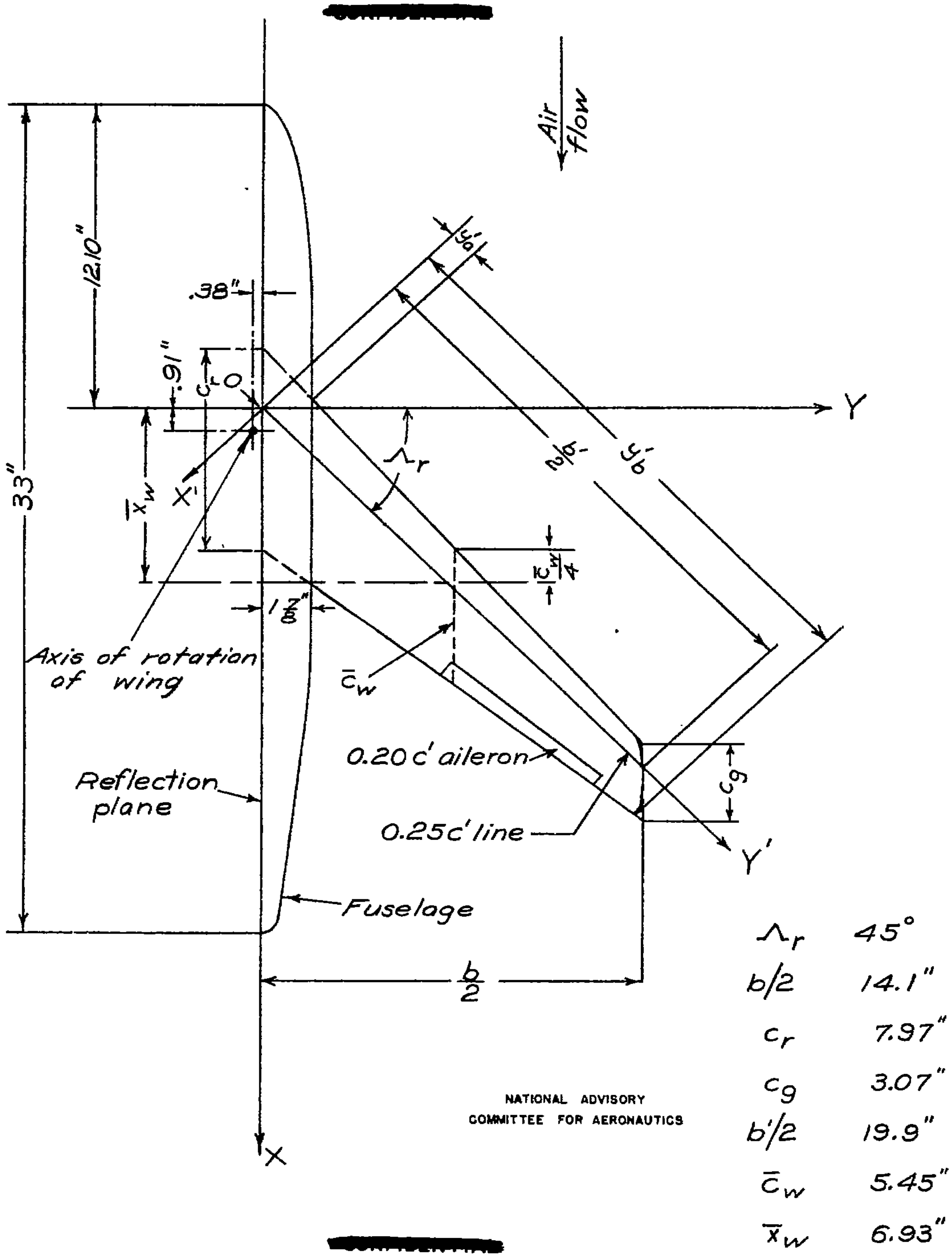

[redacted]

Figure 4.– Plan form and general dimensions of model wing-fuselage configuration with 45° sweepback.

[redacted]

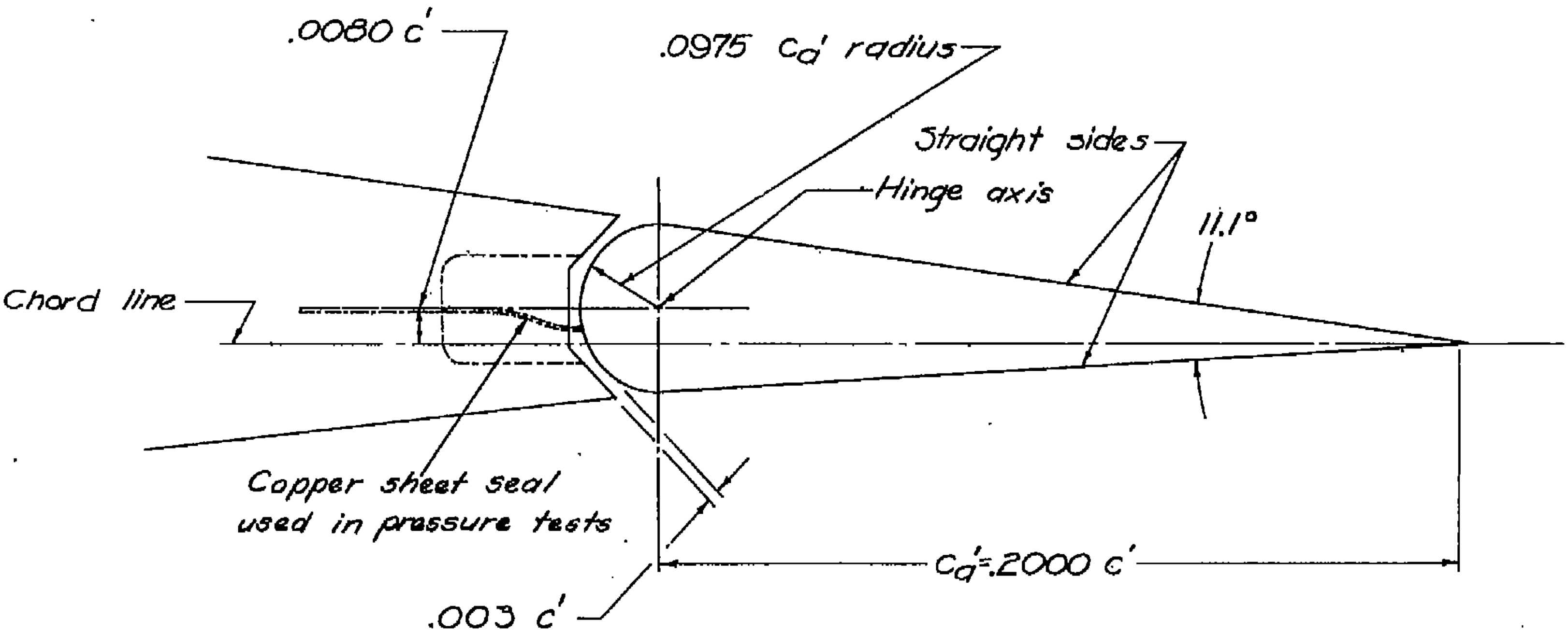

NATIONAL ADVISORY
COMMITTEE FOR AERONAUTICS

Figure 5.- Dimensions of constant-percentage-chord ailerons used on NACA 65-210 wing

[redacted]

[redacted]

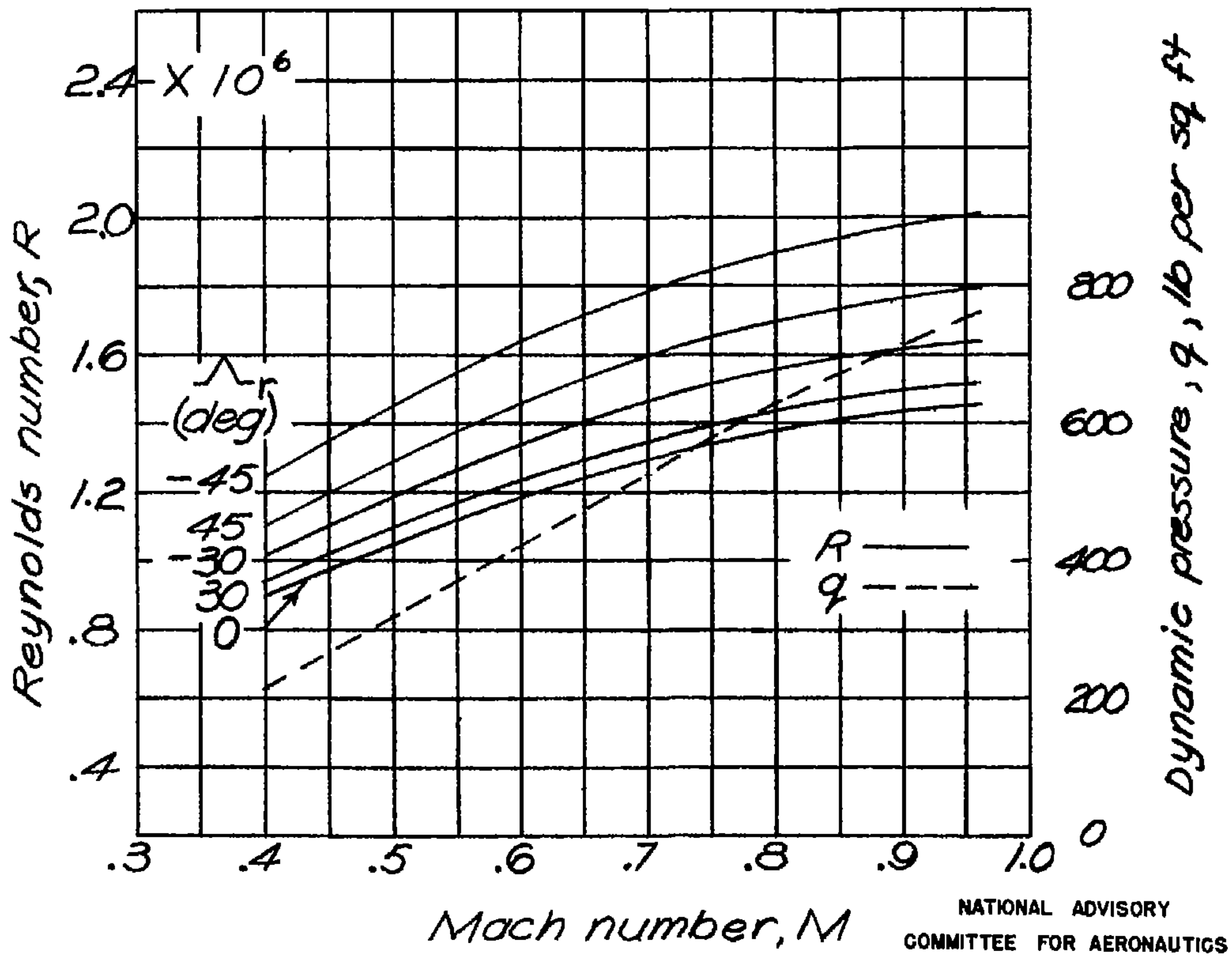

Figure 6.- Variation of Reynolds number and dynamic pressure with Mach number in the wind tunnel.

[redacted]

[redacted]

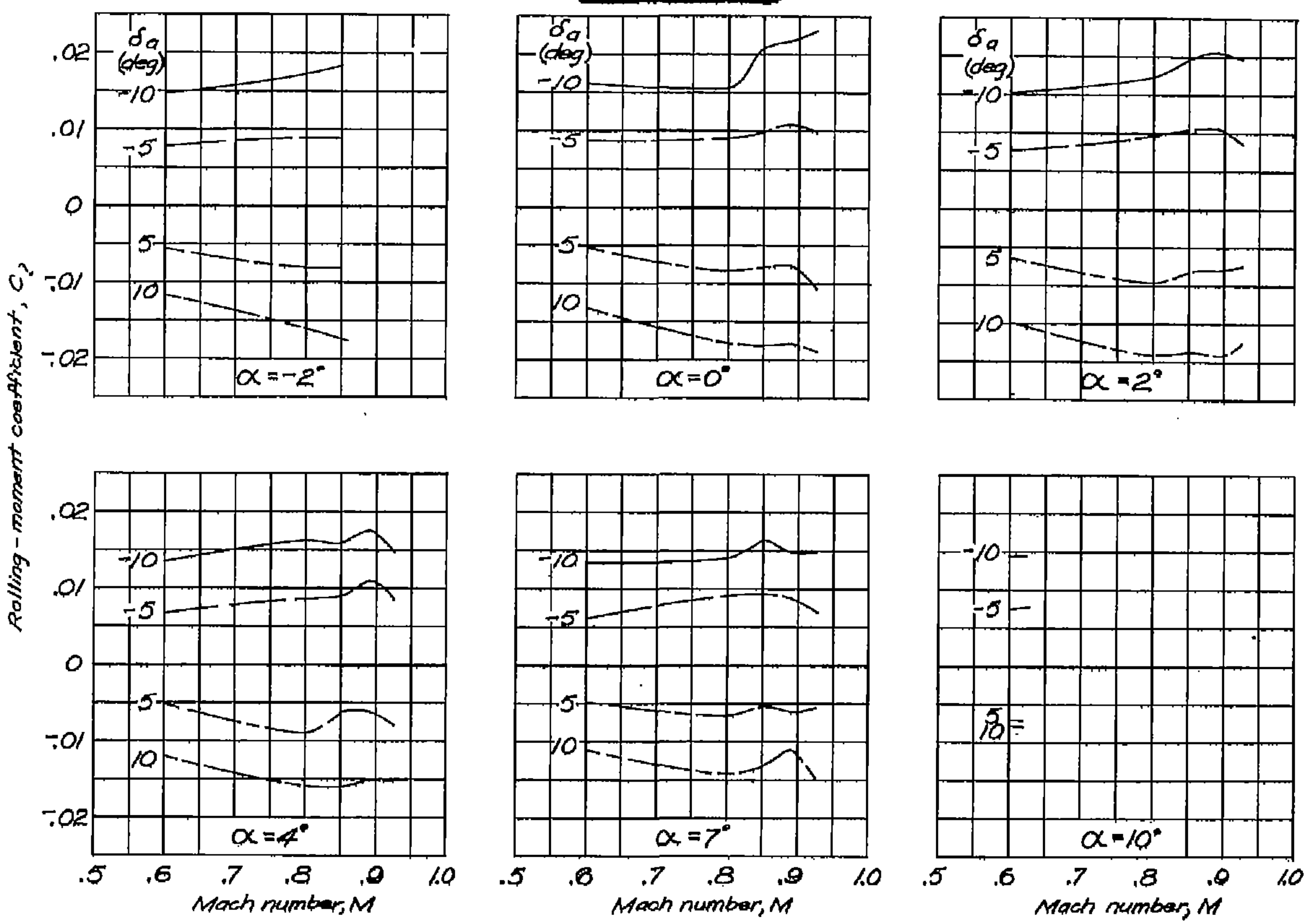

(b) $\Lambda_r = -30°$.

Figure 7.—Continued.

[redacted]

[redacted]

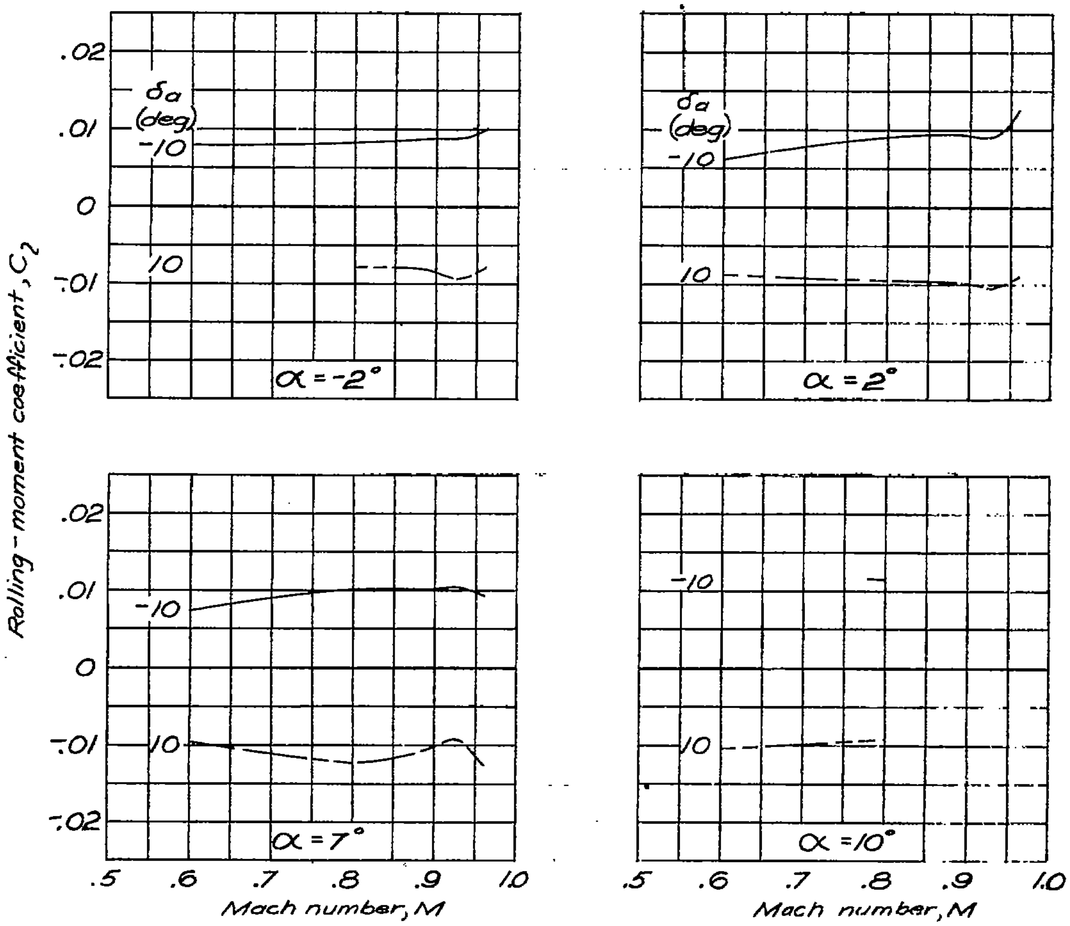

(a) $\Lambda_r = -45°$.

NATIONAL ADVISORY COMMITTEE FOR AERONAUTICS

Figure 7.— Variation of rolling-moment coefficient with Mach number. Wing with right aileron deflected; sealed aileron.

[redacted]

[redacted]

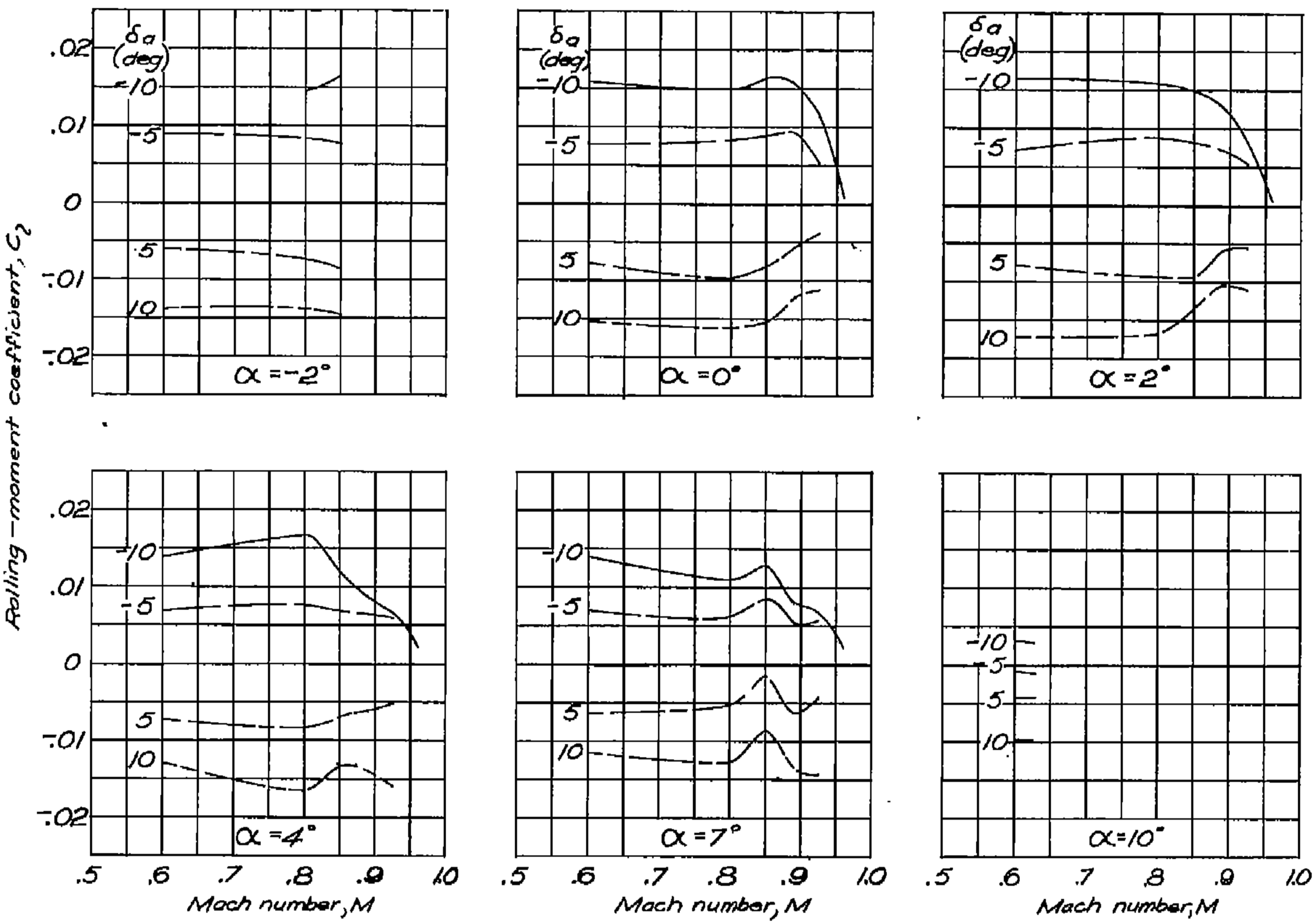

(c) $\Lambda_r = 30°$.

Figure 7.—Continued.

NATIONAL ADVISORY
COMMITTEE FOR AERONAUTICS

[redacted]

[redacted]

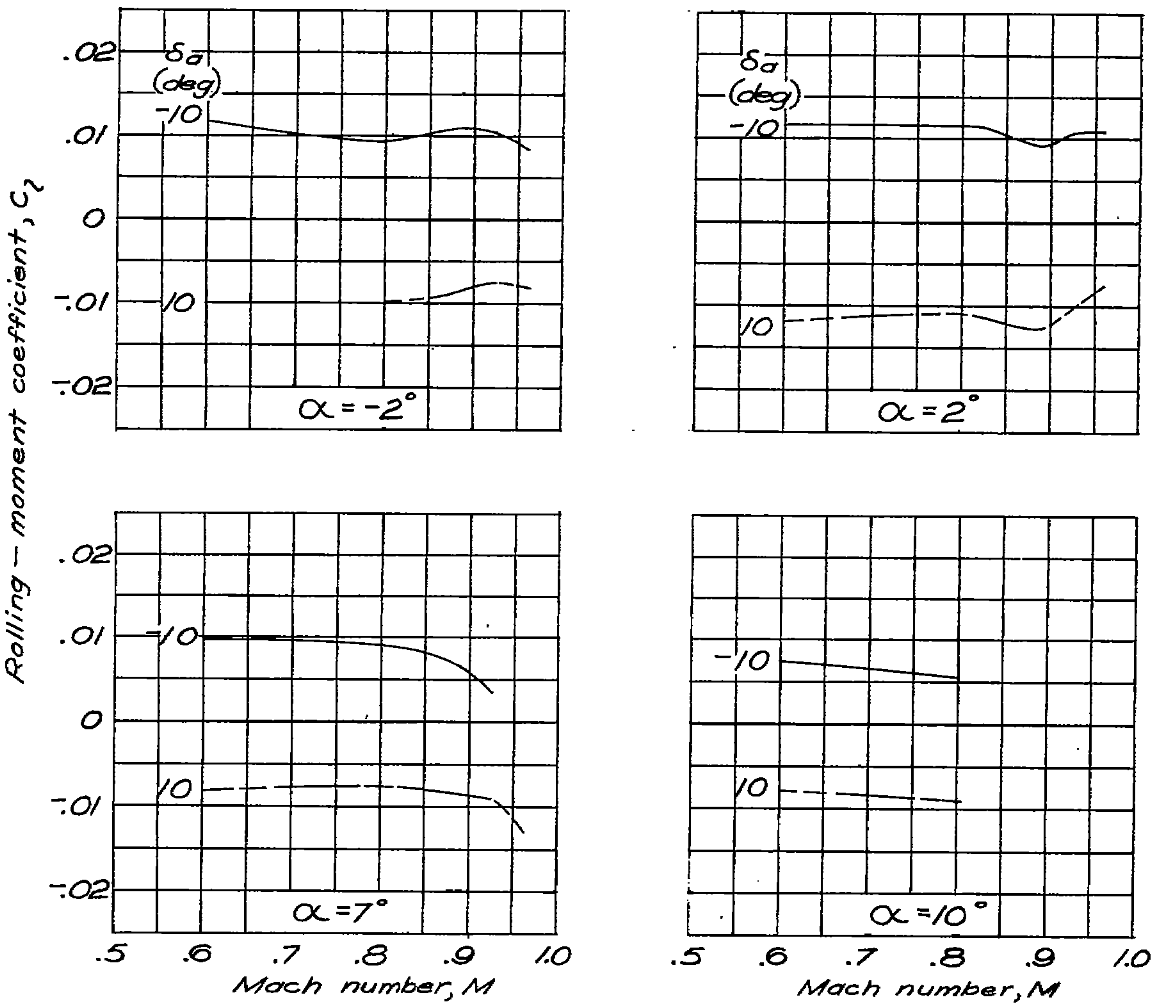

(d) $\Lambda_r = 45°$.

Figure 7.—Concluded.

NATIONAL ADVISORY COMMITTEE FOR AERONAUTICS

[redacted]

[redacted]

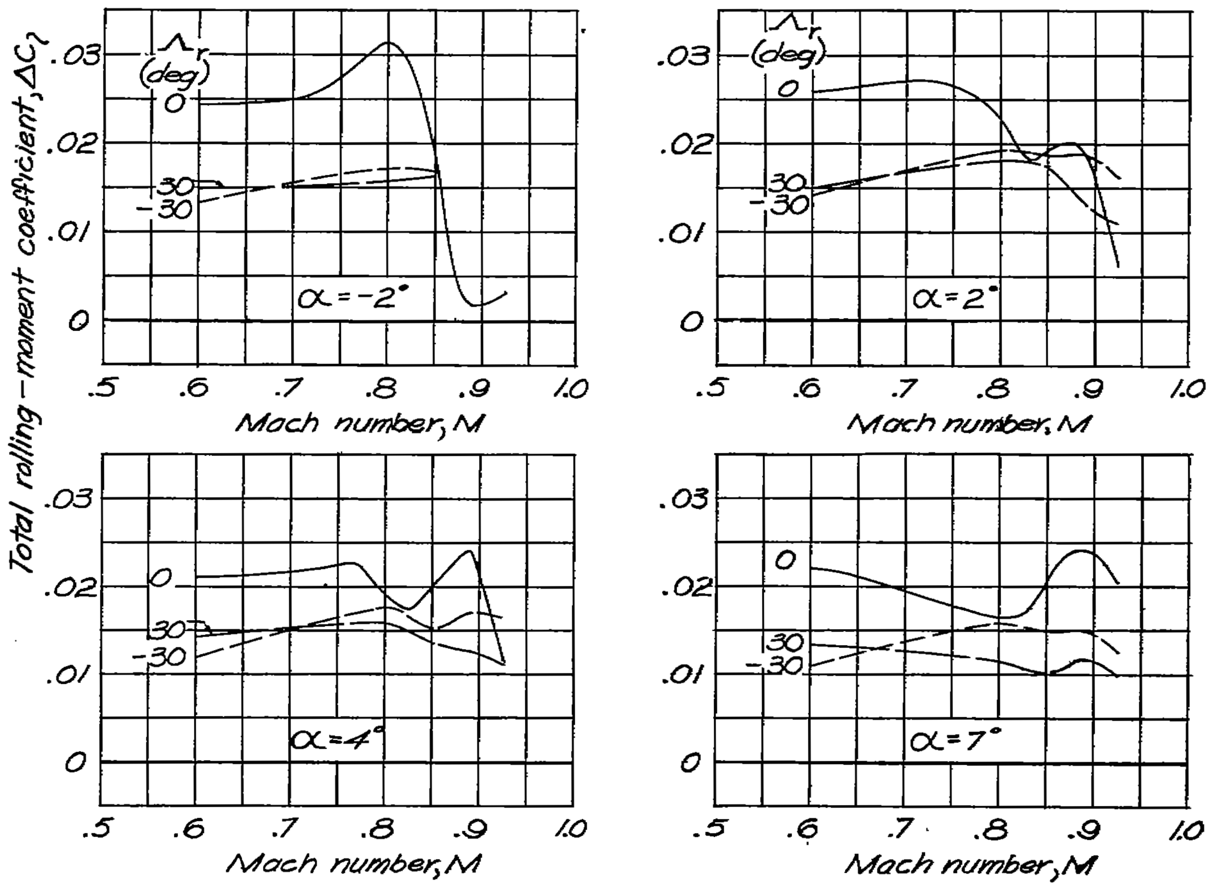

(a) $\Delta\delta_a = 10°$

Figure 8.— Variation of total rolling-moment coefficient with Mach number. Wing with ailerons at equal positive and negative deflections. Data for $\Lambda_r = 0°$ from reference 3.

NATIONAL ADVISORY COMMITTEE FOR AERONAUTICS

[redacted]

[redacted]

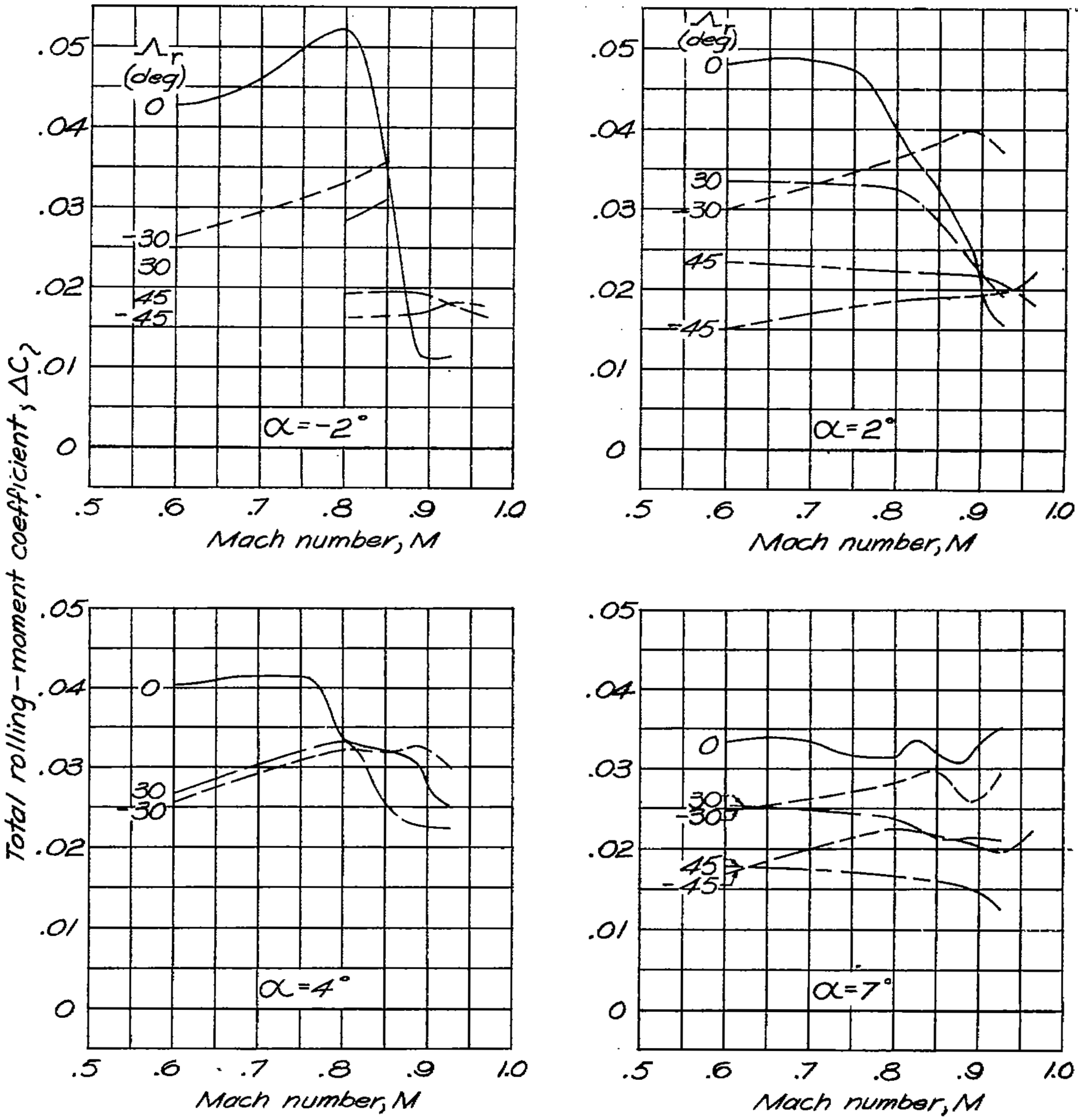

(b) $\Delta\delta_a = 20^\circ$.

Figure 8.—Concluded.

NATIONAL ADVISORY COMMITTEE FOR AERONAUTICS

[redacted]

[redacted]

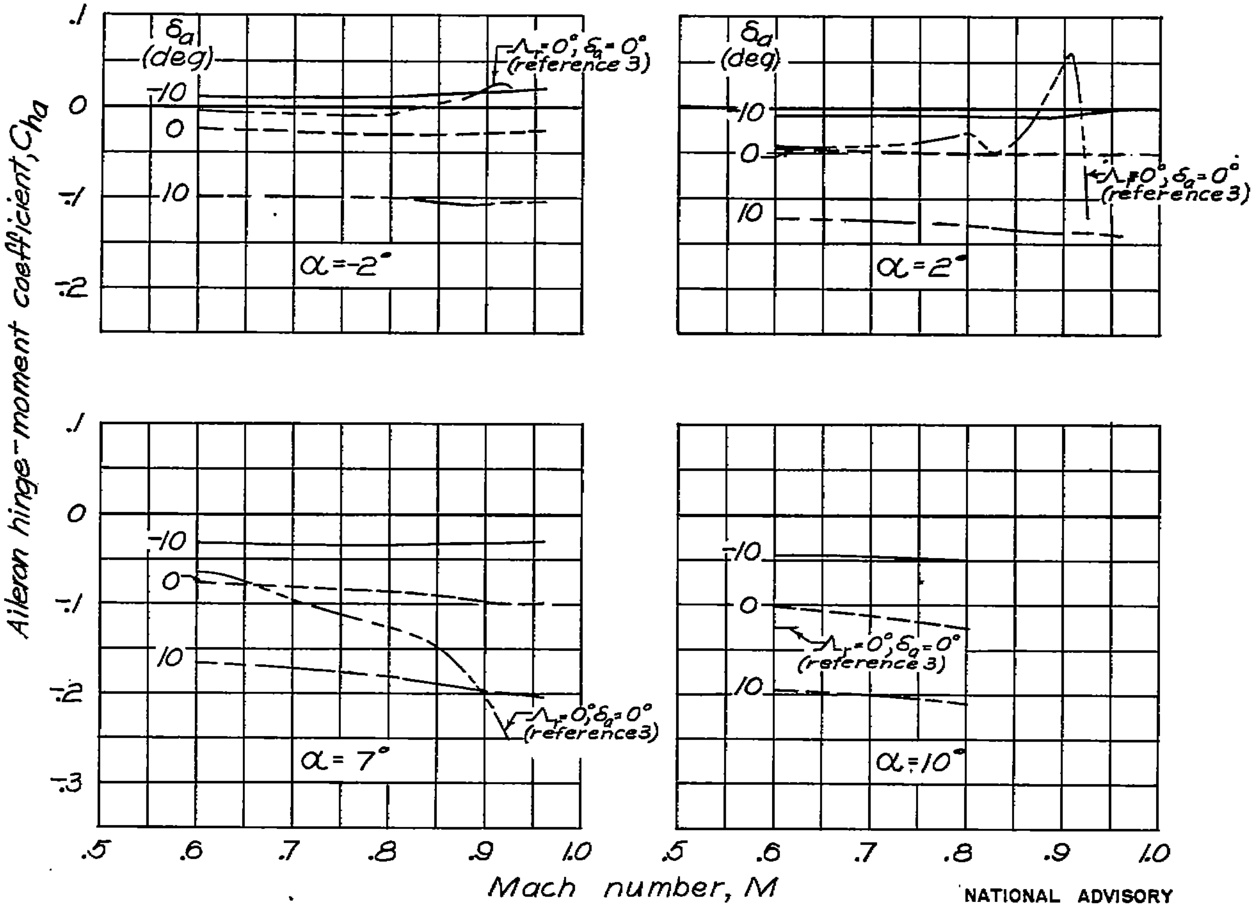

(a) $\Lambda_r = -45°$.

Figure 9.— Variation of aileron hinge-moment coefficient with Mach number. Unsealed aileron. Data for $\Lambda_r = 0°$; $\delta_a = 0°$ from reference 3.

[redacted]

[redacted]

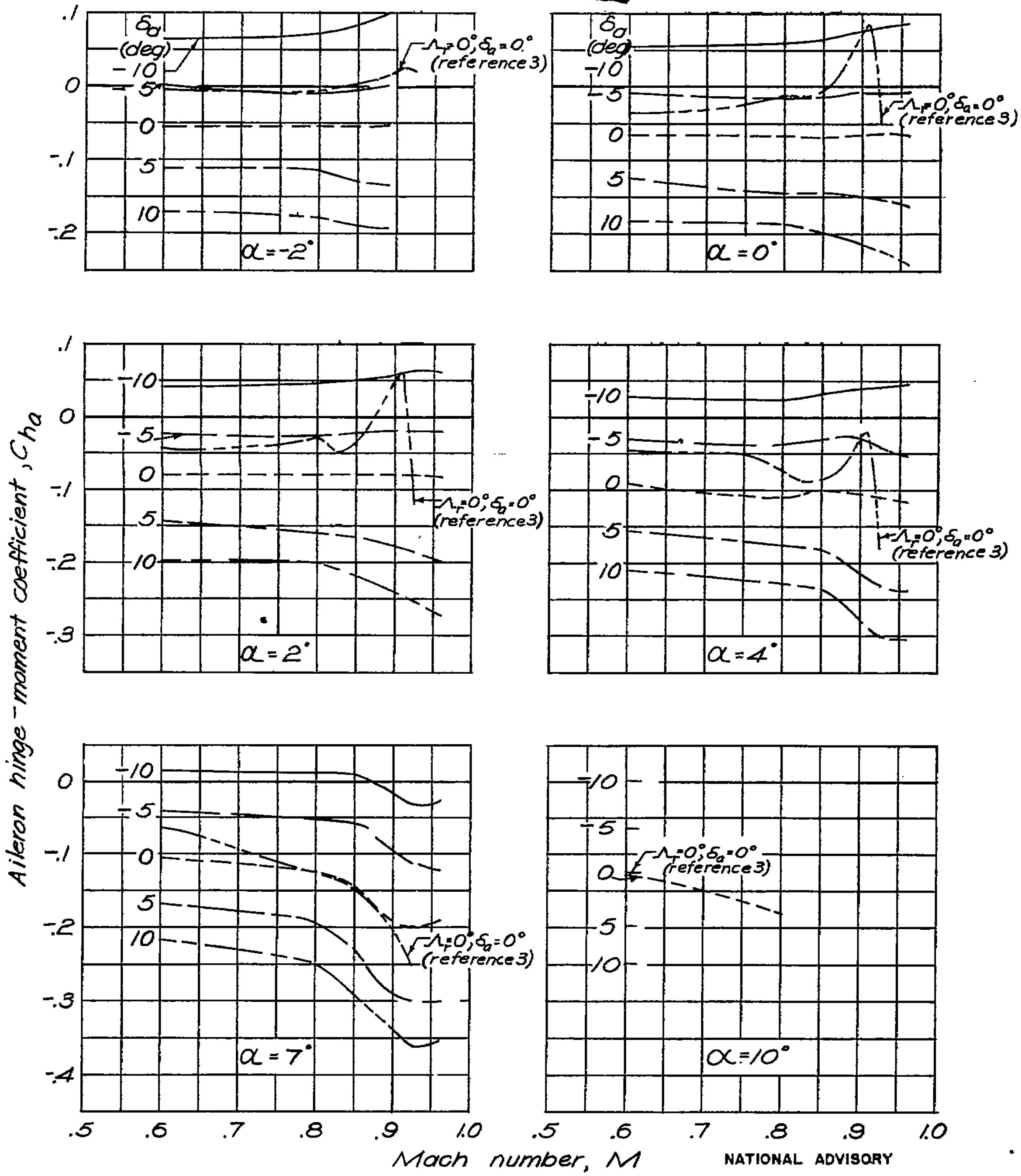

NATIONAL ADVISORY COMMITTEE FOR AERONAUTICS

(b) $\Lambda_r = -30°$.

Figure 9.—Continued.

[redacted]

[redacted]

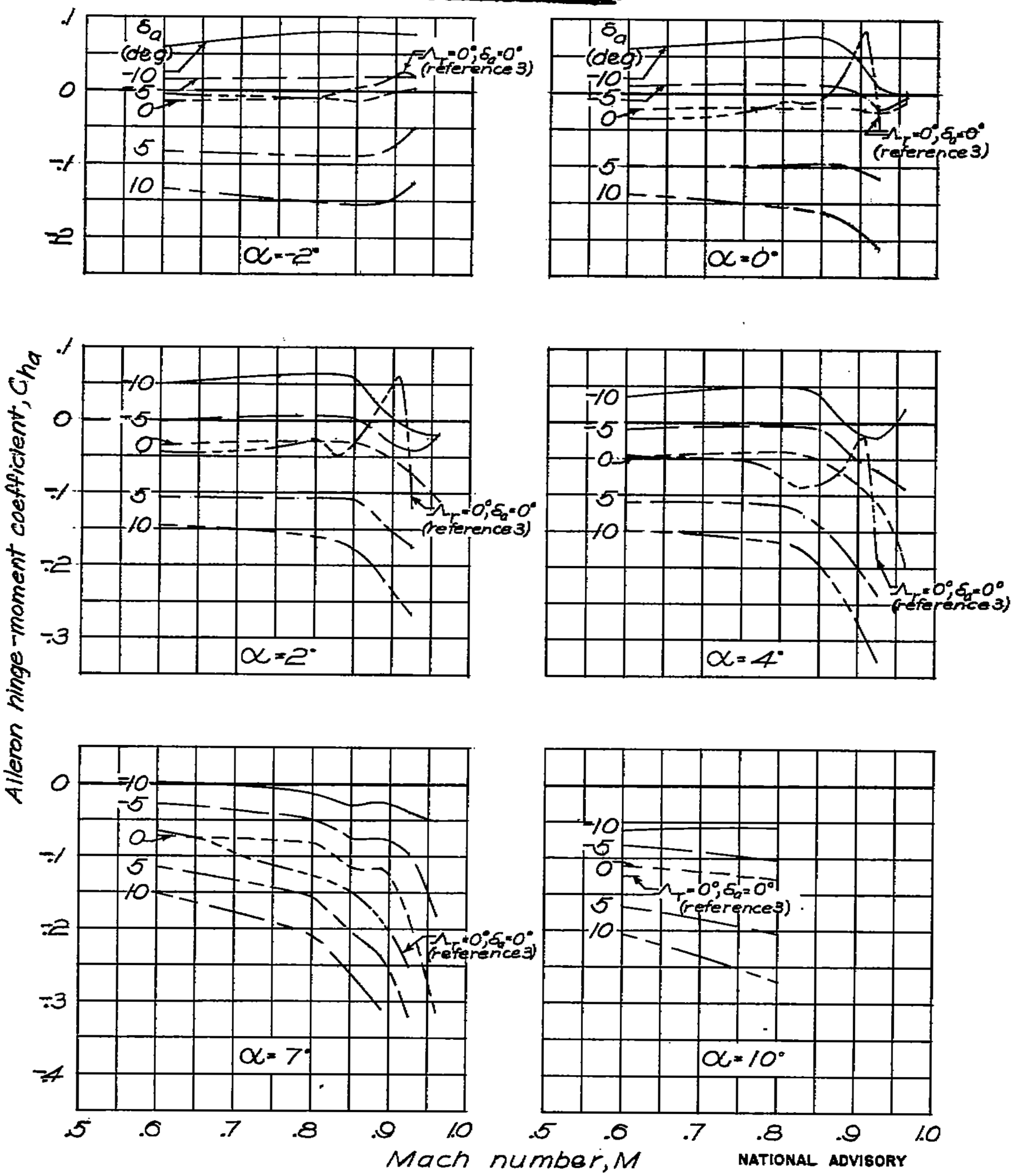

NATIONAL ADVISORY COMMITTEE FOR AERONAUTICS

(c) $\Lambda_r = 30°$.

Figure 9.- Continued.

[redacted]

[redacted]

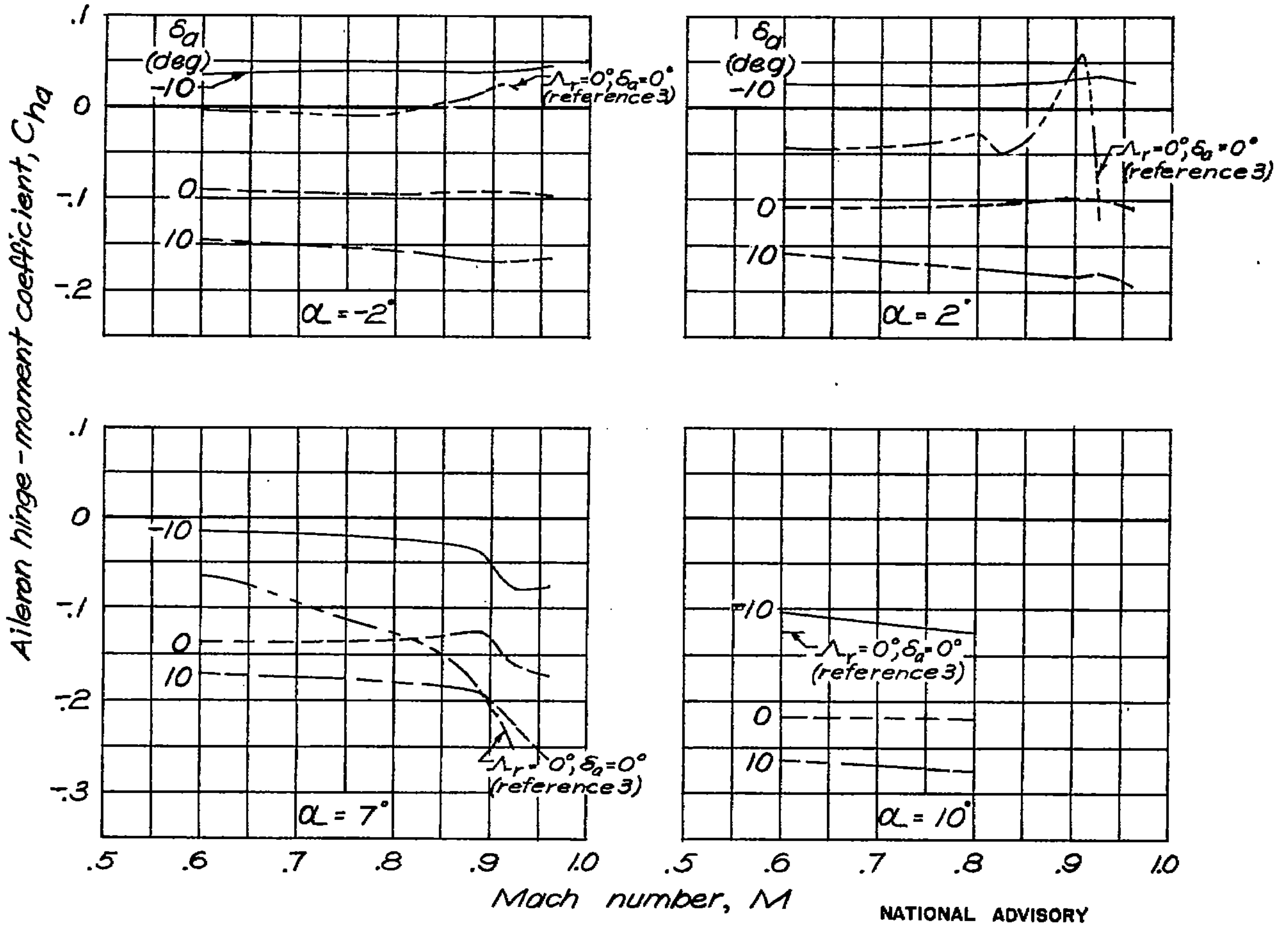

(d) $\Lambda_r = 45°$.

NATIONAL ADVISORY COMMITTEE FOR AERONAUTICS

Figure 9.—Concluded.

[redacted]

[redacted]

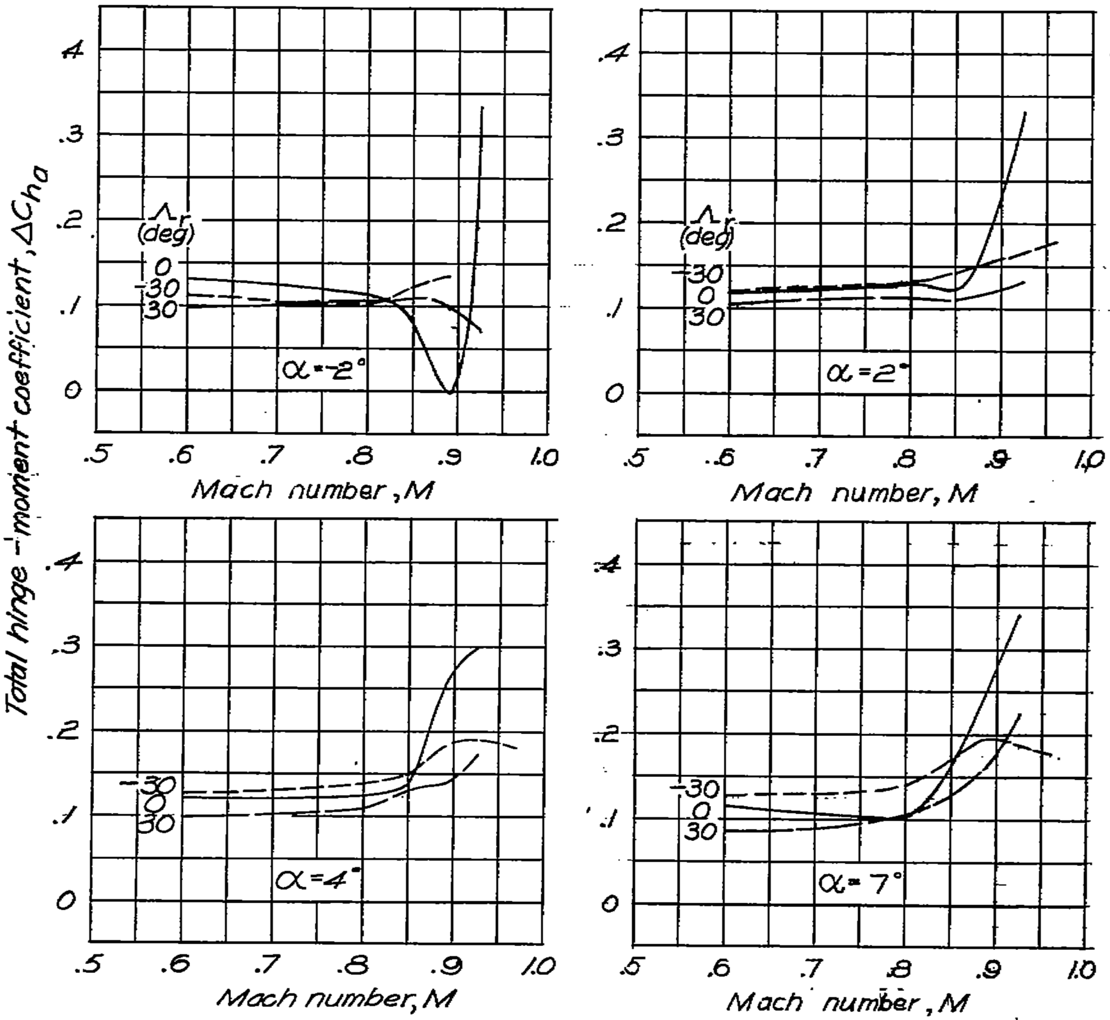

(a) $\Delta\delta_a = 10°$

NATIONAL ADVISORY
COMMITTEE FOR AERONAUTICS

Figure 10.— Variation of total hinge-moment coefficient with Mach number. Ailerons at equal positive and negative deflections; unsealed aileron. Data for $\Lambda_r = 0°$ from reference 3.

[redacted]

[redacted]

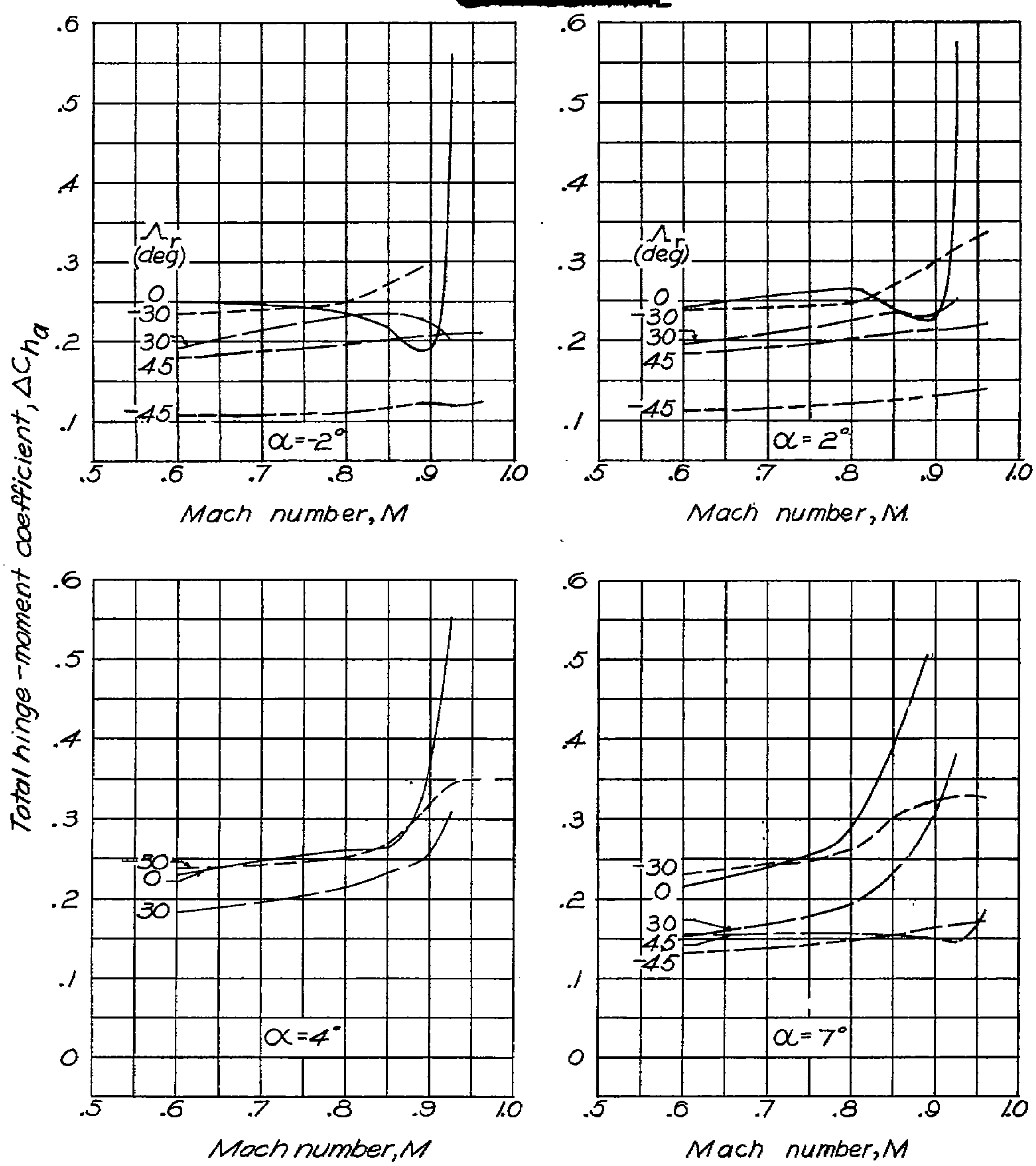

(b) $\Delta\delta_a = 20°$

Figure 10.—Concluded.

NATIONAL ADVISORY COMMITTEE FOR AERONAUTICS

[redacted]

[redacted]

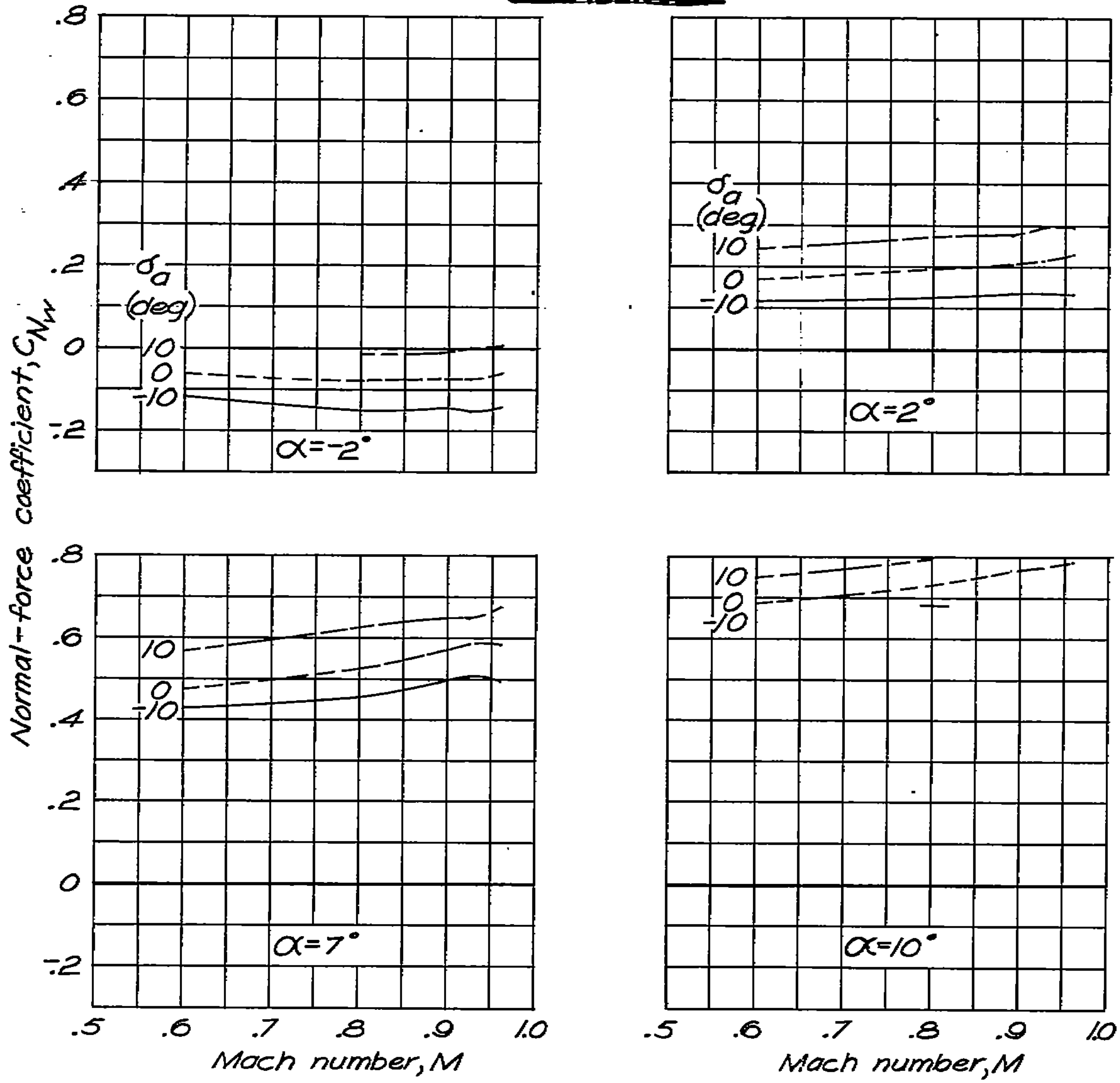

(a) $\Lambda_r = -45°$.

NATIONAL ADVISORY COMMITTEE FOR AERONAUTICS

Figure 11.— Variation of wing normal-force coefficient with Mach number. Data for $\delta_a = 0$ from reference 1.

[redacted]

[redacted]

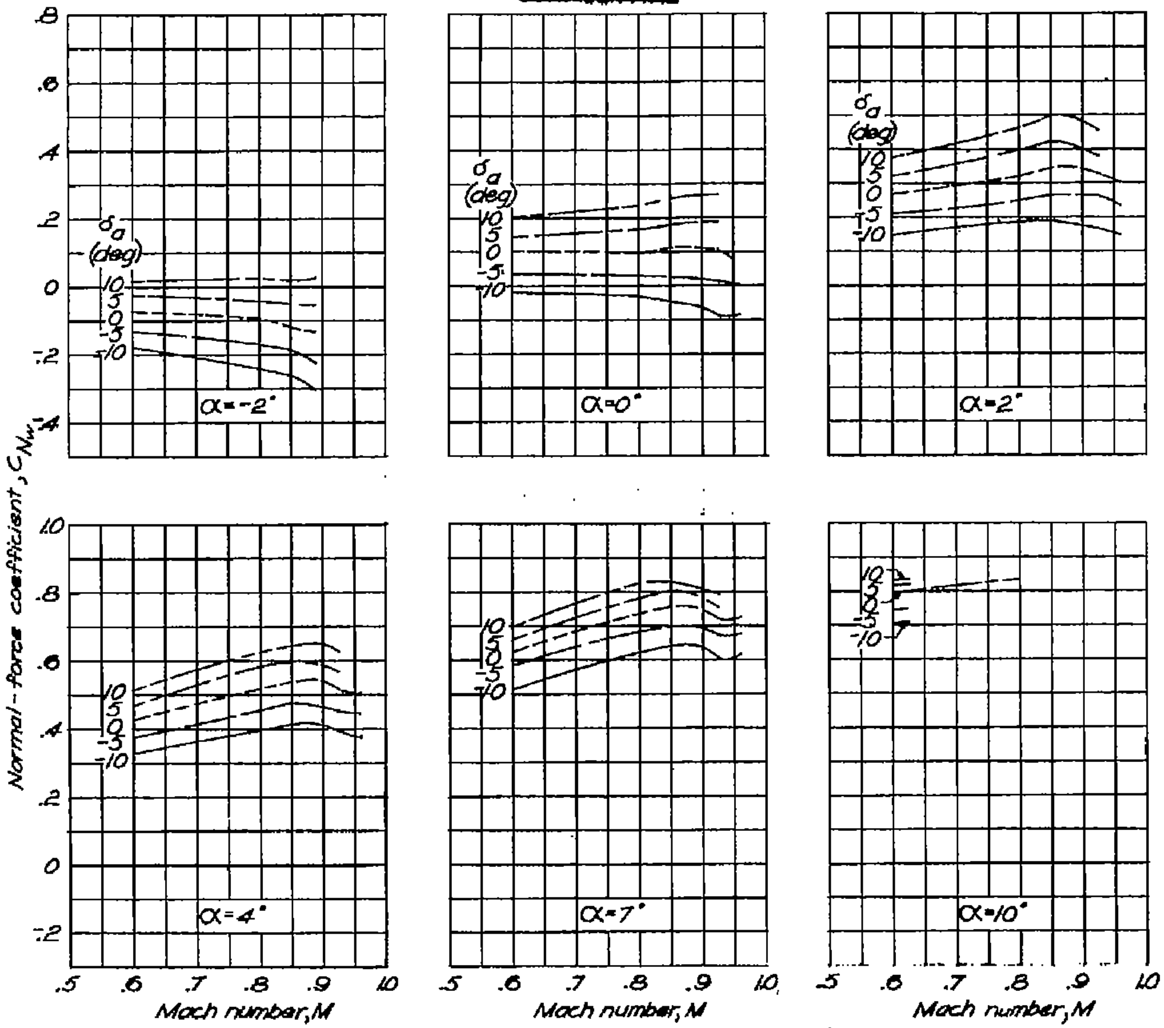

(b) $\Lambda_r = -30°$.

NATIONAL ADVISORY COMMITTEE FOR AERONAUTICS

Figure 11.- Continued.

[redacted]

[redacted]

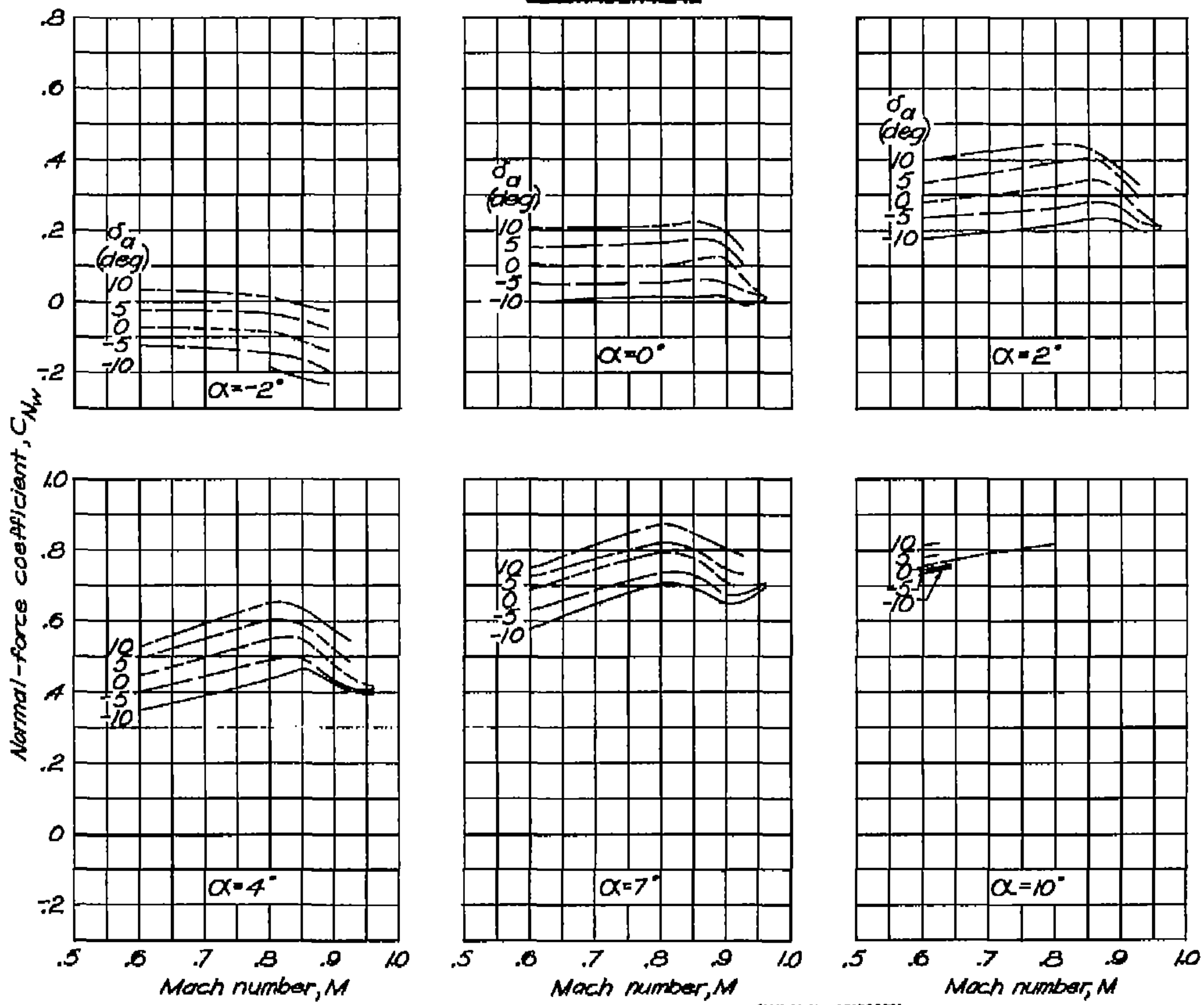

(c) $\Lambda_r = 30°$.

NATIONAL ADVISORY COMMITTEE FOR AERONAUTICS

Figure 11.— Continued.

[redacted]

[redacted]

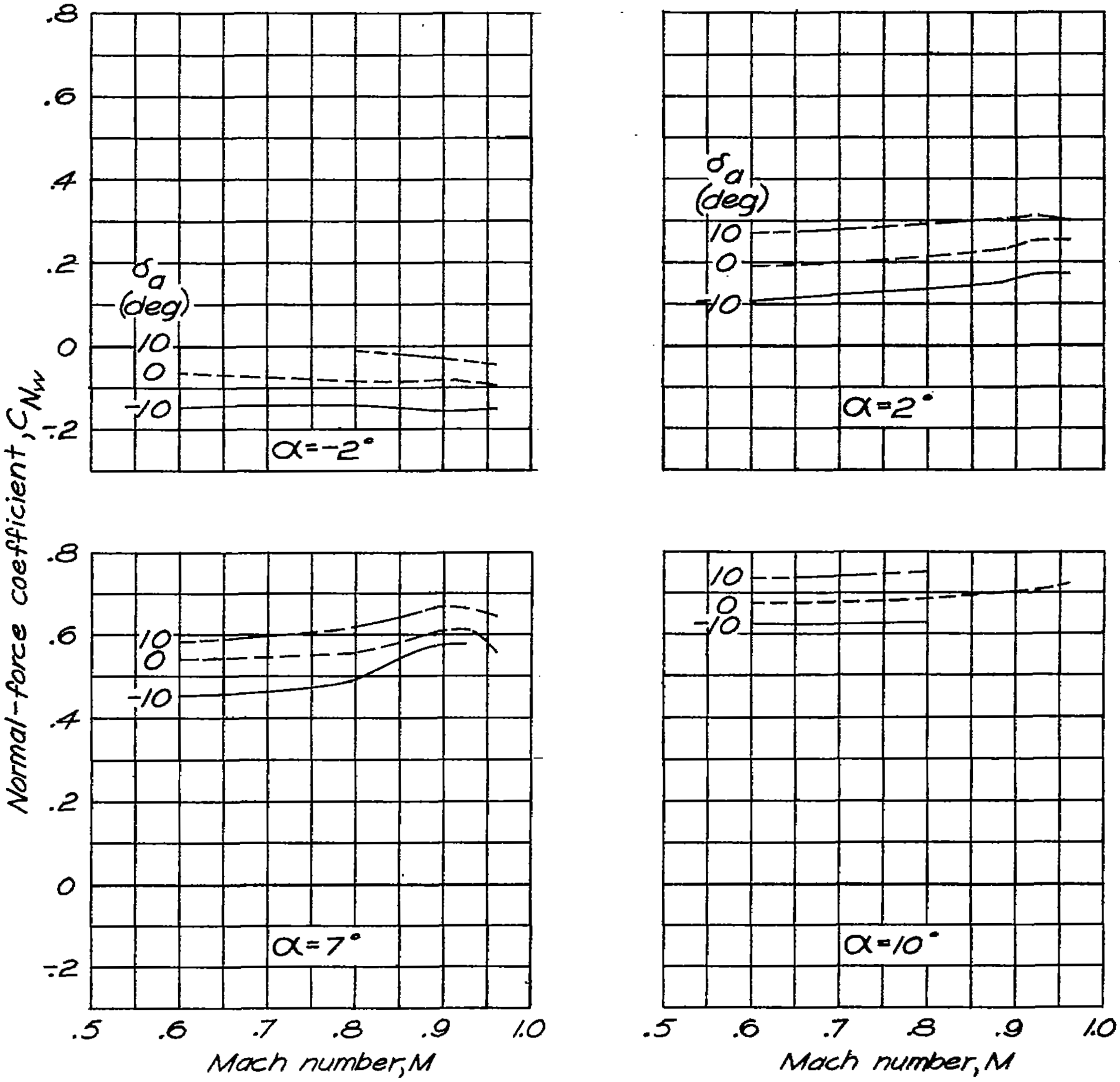

(d) $\Lambda_r = 45.°$

Figure 11.—Concluded.

NATIONAL ADVISORY COMMITTEE FOR AERONAUTICS

[redacted]

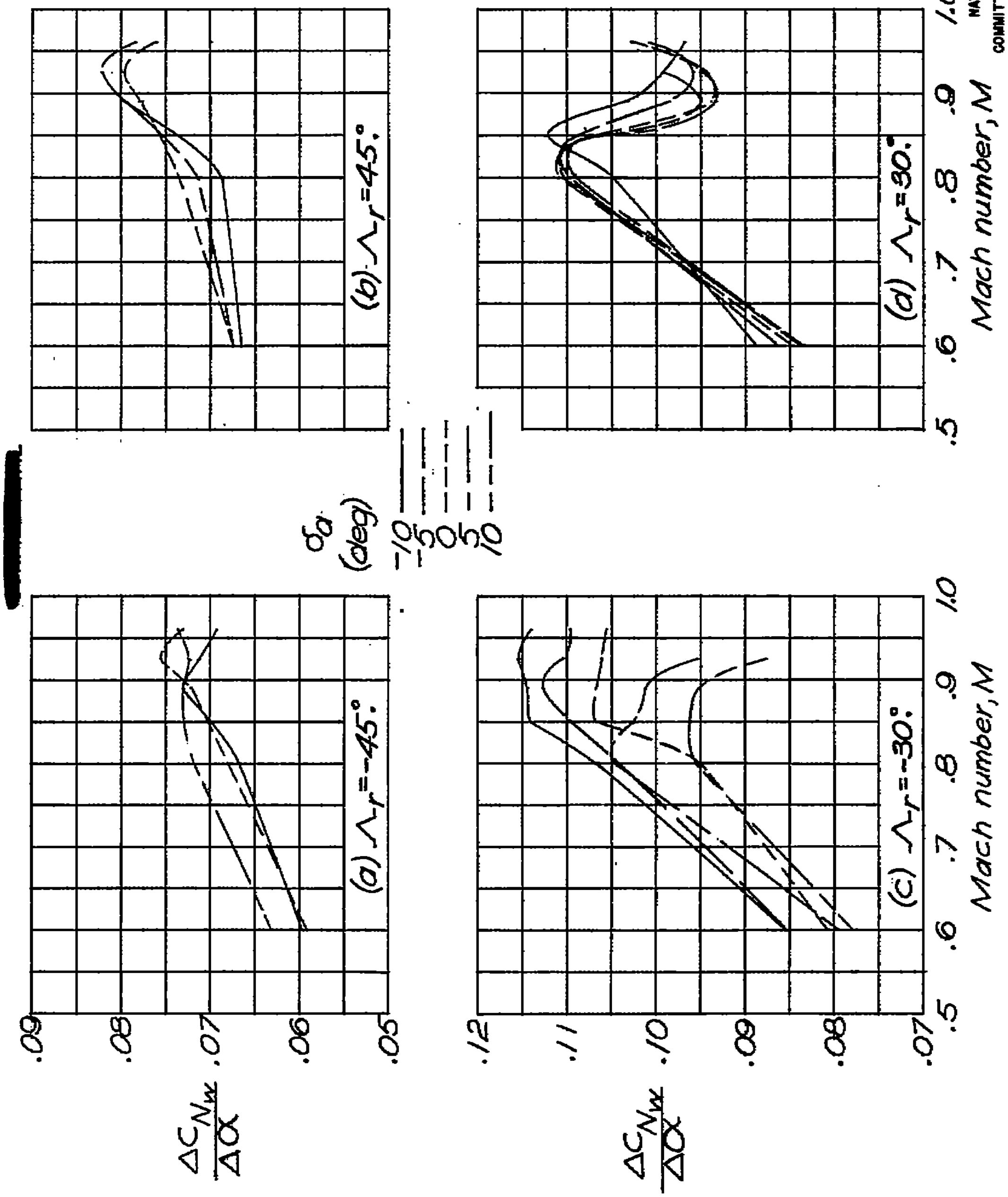

NATIONAL ADVISORY COMMITTEE FOR AERONAUTICS

Figure 12.—Variation of normal-force-curve slope with Mach number. Data for $\delta_a = 0°$ from reference 1.

[redacted]

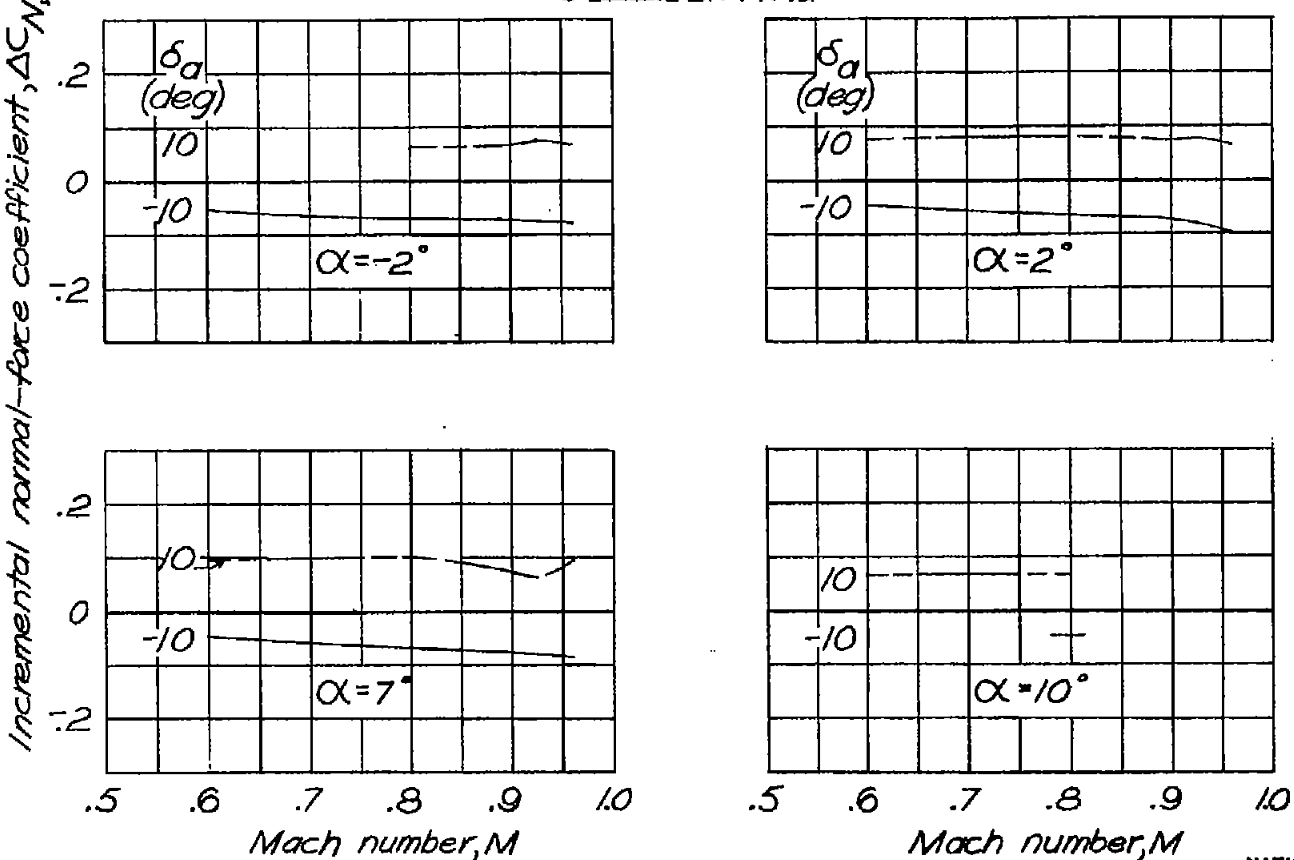

(a) $\Lambda_r = -45°$

NATIONAL ADVISORY COMMITTEE FOR AERONAUTICS

Figure 13.— Variation of change in wing normal-force coefficient resulting from aileron deflection with Mach number.

[redacted]

[redacted]

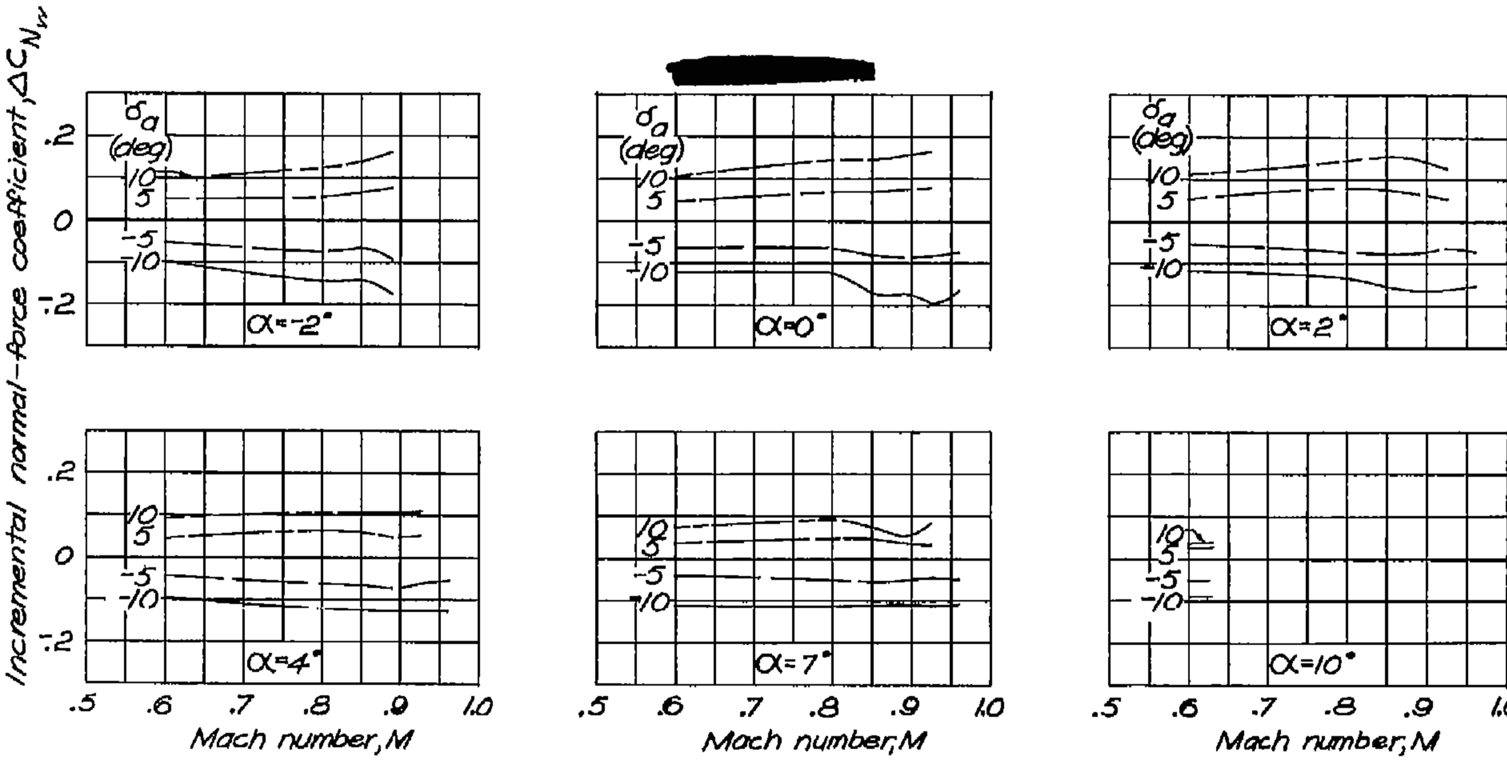

(b) $\Lambda_r = -30°$.

NATIONAL ADVISORY COMMITTEE FOR AERONAUTICS

Figure 13.– Continued.

[redacted]

[redacted]

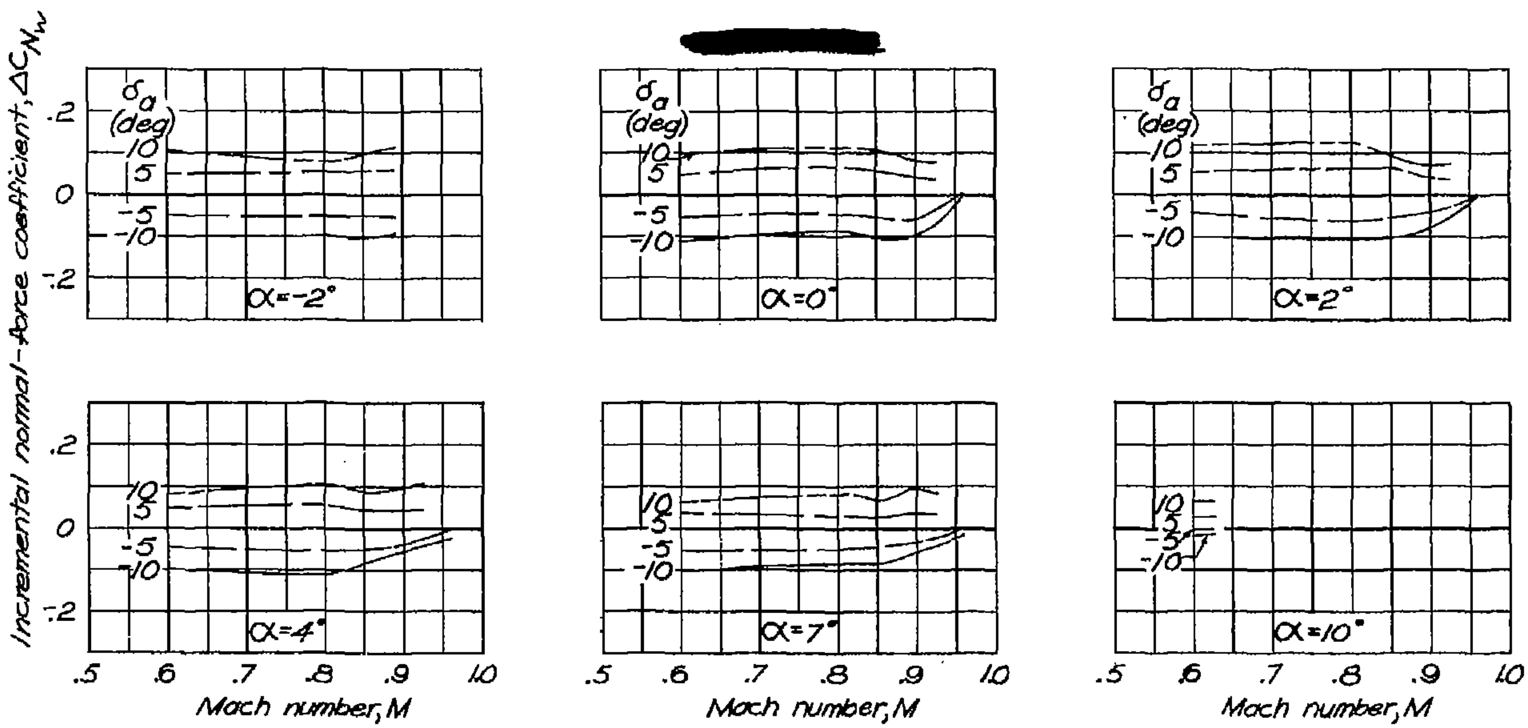

(c) $\Lambda_r = 30°$.

Figure 13.—Continued.

NATIONAL ADVISORY COMMITTEE FOR AERONAUTICS

[redacted]

[redacted]

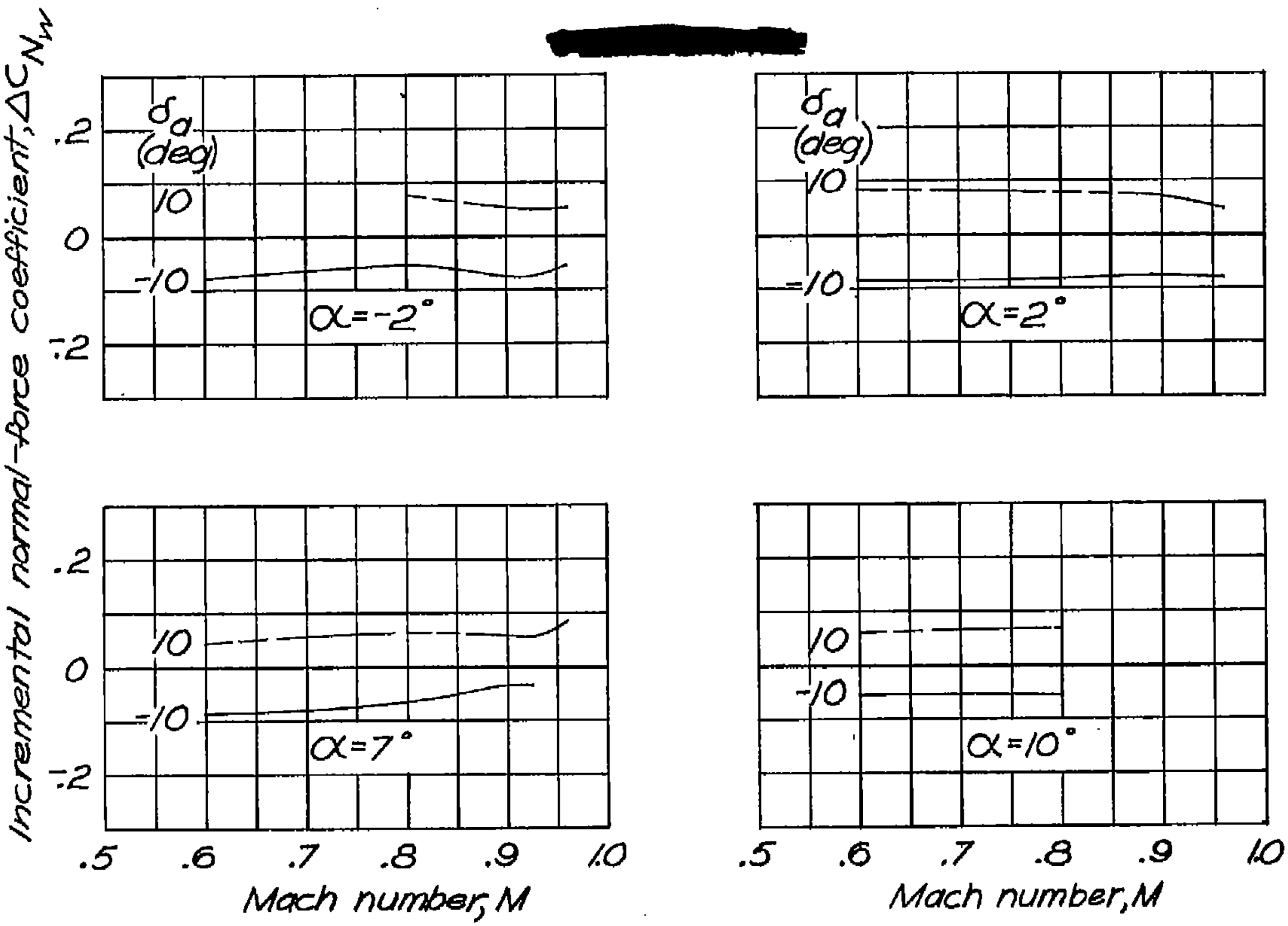

(d) $\Lambda_r = 45°$.

Figure 13.—Concluded.

NATIONAL ADVISORY
COMMITTEE FOR AERONAUTICS

[redacted]

[redacted]

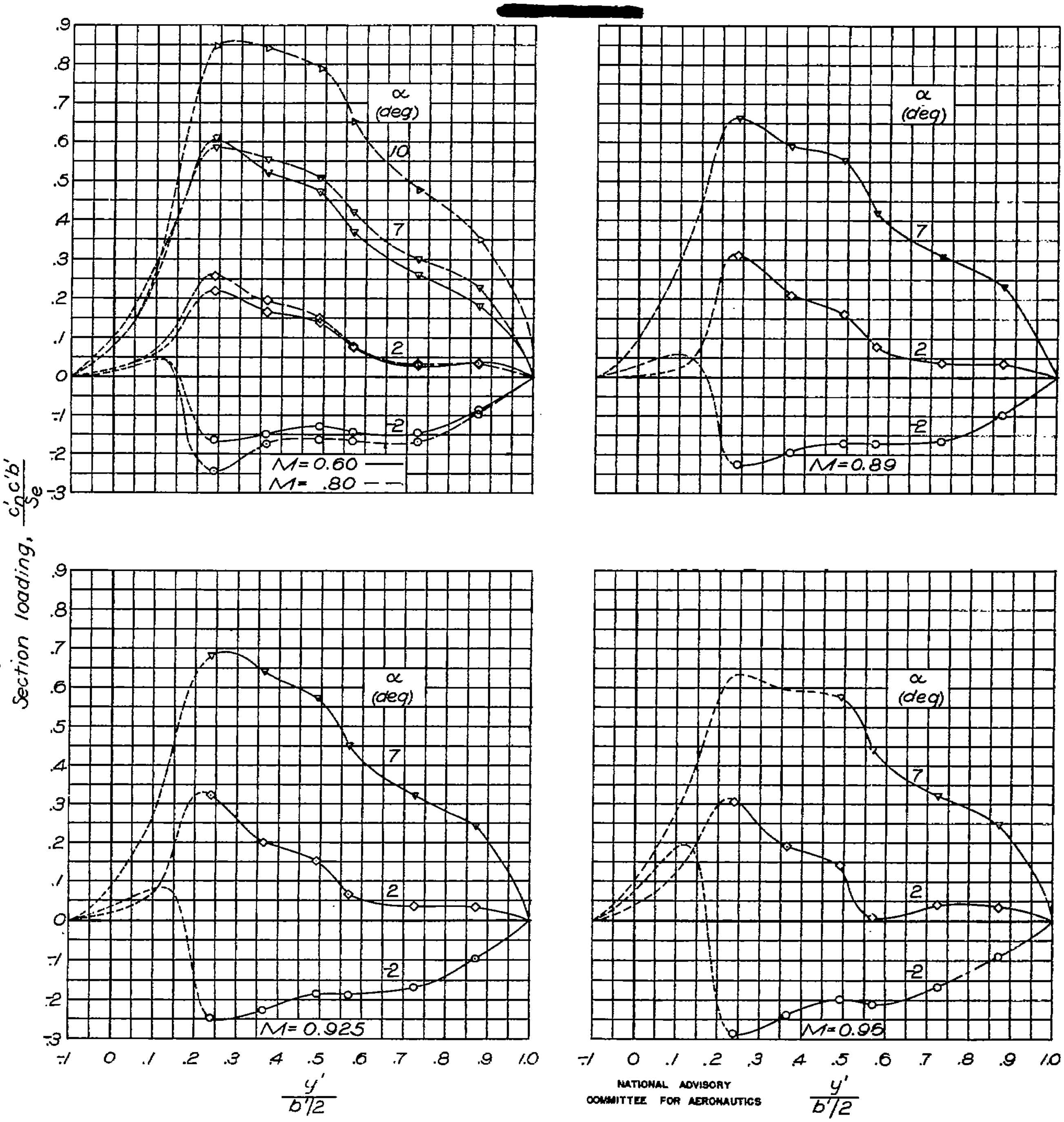

(a) $\delta_a = -10°$

Figure 14 . — Spanwise variation in section loading along Y′-axis. $\Lambda_r = -45°$.

[redacted]

[redacted]

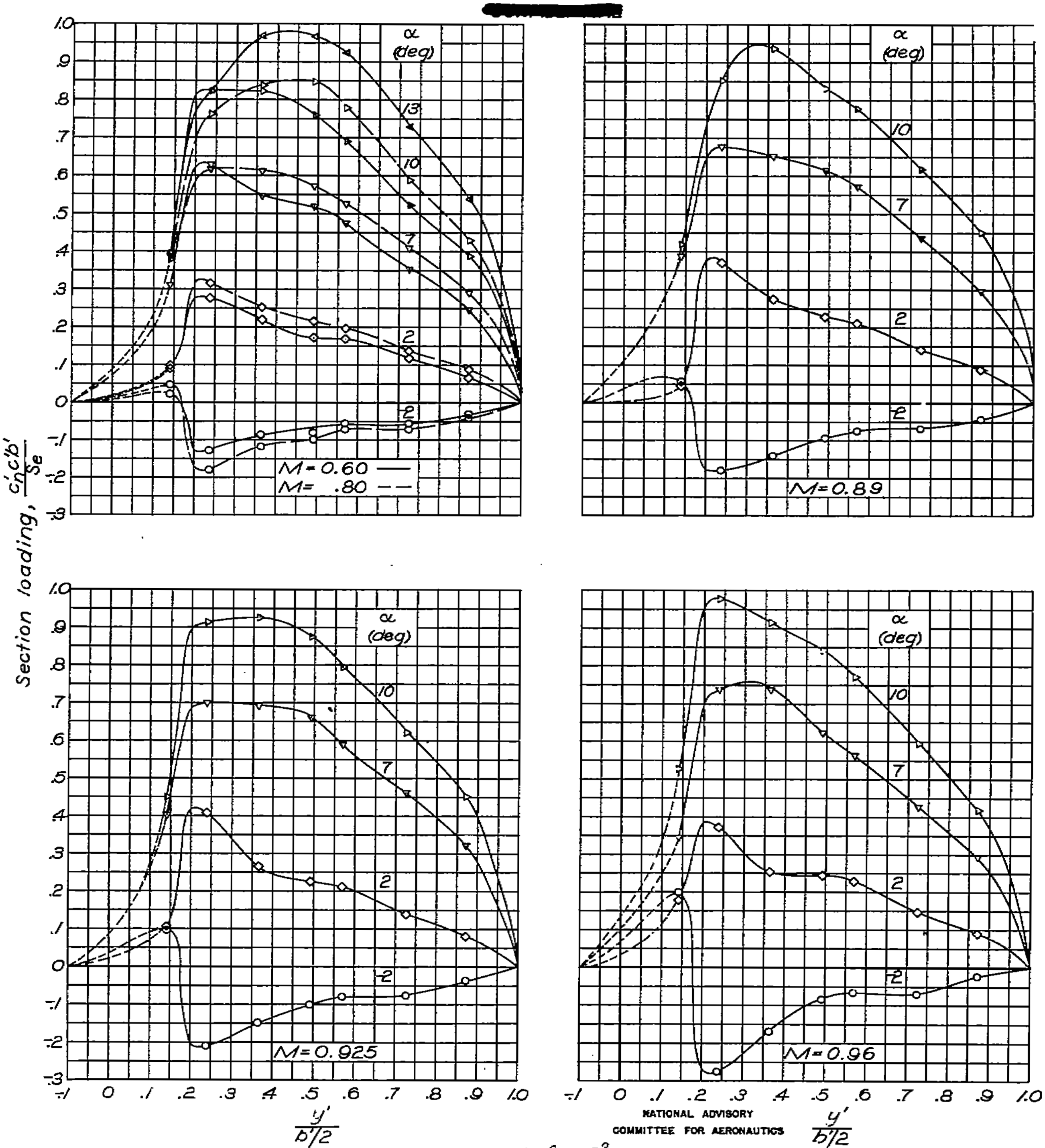

(b) $\delta_a = 0°$.

Figure 14.— Continued. $\Lambda_r = -45°$. [redacted]

[redacted]

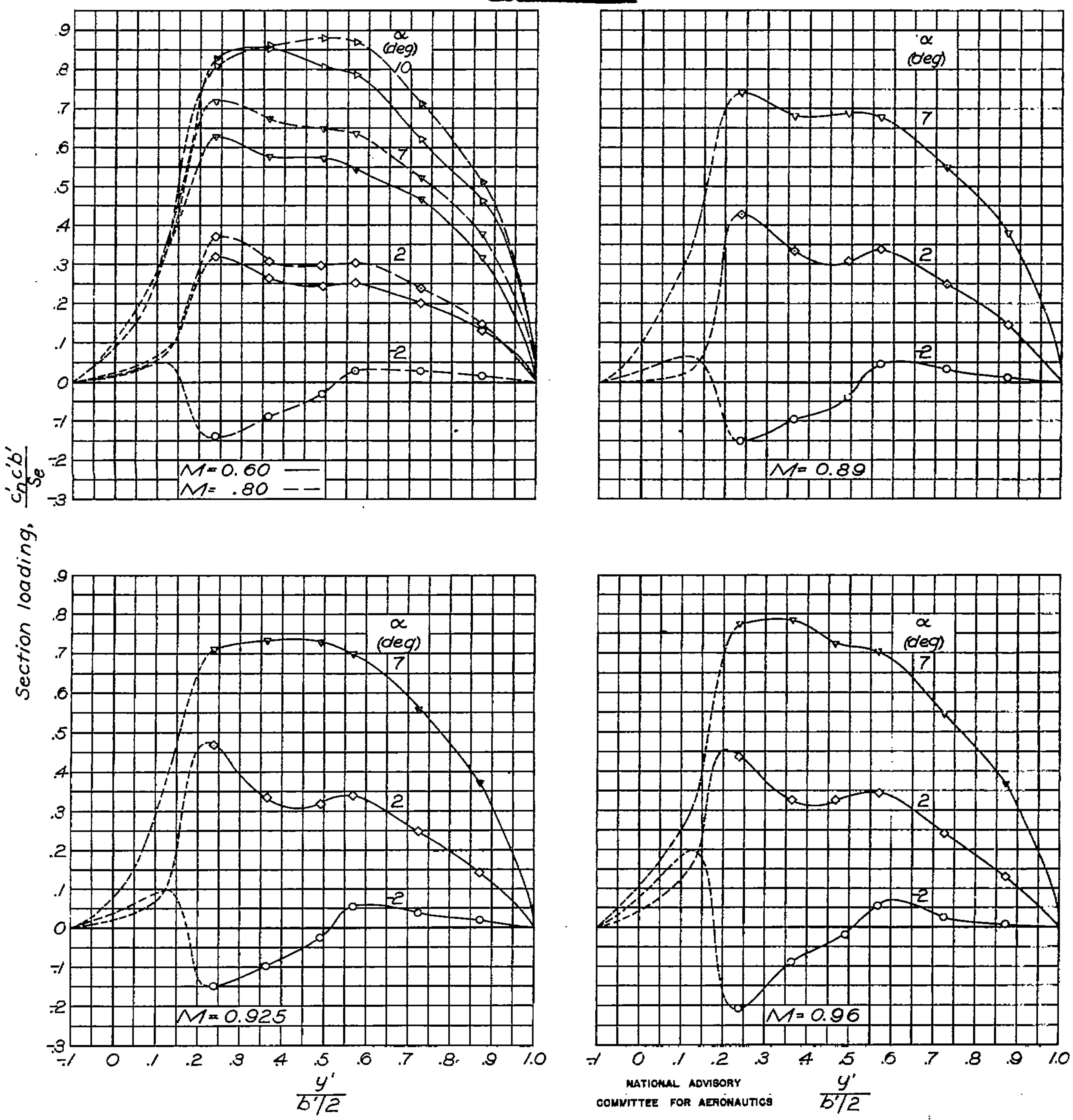

(c) $\delta_a = 9.8°$.

Figure 14 .— Concluded. $\Lambda_r = -45°$. [redacted]

[redacted]

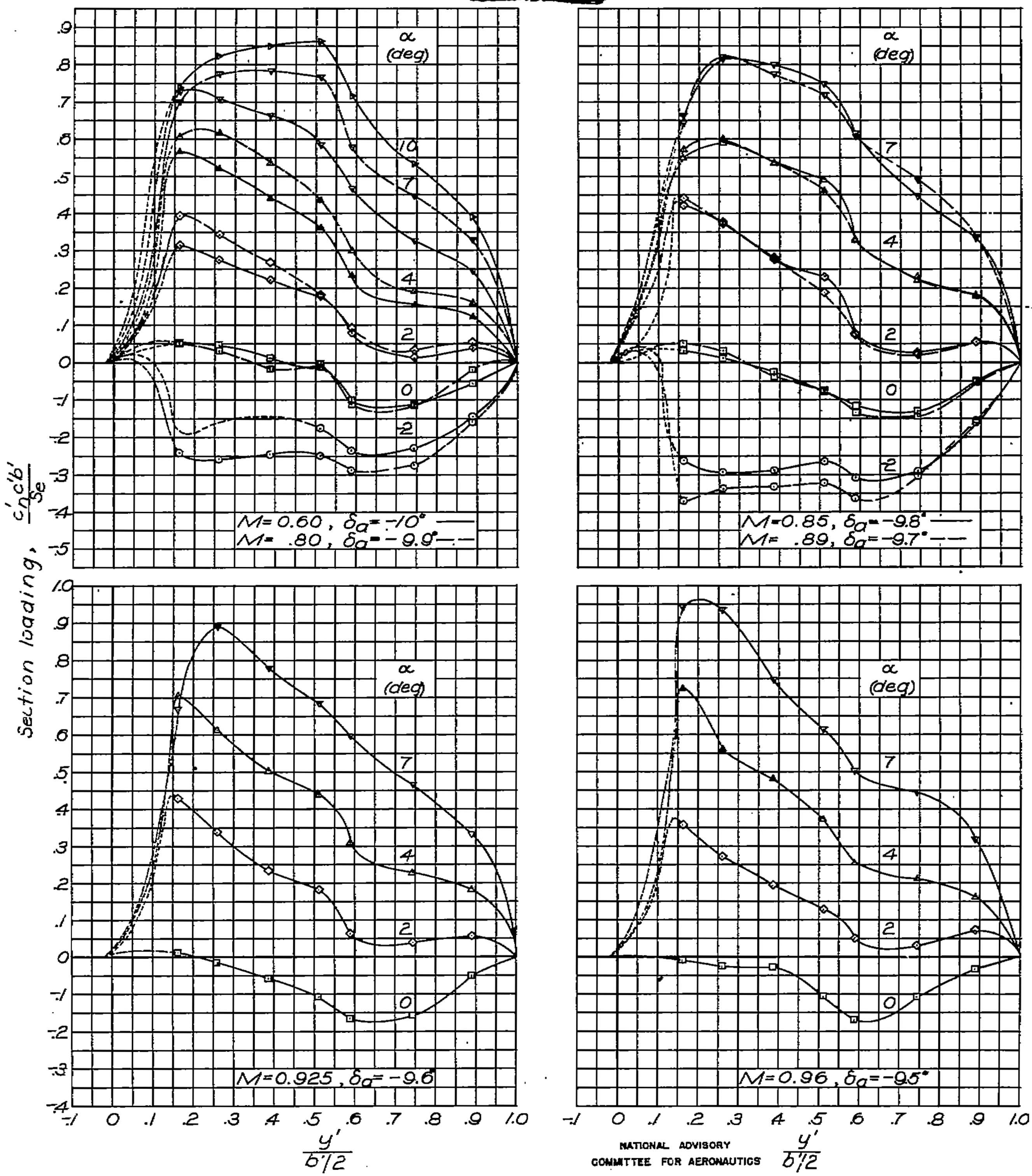

(a) $\delta_a \approx -10^\circ$. (Note individual plots.)

Figure 15 .— Spanwise variation in section loading along Y-axis. Λ_r -30°.

[redacted]

[redacted]

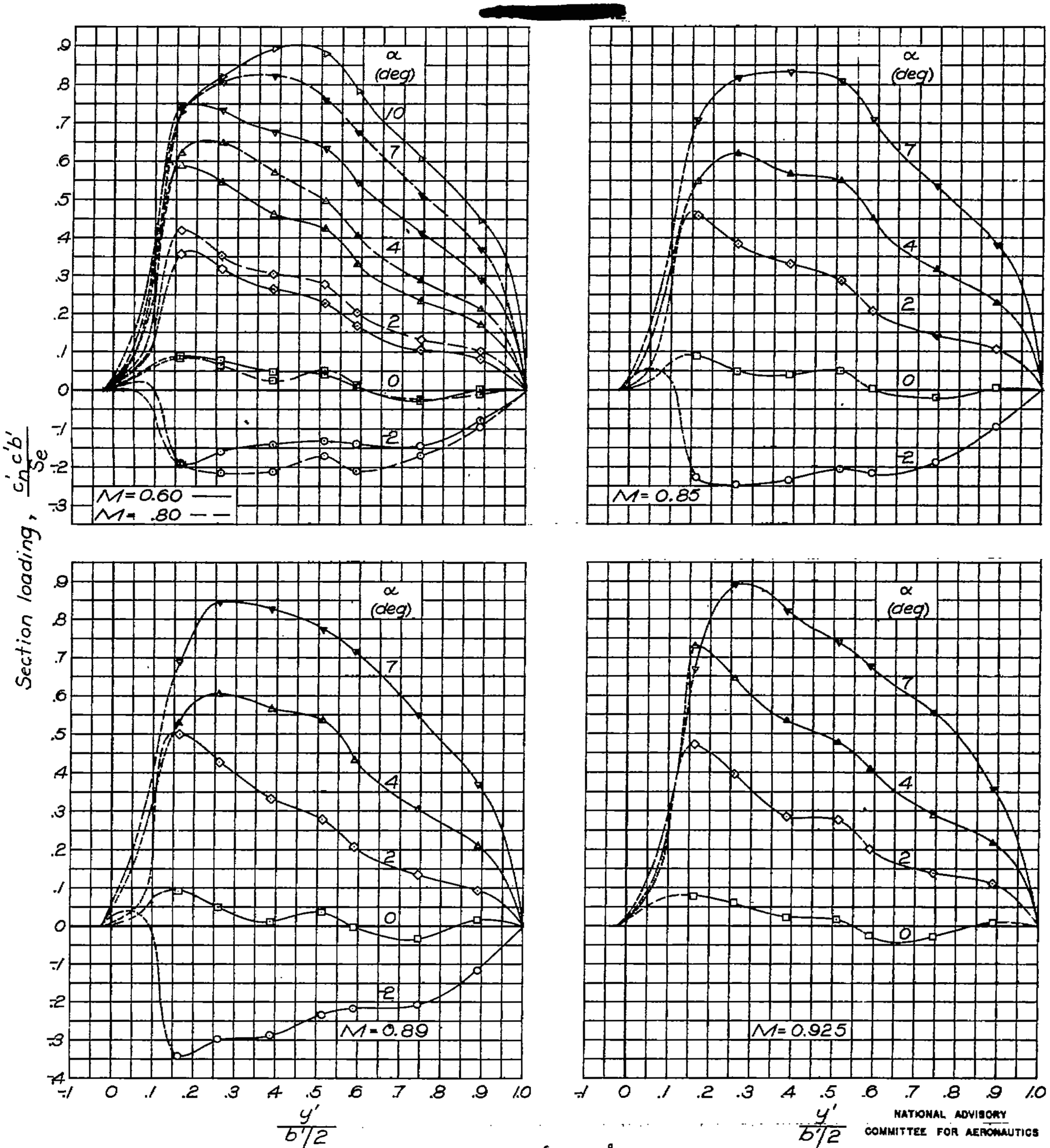

(b) $\delta_a = -5^\circ$

Figure 15 .— Continued. $\Lambda_r = -30^\circ$ [redacted]

[redacted]

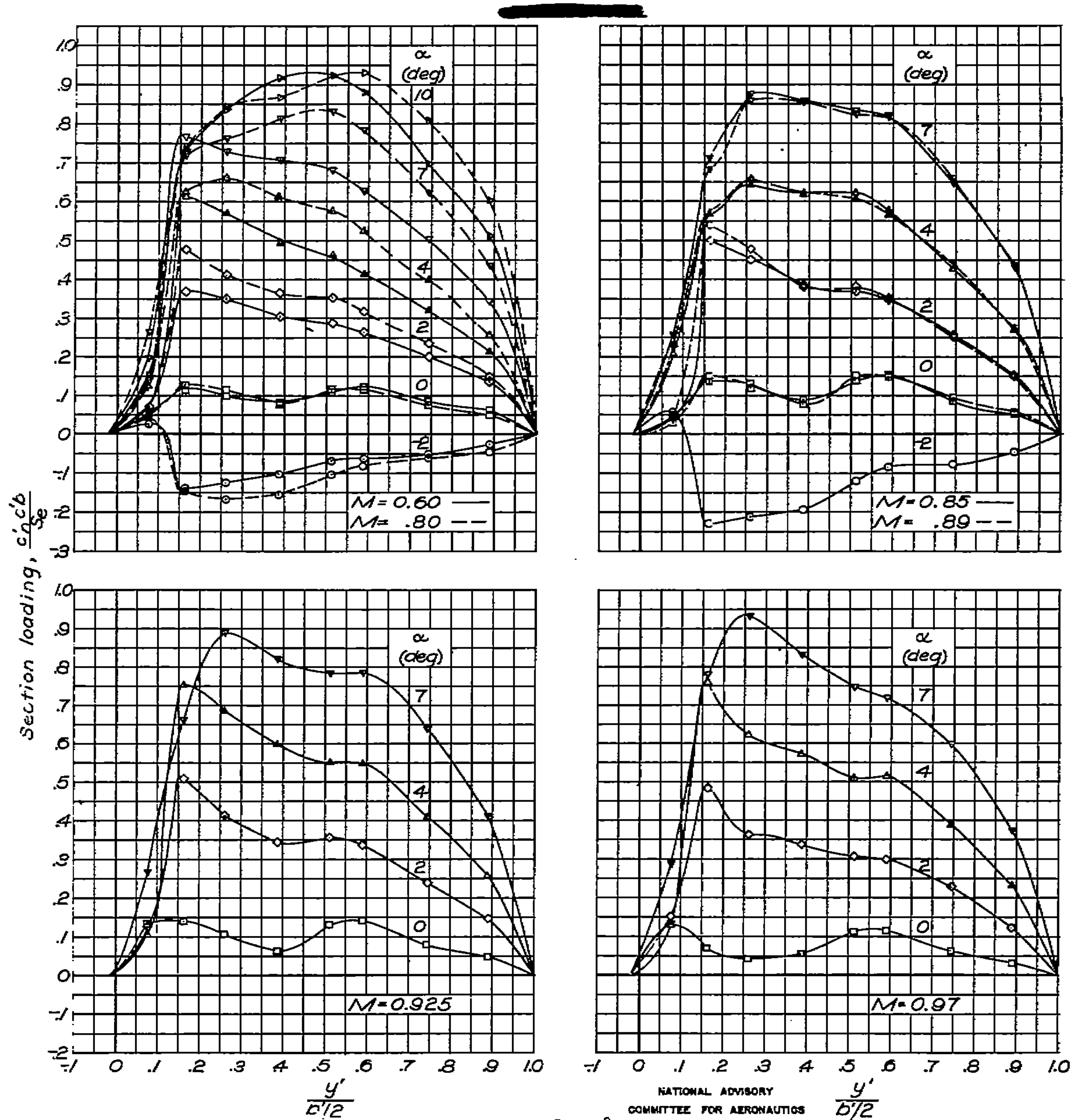

(c) $\delta_a = 0°$.

Figure 15. — Continued. $\Lambda_r = -30°$. [redacted]

[redacted]

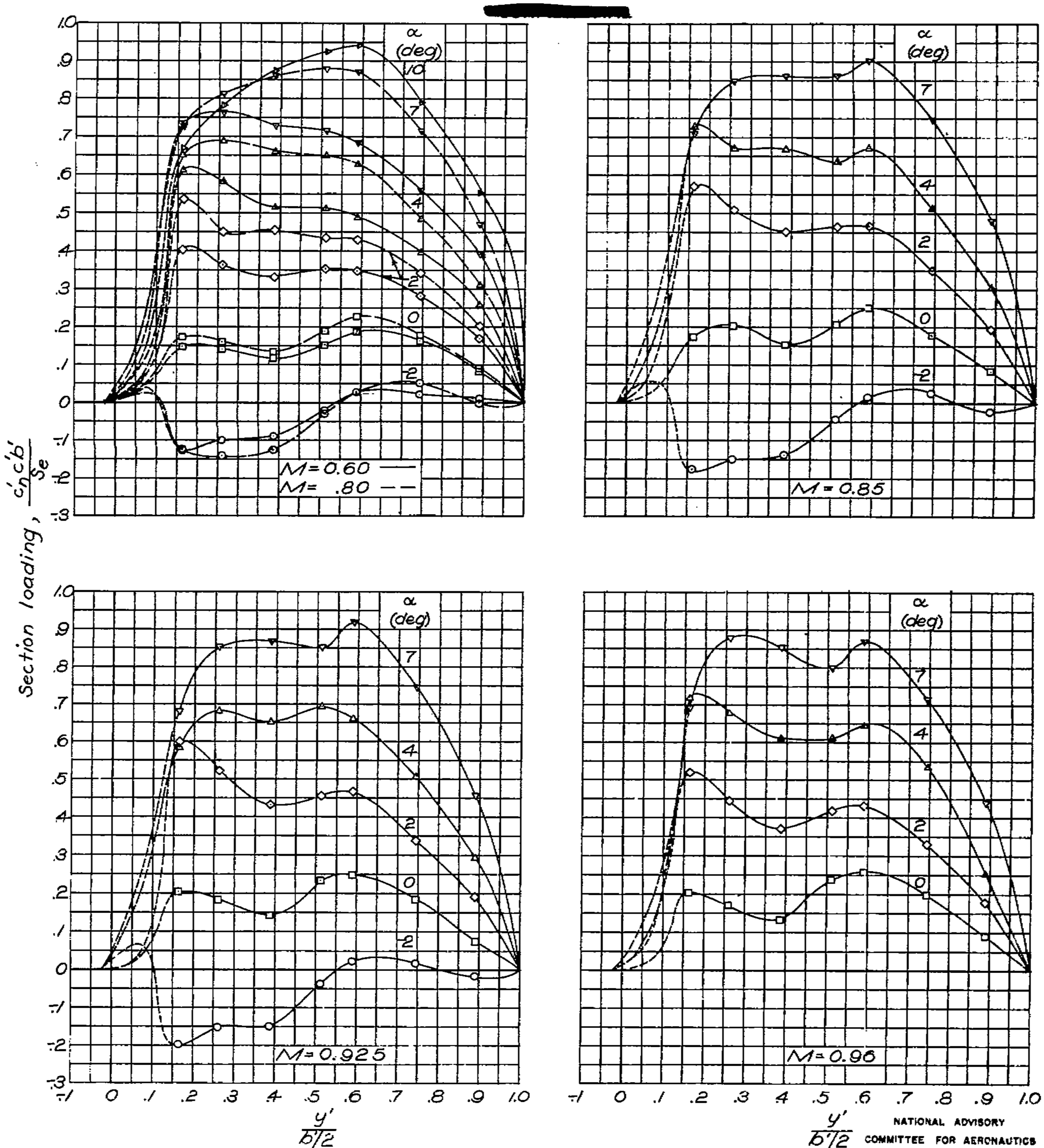

(d) $\delta_a = 5°$.

Figure 15 .— Continued. $\Lambda_r = -30°$. [redacted]

[redacted]

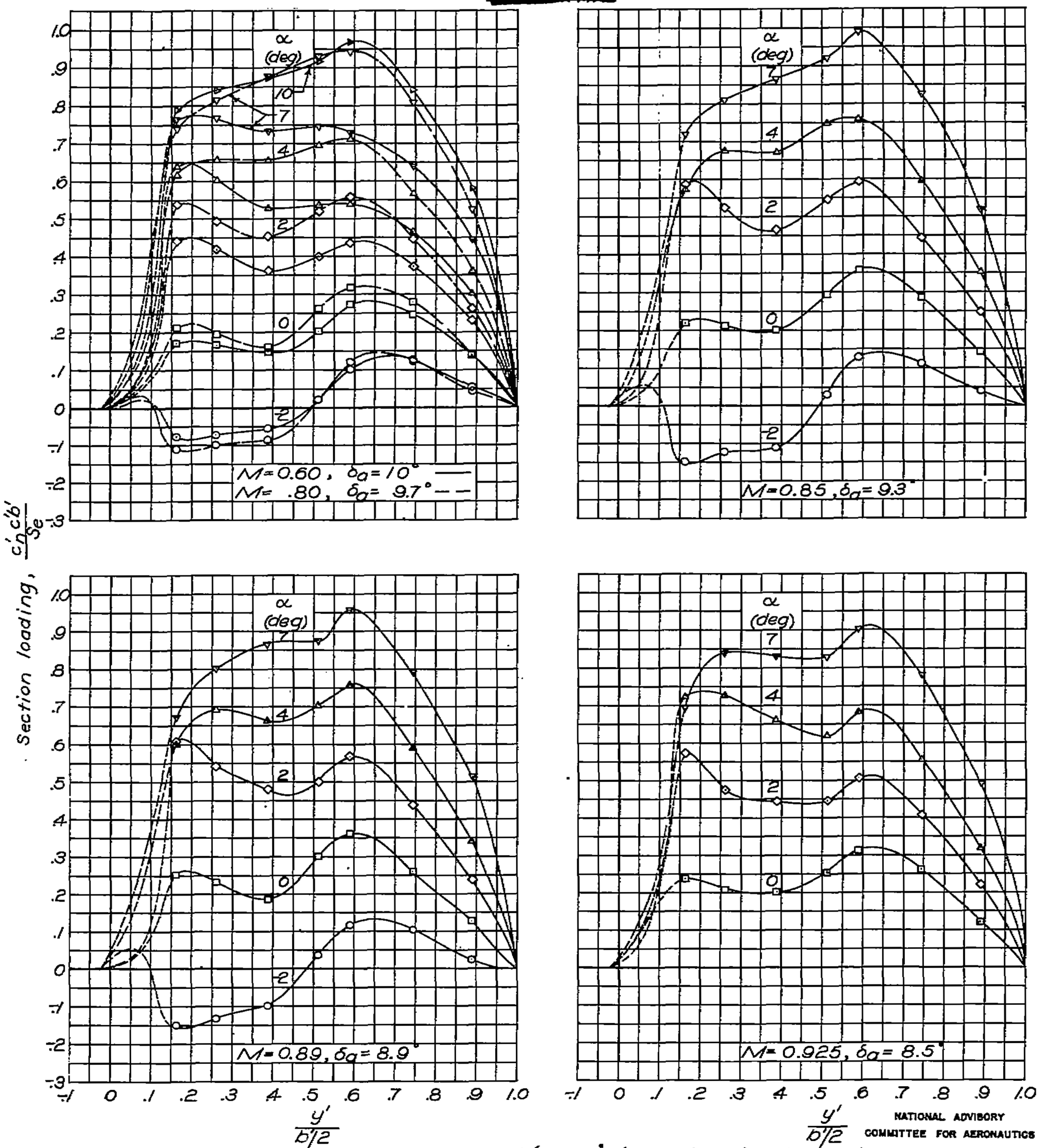

(e) $\delta_a \approx 10^\circ$. (Note individual plots.)

Figure 15. — Concluded. $\Lambda_r = -30^\circ$. [redacted]

[redacted]

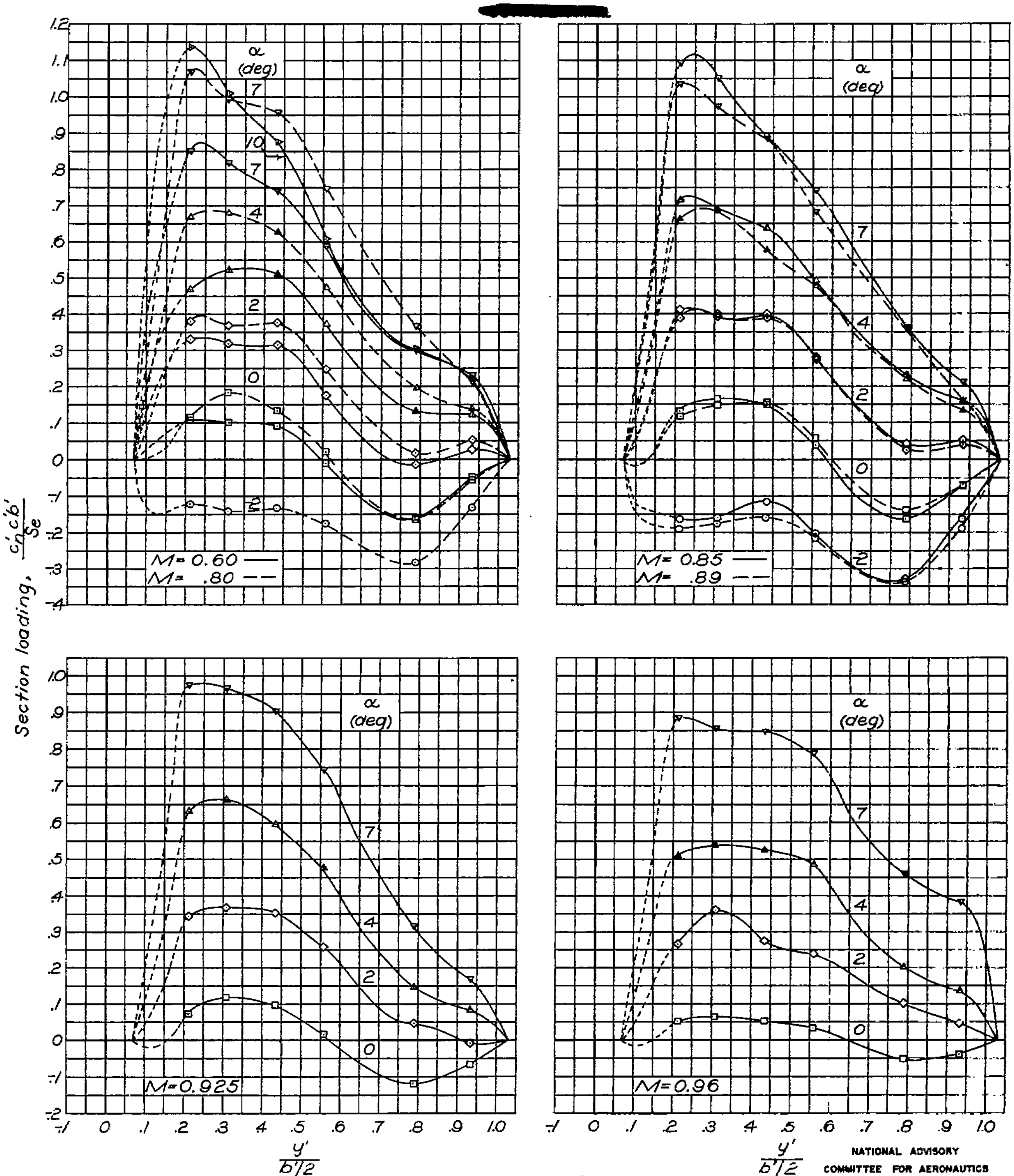

(a) $\delta_a = -10°$.

Figure 16. —Spanwise variation in section loading along Y'-axis. $\Lambda_r = 30°$.

[redacted]

[redacted]

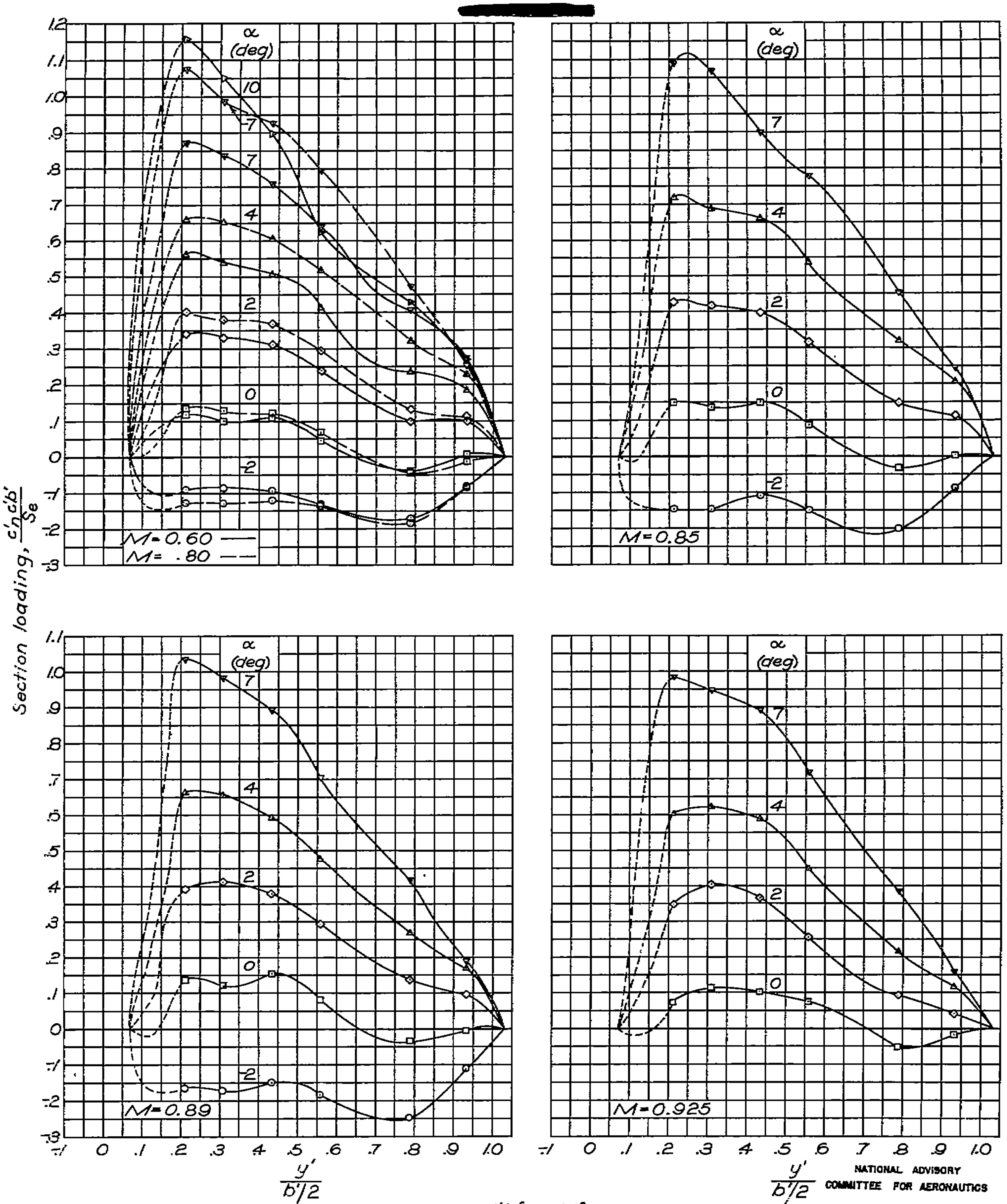

(b) $\delta_a = -5.1°$

Figure 16 .— Continued. $\Lambda_r = 30°$ [redacted]

[redacted]

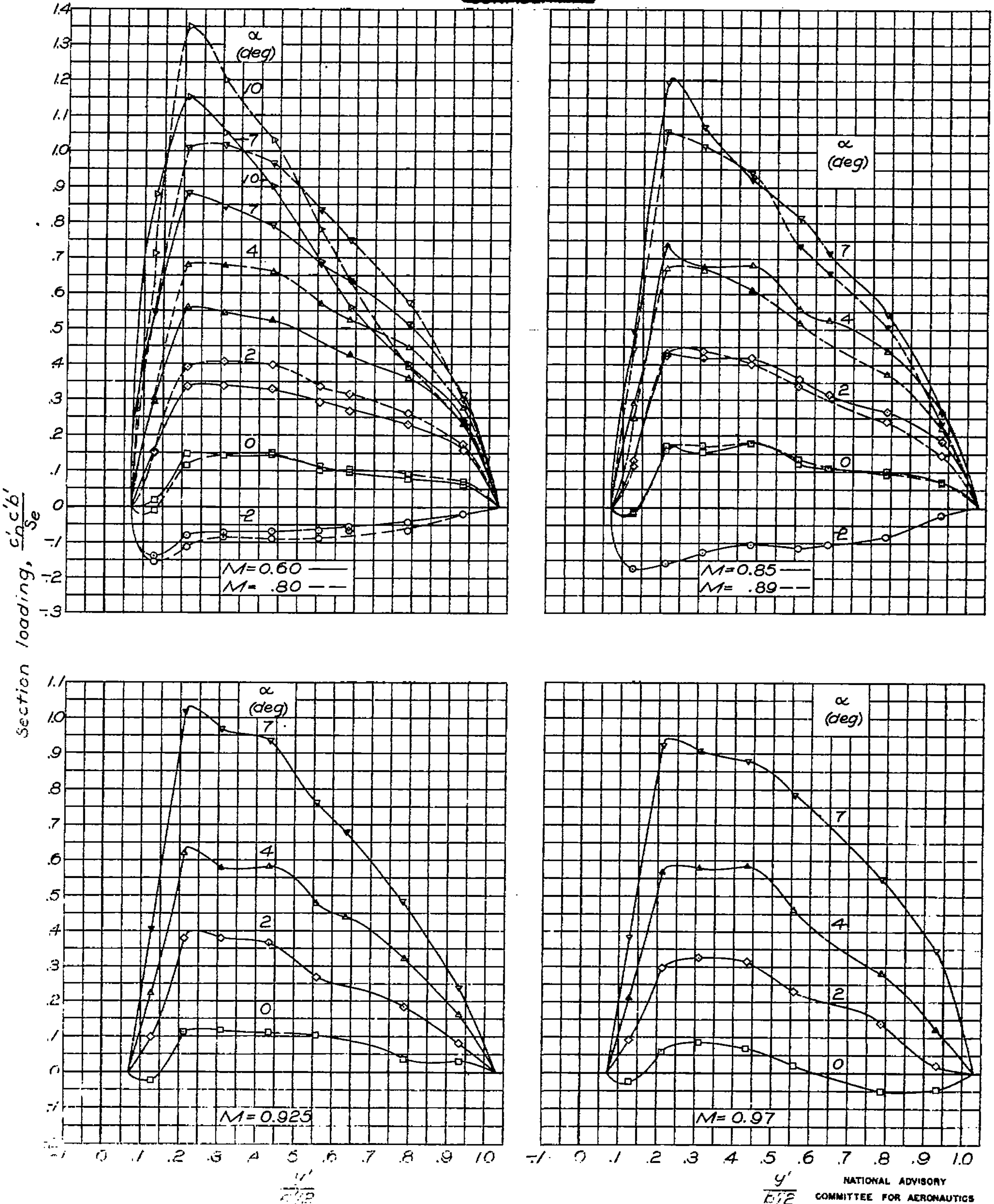

(c) $\delta_a = 0°$

Figure 16.— Continued. $\Lambda_r = 30°$ [redacted]

[redacted]

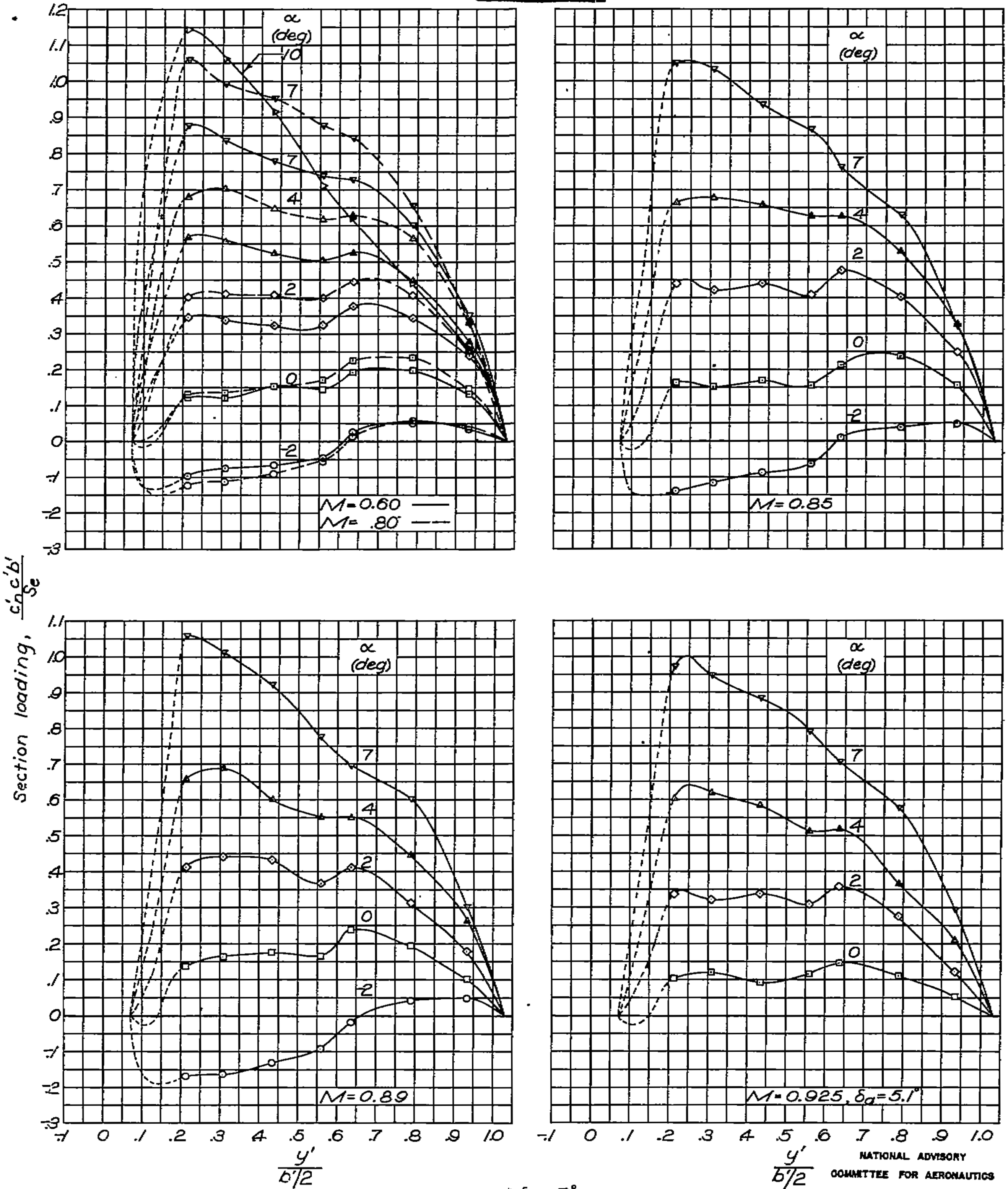

(d) $\delta_a = 5°$.

Figure 16 .— Continued. $\Lambda_r = 30°$.

[redacted]

[redacted]

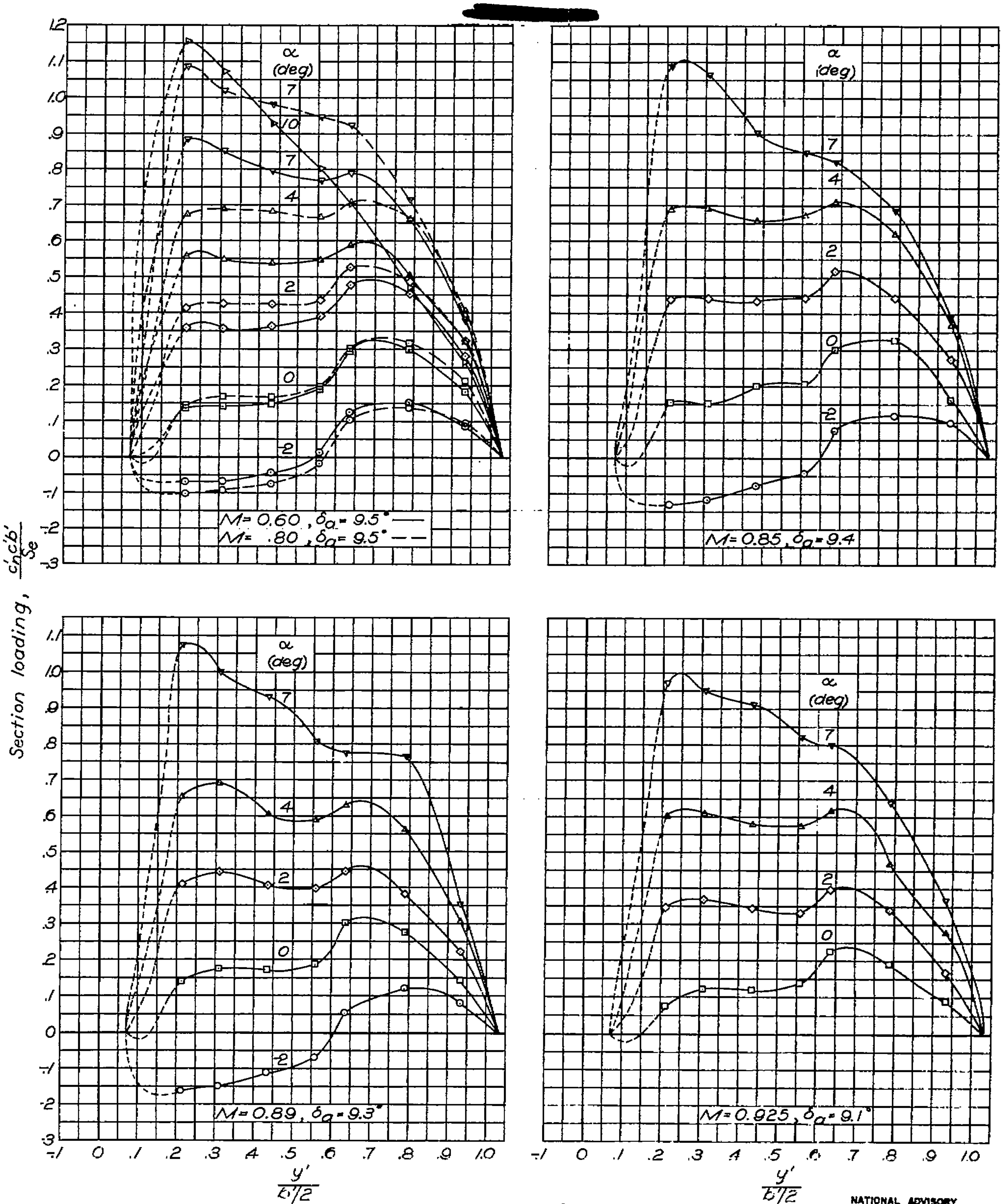

(e) $\delta_a \approx 10°$. (Note individual plots.)

NATIONAL ADVISORY COMMITTEE FOR AERONAUTICS

Figure 16 .— Concluded. $\Lambda_r = 30°$.

[redacted]

[redacted]

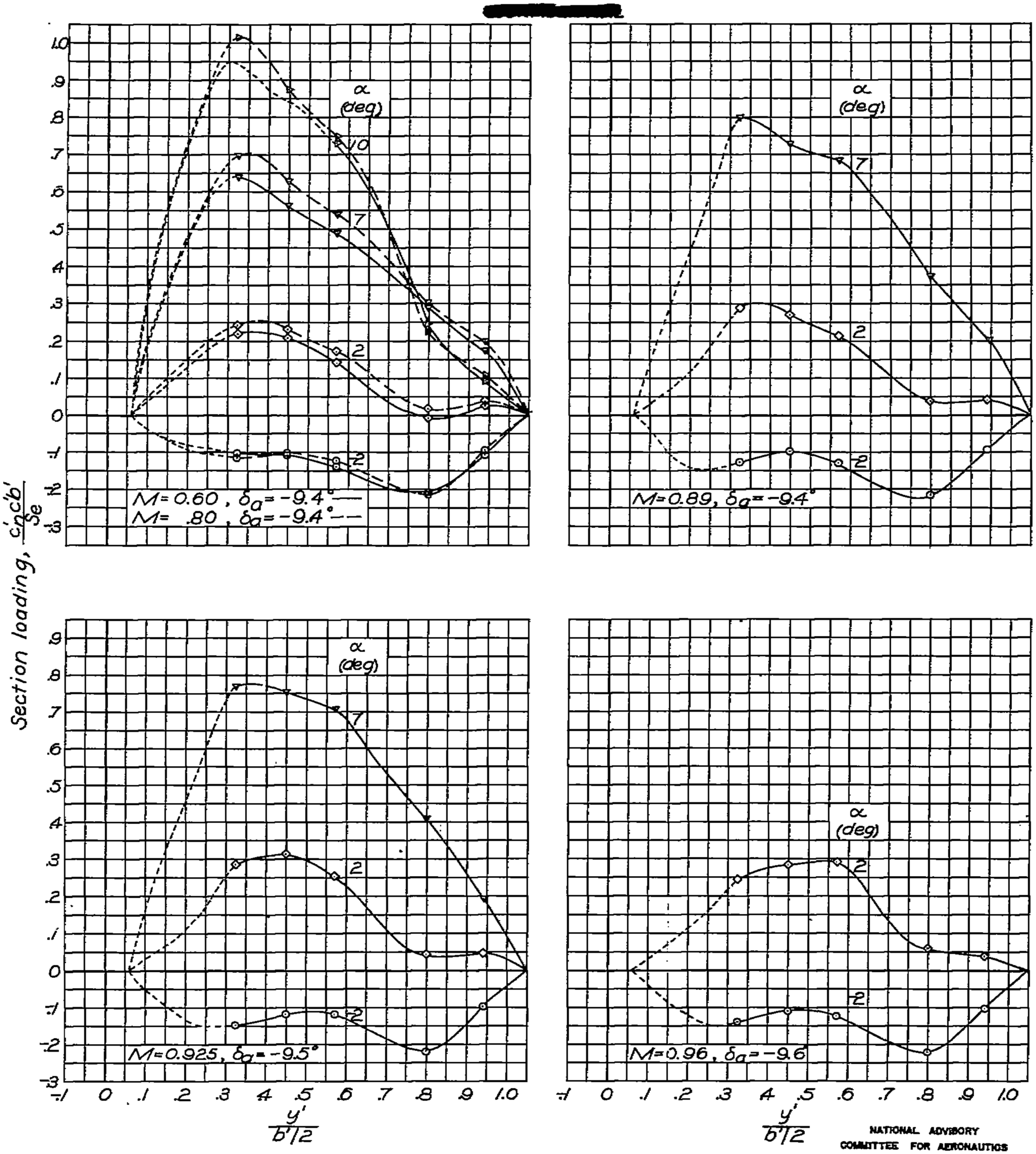

(a) $\delta_a \approx -10^\circ$. (Note individual plots.)

Figure 17 .—Spanwise variation in section loading along Y'-axis. $\Lambda_r = 45^\circ$.

[redacted]

[redacted]

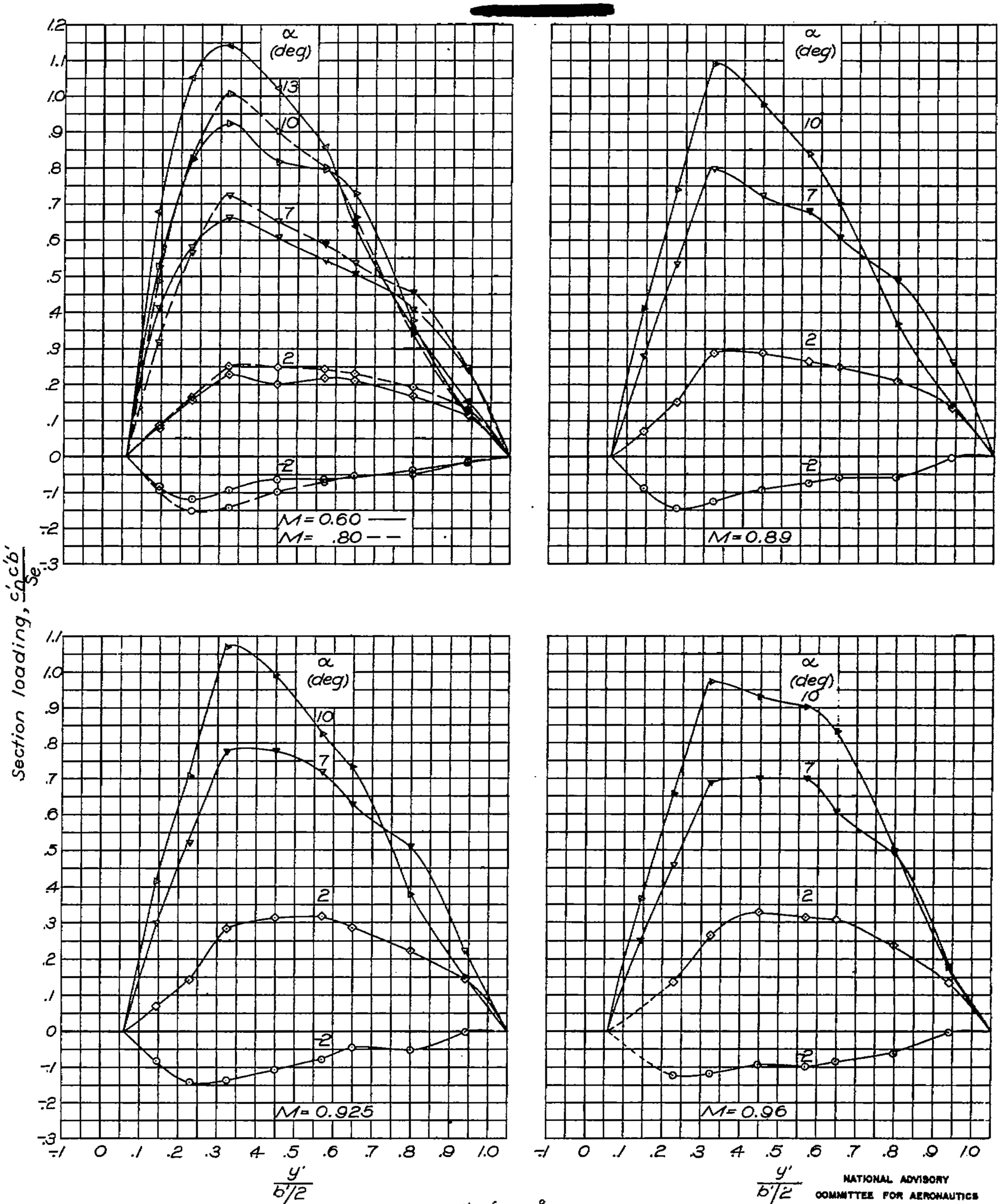

(b) $\delta_a = 0°$.

Figure 17.— Continued. $\Lambda_r = 45°$.

[redacted]

[redacted]

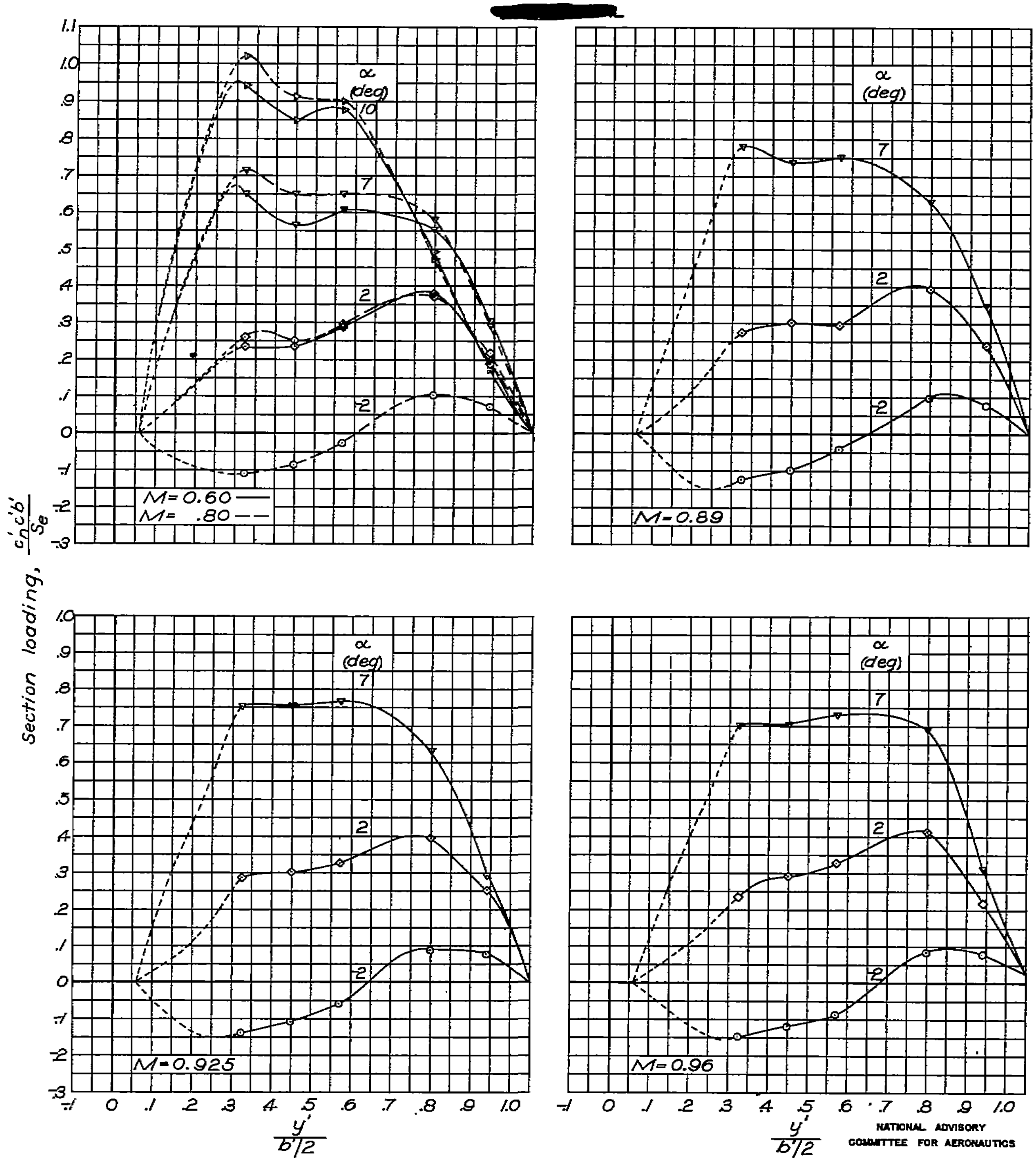

(c) $\delta_a = 10°$.

Figure 17. — Concluded. $\Lambda_r = 45°$.

[redacted]

[redacted]

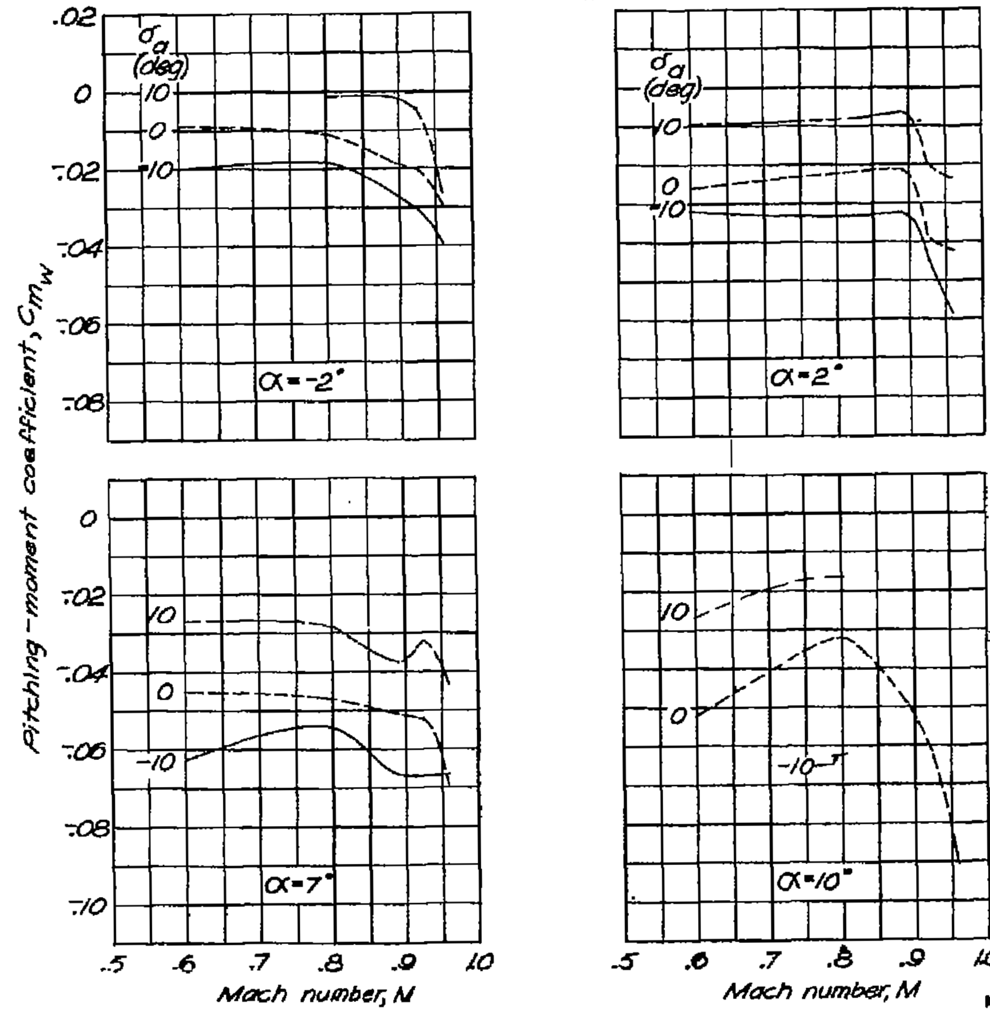

(a) $\Lambda_T = -45°$

NATIONAL ADVISORY COMMITTEE FOR AERONAUTICS

Figure 18.— Variation of wing pitching-moment coefficient with Mach number. Data for $\delta_a = 0°$ from reference 1.

[redacted]

[redacted]

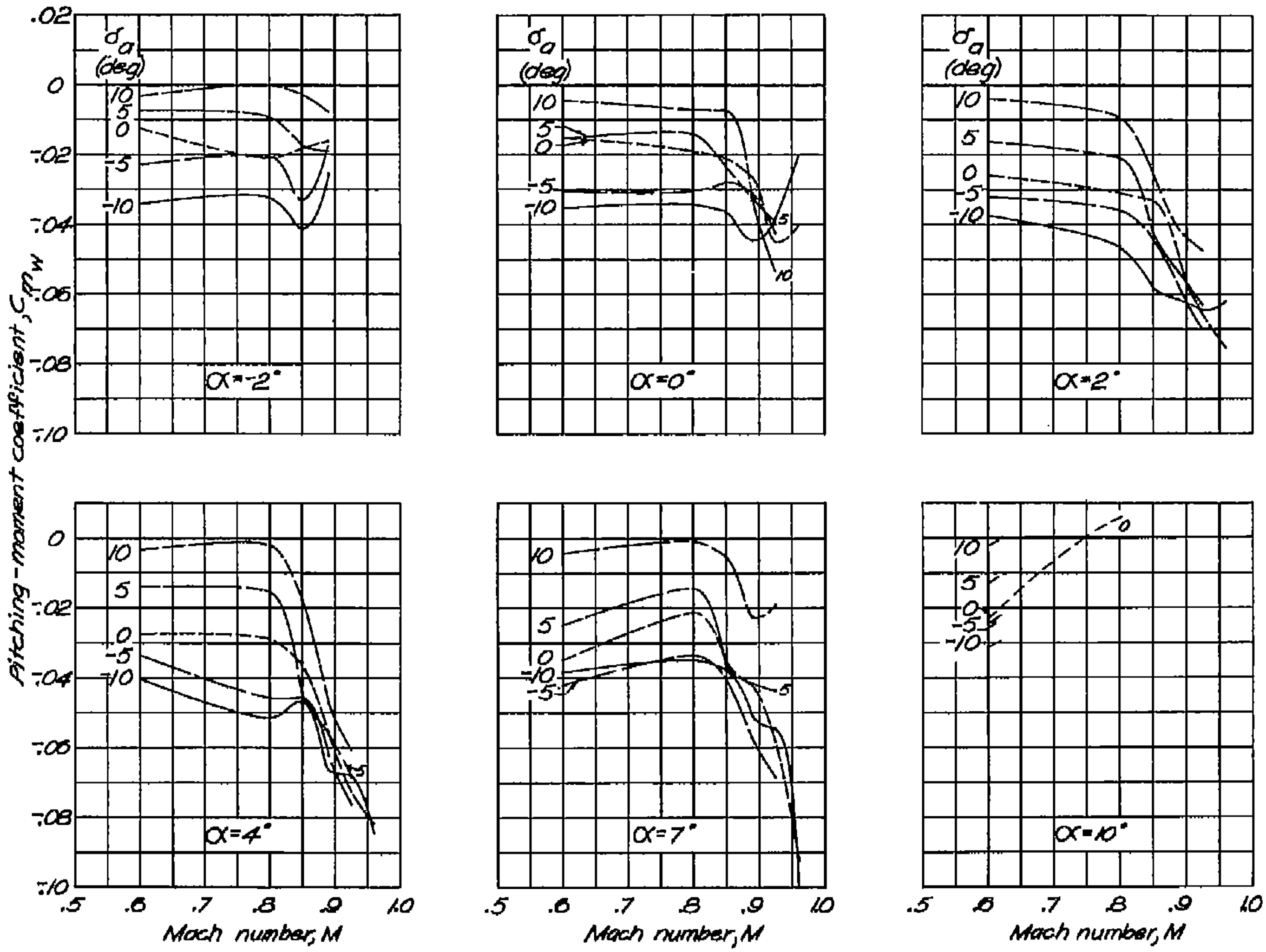

(b) $\Lambda_r = -30°$.

Figure 18.—Continued.

NATIONAL ADVISORY COMMITTEE FOR AERONAUTICS

[redacted]

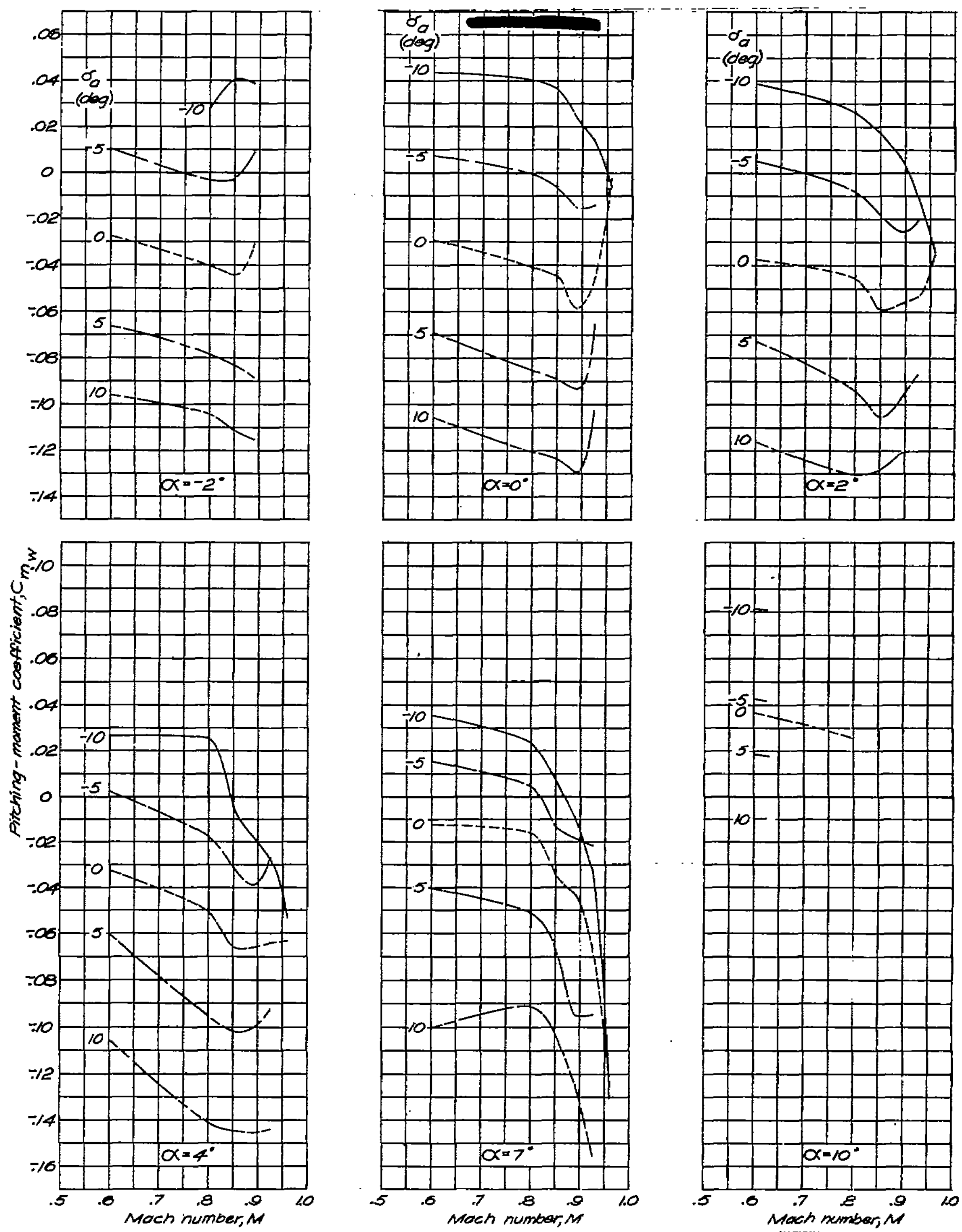

NATIONAL ADVISORY COMMITTEE FOR AERONAUTICS

(c) $\Lambda_r = 30°$.

Figure 18.—Continued.

[redacted]

[redacted]

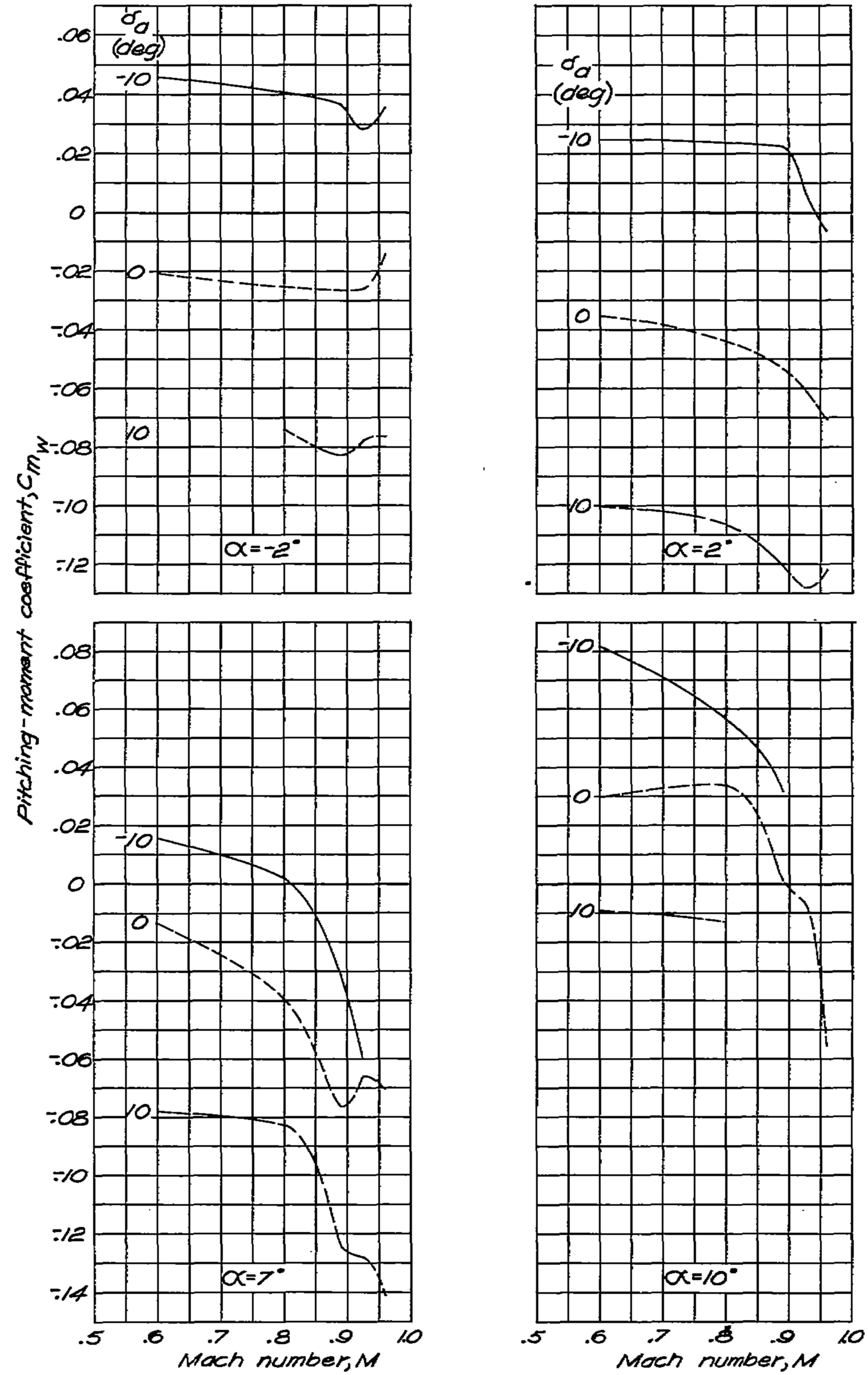

(d) $\Lambda_r = 45°$

Figure 18.—Concluded.

[redacted]

[redacted]

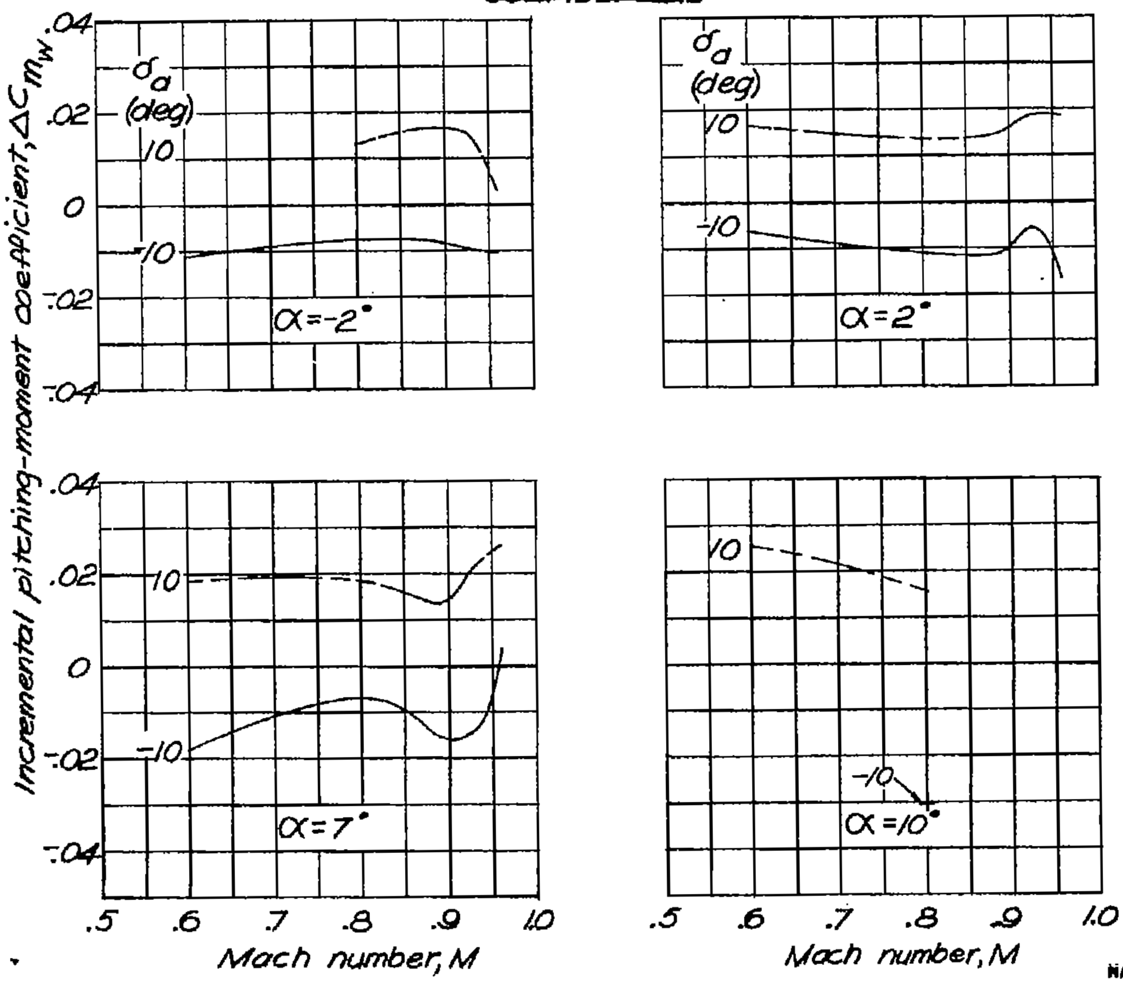

(a) $\Lambda_r = -45°$.

NATIONAL ADVISORY COMMITTEE FOR AERONAUTICS

Figure 19.—Variation of change in wing pitching-moment coefficient resulting from aileron deflection with Mach number.

[redacted]

[redacted]

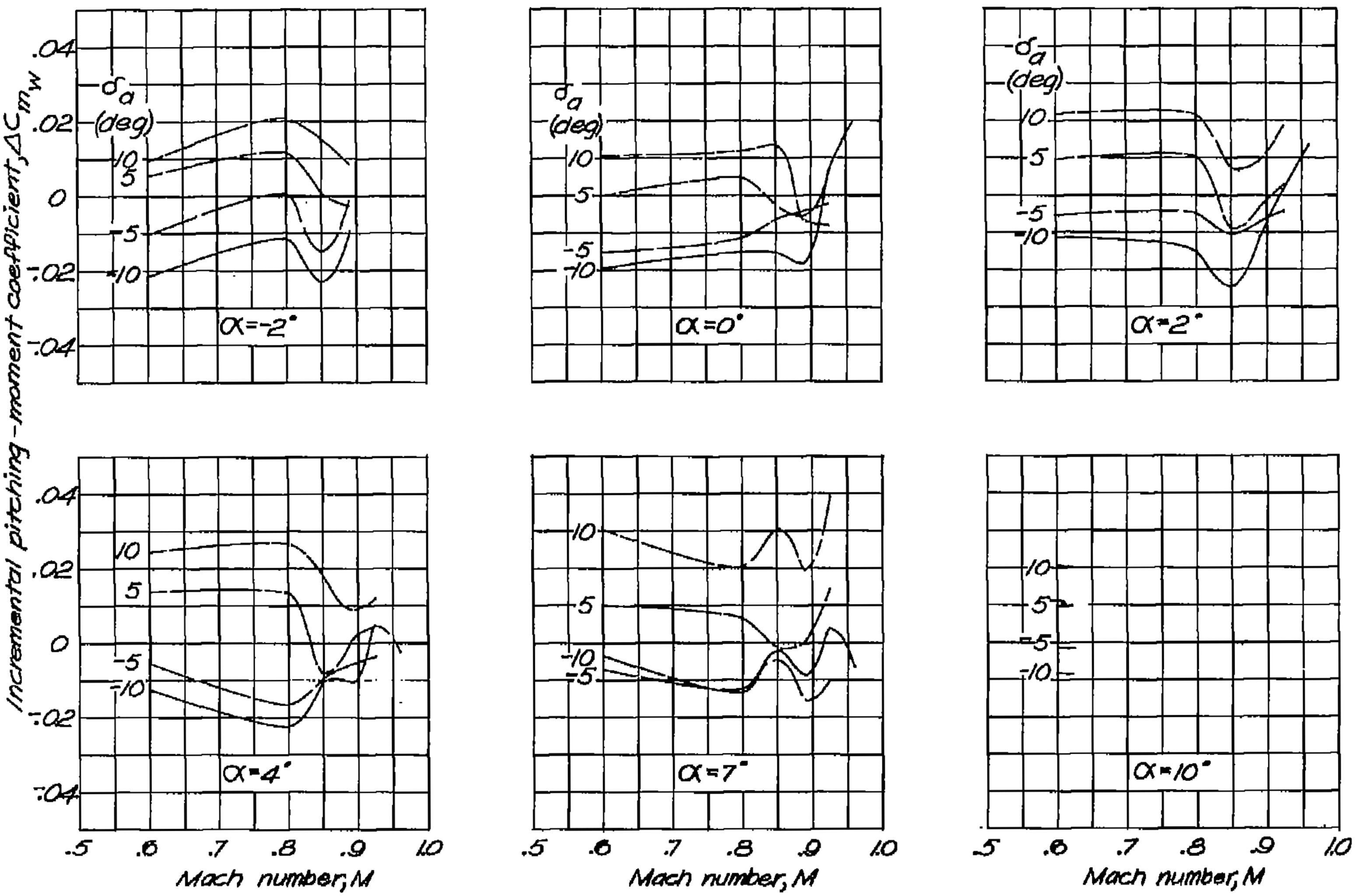

(b) $\Lambda_r = -30°$.

Figure 19.—Continued.

NATIONAL ADVISORY
COMMITTEE FOR AERONAUTICS

[redacted]

[redacted]

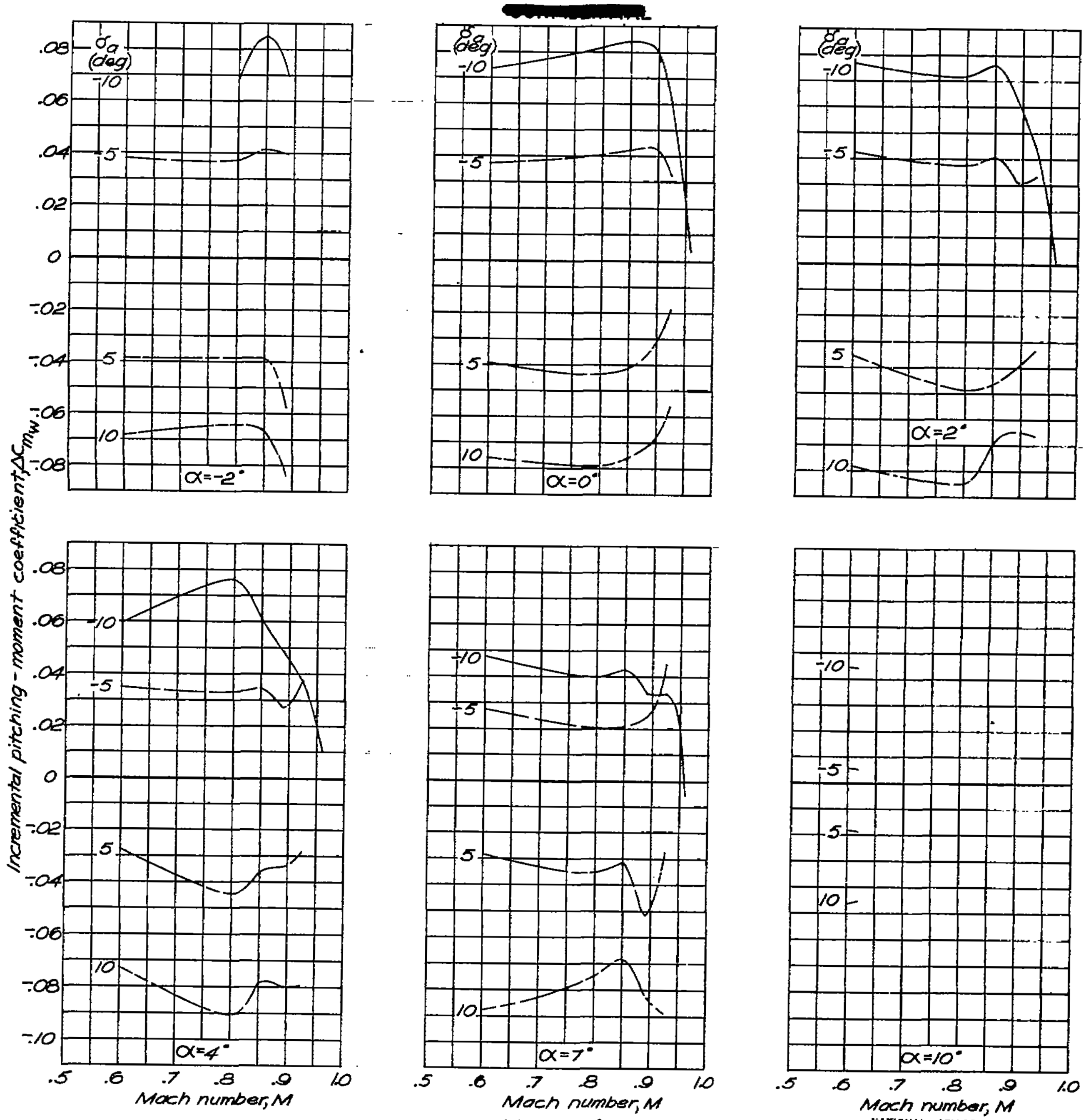

(c) $\Lambda_r = 30°$.

Figure 19.—Continued.

[redacted]

UNCLASSIFIED

[redacted]

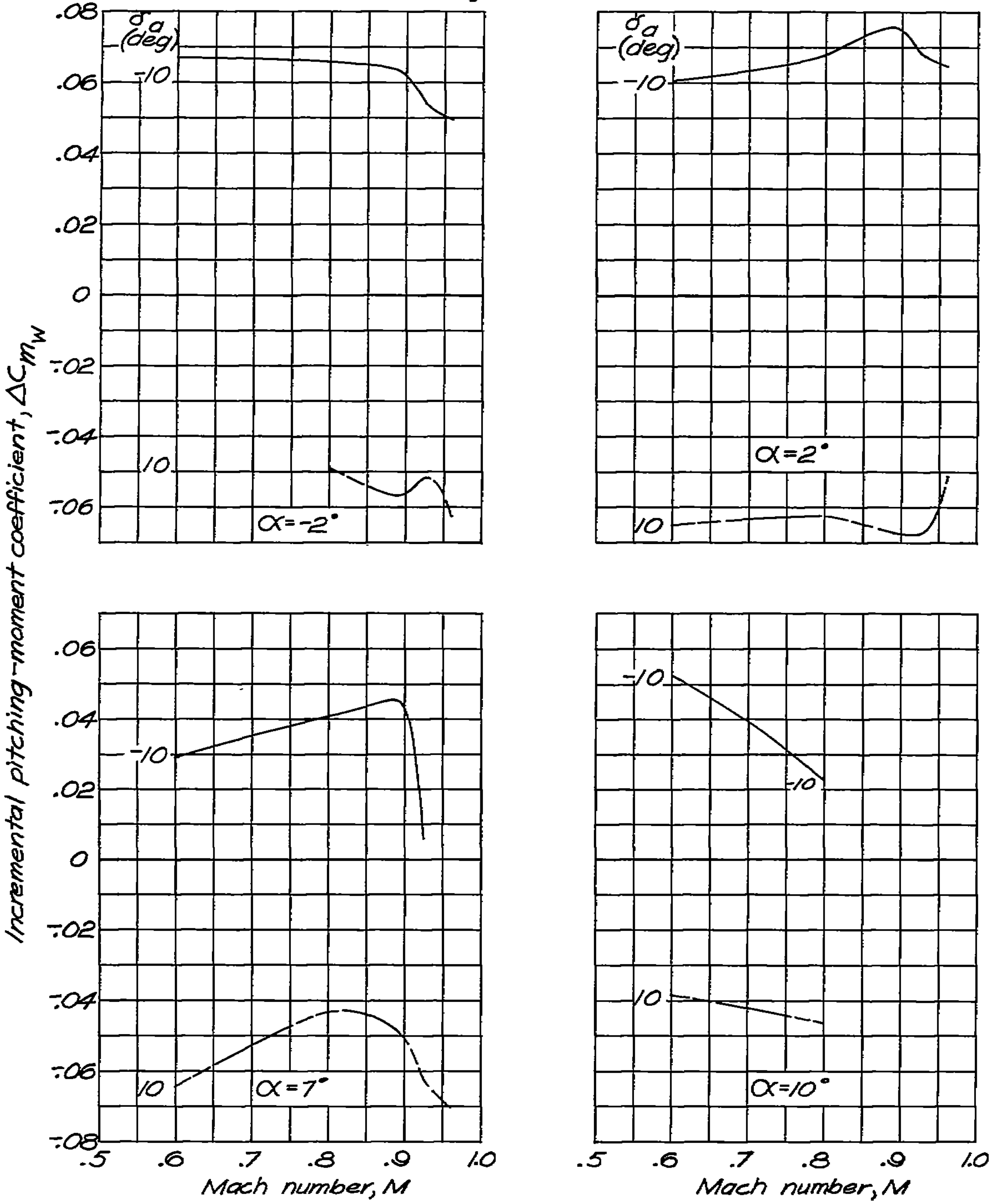

(d) $\Lambda_r = 45°$.

Figure 19.—Concluded.

NATIONAL ADVISORY COMMITTEE FOR AERONAUTICS

[redacted]

UNCLASSIFIED